UNIVERSITY OF MINNESOTA
ST. ANTHONY FALLS HYDRAULIC LABORATORY

Project Report No. 239

INFLUENCE OF WAVES ON AIR–WATER TRANSFER OF LOW SOLUBILITY GASES

By

Ekaterini I. Daniil

and

John S. Gulliver

Prepared for

LEGISLATIVE COMMISSION ON MINNESOTA RESOURCES
MINNESOTA STATE LEGISLATURE

December 1987

Minneapolis, Minnesota

University of Minnesota
St. Anthony Falls Hydraulic Laboratory
Mississippi River at 3rd Avenue S.E.
Minneapolis, Minnesota 55414

Project Report No. 239

INFLUENCE OF WAVES ON AIR-WATER TRANSFER OF LOW SOLUBILITY GASES

by

Ekaterini I. Daniil

and

John S. Gulliver

Prepared for

LEGISLATIVE COMMISSION ON MINNESOTA RESOURCES
MINNESOTA STATE LEGISLATURE

December, 1987

ABSTRACT

Water quality of rivers and reservoirs or lakes is a main component of the quality of life in a state like Minnesota, where free surface waters are abundant. A major key to managing water quality is dissolved oxygen concentration. Low oxygen concentrations result in fish kills, gaseous releases from sediments, and the release of toxic chemicals from sediments. The understanding of oxygen dynamics is therefore imperative in order to predict the impact of future developments along a river. One of the main ways of oxygen replenishment is the transfer of oxygen from air into the water through the water surface (reaeration). Reaeration in river-reservoir systems occurs most effectively through the turbulence of flowing water, turbulence and surface waves caused by the wind, and air entrainment caused by flow over hydraulic structures.

Recent studies of air-water gas transfer and comparisons between large and small wind wave flume data have indicated the potential importance of waves in the gas transfer process. Experimental evidence is presented in this paper showing that non-breaking deep-water gravity waves significantly influence gas transfer. Experiments were performed in a flume with a mechanical wave maker. Oxygen was used as a tracer gas, and the flume was chemically deoxygenated. Oxygen concentrations and wave characteristics were recorded over time at various locations along the flume. Horizontal mass transport was determined from conductivity measurements, using salt as a conservative tracer. Semi-empirical correlations of the transfer velocity and the wave characteristics were obtained. The transfer velocity is shown to increase proportionally to both wave height and frequency. Comparison against data reported in the literature indicates that approximately 50 percent of the observed gas transfer in wind wave flume experiments can be attributed to non-breaking waves. The presence of bubbles or bubble entraining breaking waves enhances the transfer velocity considerably. Visual correlation between breaking intensity and the transfer coefficient was very good, although the relation has not been quantified.

CONTENTS

LIST OF FIGURES

LIST OF TABLES

LIST OF SYMBOLS

A	surface or cross-sectional area
A	factor in the equation of Dobbins [1965] = $9.68+0.054(T-20)$
A_1	net area over which the particles in a vertical line travel in one wave period
B	factor in the equation of Dobbins [1965] = $0.976+0.137(30-T)^{3/2}$
B_F	$= 1+F^2$ in the Dobbins' equation
BOD	biochemical oxygen demand
C	D.O. concentration
c	celerity
c_g	group velocity
C_a, C_w	concentration of the chemical in air, water respectively
C'_s	saturation concentration of oxygen at p = 760 mm Hg
C_s	actual saturation concentration
$c(z)$	displacement of particle at depth z in the horizontal direction over one wave period
$C_{0,t}$	bulk oxygen concentration at time 0,t, respectively
C_4	=0.9+F in the Dobbins equation
D_{ij}	Longitudinal dispersion coefficient between point i and j $[L^2T^{-1}]$
D_m	molecular diffusivity $[L^2T^{-1}]$
D.O.	dissolved oxygen
dp/dx	air pressure gradient in the longitudinal direction
D_x	longitudinal dispersion coefficient $[L^2T^{-1}]$
E	factor in equation of Dobbins [1965]
F	$= U/\sqrt{gH}$ Froude number

F	Fetch (in the evaluation of the experimental data)
f	wave frequency
f_c	temperature correction factor
f_E	factor quantifying any enhancement in the value of K_L due to chemical reactivity of the gas in the water
g	acceleration of gravity
H'	Henry's law constant
h,H	water depth (H in literature review)
H	characteristic wave height
h_r	reference water depth
I	index for numbering of points
J	gas flux across the air-water interface $[M\ L^{-2}\ T^{-1}]$
K	overall transfer coefficient $[LT^{-1}]$
K_a	gas film coefficient or transfer coefficient for chemically unreactive gas in air
k_{comp}	computed value of conductivity
K_d	coefficient of carbonaceous oxidation
k_{expt}	measured value of conductivity during the experiment
K_{ij}	$= D_{ij}/L_{ij}$ coefficient of horizontal transfer
k_L	liquid film coefficient based on common logarithms (base 10)
K_L	liquid film coefficient or transfer coefficient of a gas into the water
K_n	coefficient of nitrogenous oxidation
k_T	conductivity at temperature T
K_1	deoxygenation coefficient
k_2	reaeration coefficient based on common logarithms (base 10) $[T^{-1}]$
K_2	reaeration coefficient $[T^{-1}]$
K_{2G}	tracer-gas transfer coefficient $[T^{-1}]$

L	wave length
L_a	L(x) at the point where the waste is added to the stream
L_i	length of i-th control volume
L_{ij}	distance between point i and j
L,L(x)	carbonaceous BOD (CBOD) at location x.
N(x)	nitrogenous BOD
p	atmospheric pressure in mm Hg
p'	fraction of day over which photosynthetic production takes place
P_m	maximum photosynthetic oxygen production
P(x,t)	algal photosynthetic oxygen source.
Q	volumetric flow rate
r	average rate of surface renewal (T^{-1})
r	correlation coefficient (when given in parenthesis after equations)
r^2	coefficient of determination
r_a	resistance to gas transfer in the air
RMS	root mean square value
R_{sh}	shear Reynolds number
RUN	code number of experiment
r_w	resistance to gas transfer in the water
R(x)	algal respiration sink
S	channel slope in predictive equations
S	source or sink term in the transport equation
s	wave slope [$=(\pi/\sqrt{2})H/L$]
Sc	Schmidt number ($= \nu/D_m$)
S_c	pressure adjusted channel slope
S_e	slope of energy gradient

$S(x)$	benthic bacterial respiration sink
T	wave period
T	temperature (°C)
t	time
T_r	reference temperature
t_s	time at which photosynthetic production begins
U	mean stream velocity
$\overline{u'}$	longitudinal turbulent intensity
$\overline{U}_A$	air velocity
$\overline{U}_W$	water velocity
u_*, u_{*c}	shear velocity
u_{*s}	surface shear velocity
V	volume
x	distance in the longitudinal direction
z	distance in the vertical direction

Greek letters

α	coefficient quantifying the effect of pollution on the reaeration coefficient
δ	film thickness
ΔC	difference in concentration
Δt	time difference
θ, θ'	temperature correction coefficient
Λ	turbulent macroscale of the flow
μ	dynamic viscosity
ν	kinematic viscosity
ρ	water density
ρ_a	air density

σ	standard deviation
ϕ	concentration

Units

L	length
M	mass
T	time

ACKNOWLEDGEMENTS

This research was supported by the Environmental Engineering Program of the National Science Foundation, Grant No. CEE-8205078, and the Legislative Commission on Minnesota Resources. The cost of computer time was covered by a grant from the University of Minnesota Computer Center. Pat Swanson edited and word processed the manuscript.

I. INTRODUCTION

Interest in the exchange of gases between the atmosphere and underlying water bodies and its effect on water quality dates back to the beginning of the century. One of the first papers presented was "The Atmospheric Reaeration of Sewage Polluted Streams," by Streeter [1926] in the first symposium about stream pollution. More than 50 years later an international symposium on gas transfer at water surfaces was held at Cornell University in 1983. Papers from this symposium are published by Brutsaert and Jirka [1984]. The editors in the foreword of the book note:

> "Interfacial mass transfer is, by its very nature, highly complex. The air and water are usually in turbulent motion, and the interface between them is irregular, and disturbed by waves, sometimes accompanied by breaking, spray and bubble formation. Thus, the transfer involves a wide variety of physical phenomena occurring over a wide range of scales. As a consequence, scientists and engineers from diverse disciplines and problem areas, have approached the problem, often with greatly differing analytical and experimental techniques and methodologies."

All these indicate that air-water gas transfer is still an important issue, and interest in it has increased in recent years. This is due to the growing concerns over environmental pollution and the movement of atmospheric pollutants. Many of these pollutants are ultimately transferred across the air-water interface and as a result problems concerning aesthetics, eutrophication and toxicity develop. These problems are not only of environmental importance, but of economic significance as well, considering the cost of treatment and control methods required to address them. Water bodies, especially the oceans, also represent a sink for greenhouse gases, like carbon dioxide, methane and chlorofluorocarbons, which have an impact on climatic variations.

Gas transfer through a river-reservoir system is controlled both by the flow and the weather. High winds create extra turbulence on the water surface as well as wind waves that can significantly enhance the gas transfer rate and increase the dissolved oxygen concentration of a water body. This should also be taken into consideration when field surveys are planned. The gas transfer on reservoirs and lakes is significantly lower on calm days than on windy days.

As projected water quality and required wastewater treatment are highly sensitive to the estimate of gas transfer rate, accurate estimations, as well as further research in the area to provide more in-depth understanding of the phenomena involved, are required.

Traditionally, the transfer of oxygen gas (reaeration) has been of most interest and is the main subject of the research presented here, since the dissolved oxygen (D.O.) present in surface waters is often used as an index of water quality. This is based on the fact that biological systems in water are quite sensitive to D.O. concentrations.

Reaeration and photosynthetic activity of plants are the two main sources of D.O. and represent the natural purification capacity of a water body. Consequently, they impose a limit on its capacity to assimilate organic waste, such as municipal and industrial sewage. The utilization of oxygen by organic material can turn the water body anaerobic, cause fish mortality, and damage the entire ecosystem.

A large number of predictive equations for reaeration exist. However, they give a wide range of values of the reaeration coefficient for the same flow parameters. This has been generally attributed to the fact that some important parameters have not been included in the existing models, two such parameters being wind and waves.

Some measurements of wind influenced gas transfer coefficients have been made in wind wave flumes, and the transfer velocity has been related to wind shear. In several studies, the authors have noted the rapid increase in air-water gas transfer velocity, that occurs with the onset of waves on water. However, little systematic investigation of the effects of waves on gas transfer in wind tunnels has been done. The effect of waves should, therefore, be studied separately, where the effect of wind shear and associated turbulence is not present.

An experimental investigation of the effect of deepwater waves on oxygen transfer is presented here.

II. LITERATURE REVIEW

A. Background

Air water gas transfer is a complex phenomenon including a number of different subjects as fluid mechanics, wave dynamics, turbulence, molecular diffusion, equilibrium chemistry, and surfactants chemistry. Despite a remarkable increase of knowledge and experimental skill in some areas pertinent to the field, surprisingly little is still known on the subject. On the one hand, this is due to the fact that the rate of transport is controlled by a region very near the interface and the actual mechanism remains a subject of debate. On the other hand, no attempt has been made to incorporate the various processes involved into an integrated model. Thus, every model has a limited perspective, neglecting a number of parameters which are out of the field of interest of the researcher.

The flux of any dissolved chemical across the air-water interface is often given by the equation

$$J = K(C_a/H' - C_w) \tag{1}$$

where J = flux/unit projected surface area $[MT^{-1}L^{-2}]$

K = overall transfer coefficient [L/T],

C_a = concentration in air $[ML^{-3}]$,

H' = Henry's law constant, an equilibrium constant, and

C_w = concentration of the dissolved chemical in water.

C_a/H is often called the saturation concentration, C_s.

With this formulation, using a projected area, any increase in surface area due to waves or other forms of roughness is incorporated into the overall transfer coefficient. The overall transfer coefficient can be thought of as the reciprocal of the resistance to the gas flow. In the case of air-water gas transfer, this resistance can be split into resistances in the air (r_a) and in the water (r_w) and the followng relation holds [Liss, 1983]:

$$\frac{1}{K} = r_w + r_a = \frac{1}{f_E K_L} + \frac{1}{H' K_a} \tag{2}$$

where K_L = liquid film coefficient, representing transport in the water;

K_a = gas film coefficient, representing transport in the air; and

f_E = an enhancement factor accounting for the reactivity of the gas in water, e.g. $SO_2 \rightarrow H_2SO_4$. $f_E = 1$ for a chemically unreactive gas.

The gas film coefficient depends upon the forced convection and natural convection of the air and is fairly well understood from studies on evaporation and heat transfer [Gulliver and Stefan, 1986; Sill 1983], which are controlled by the air side of the interface. Henry's law constant (related to the saturation concentration) is a function of temperature, pressure, salinity, etc., and is well studied for the more common gases such as O_2, N_2, and CO_2. It is usually found from a ratio of the vapor pressure to the solubility of the chemical. There is a wide variety of compounds for which data on Henry's law constant is currently being collected [Gerrard, 1980]. The 17 volume IUPAC Solubility Data Series published by Pergamon Press is an indication of the extensive amount of work being performed in this area.

The liquid film coefficient is influenced by the ordering of water molecules into a "film" on the water surface, and the important process is the breakdown of this film by fluid motion.

Gas transfer may be divided into three categories:

1) gas phase controlled, when $r_a >> r_w$ e.g. H_2O, SO_2, SO_3, $HgCl_2$, $HgClCH_3$, and toxaphene,

2) liquid phase controlled, when $r_w >> r_a$, e.g. O_2, N_2, CO_2, SF_6, Hg, $Hg(CH_3)_2$ and the noble gases, in which case $K \simeq K_L$ for a chemically unreactive gas, and

3) a category when neither resistance can be neglected. There are only a few gases in this category (i.e. HCHO, H_2S for pH $\geq$ 8), but air-water transfer of several intermediate and high molecular weight organic compounds (e.g. DDT, PCB's, napthaline, dieldrin, and chlordane) is also subject to transfer resistance from both media.

The liquid film coefficient is the topic of this paper. It relates to low solubility and relatively unreactive compounds, where transfer is controlled by water phase or by both phases. Experimental results presented in this paper were obtained using oxygen as a tracer gas. The liquid film coefficient for oxygen will be referred to as the oxygen transfer coefficient. The results are expected to be applicable to compounds in category 2 and to the liquid side resistance of compounds in category 3.

B. The Reaeration Coefficient

For oxygen Eq. (1) can be written as:

$$J = K_L(C_s - C)$$

where K_L = oxygen transfer coefficient or liquid film coefficient for oxygen into the water [L/T],

C = dissolved oxygen (D.O.) concentration at a reference depth, usually at mid-depth for rivers, and

C_s = saturation concentration.

The saturation concentration depends on the pressure, the temperature and the chlorinity of the water. Tables giving $C_s = f(T,\text{chlorinity})$ are available and the effect of pressure is taken into account by multiplying by the term p/760, where p is the atmospheric pressure in mm Hg.

For a well-mixed water body of volume V and surface area A (available for oxygen transfer), assuming that C is changed only due to reaeration, we get:

$$V \frac{dC}{dt} = J\,A = K_L\,A\,(C_s - C)$$

or

$$\frac{dC}{dt} = K_L \frac{A}{V}(C_s - C) = \frac{K_L}{H}(C_s - C) = K_2(C_s - C) \qquad (3)$$

where H = mean depth, and $K_L = K_2 H$.

Upon integration, equation (3) yields:

$$\ell n \frac{C_s - C_o}{C_s - C_t} = \frac{K_L}{H} t = K_2 t \qquad (4)$$

where C_o, C_t = bulk concentration of oxygen at time 0, and t, respectively.

K_2 = reaeration coefficient, with units of a rate coefficient $[T^{-1}]$ and is often used when results are reported.

Equation (4) serves as a basis of the practical evaluation of the reaeration coefficient. Herein, K_L will be referred to as oxygen transfer coefficient. Since gas transfer is a surface phenomenon, K_L is the coefficient describing the process.

In the literature, expressions similar to Eq. (4), but employing common logarithms (base 10), have also been used. In this way, a "new" mass transfer coefficient is defined:

$$k_L = \frac{K_L}{2.303} \quad ; \quad k_2 = \frac{K_2}{2.303} \tag{5}$$

The reason for this is that data were plotted on semi-log paper and k_2 was estimated directly from the graph. This is an additional cause of confusion and one must be careful, when using the various equations appearing in the literature. Now that desk calculators and computers are widely available, the use of k_L and k_2 should be eliminated. Unfortunately, even in recent publications [Nemerow, 1985] equations for k_2 are still given and the confusion is perpetuated.

C. Models of D.O. in Streams

Gas transfer across the air-water interface is a source (or sink) term in the transport equation. Gas transfer cannot be measured directly. Therefore, the influence of the rest of the terms in the transport equation on the concentration has to be known in order to estimate gas transfer. The correct choice of transport equation affects the accuracy of gas transfer measurements significantly. Data from earlier studies are not always reliable because certain processes were neglected. In a laboratory setup some sources of error can be eliminated, but still caution should be used. For these reasons a review of the models used for D.O. in streams will be presented.

1. Deterministic models

The first model in this area was presented by Streeter and Phelps [1925] and has the following formulation:

$$\frac{dD}{dt} = K_1 L - K_2 D \tag{6}$$

$$L = L_a \exp(-K_1 t) \tag{7}$$

where:

$D = C_s - C$ = D.O. deficit,

L = carbonaceous BOD (CBOD),

K_1 = deoxygeneration coefficient [T^{-1}], and

L_a = L at the point where the waste is added to the stream.

In this model, only oxidation of CBOD and reaeration process are considered. However, processes other than these may also be important. Streeter and Phelps, although they included only these two processes in their model, were aware of the possible effects of inflow along the reach, sedimentation and scouring in the reach and photosynthesis.

Gradually, more complete models were developed to include nitrogenous BOD, organic N_2, ammonia, nitrates, respiration (phytoplankton mass), phosphorus and orthophosphorus.

O'Connor [1970] gives the following formulation.

$$\frac{\partial C}{\partial t} = -\frac{Q}{A}\frac{\partial C}{\partial x} + K_2(C_s - C) - K_d\, L(x)$$

$$- K_n\, N(x) + P(x,t) - R(x) - S(x) \qquad (8)$$

where:

Q = volumetric water flow $[L^3\ T^{-1}]$,

A = cross-sectional area,

K_2 = reaeration coefficient $[T^{-1}]$,

K_d = coefficient of carbonaceous oxidation $[T^{-1}]$,

$L(x) = L_o e^{-K_d x/U}$, $U = Q/A$, carbonaceous BOD,

K_n = coefficient of nitrogenous oxidation $[T^{-1}]$,

$N(x) = N_o e^{-K_n x/U}$, nitrogenous BOD,

$R(x)$ = algal respiration sink,

$S(x)$ = benthic bacterial respiration sink,

$P(x,t)$ = algal photosynthetic oxygen source,

$P(t) = P_m \sin[\pi/p'(t-t_s)]$ when $t_s \leq t \leq t_s+p'$

$= 0$ when $t_s+p' \leq t \leq t_s+1$,

P_m = max photosynthetic oxygen production,

t_s = time at which the source begins (days), and

p' = fraction of the day over which the source is active (usually between sunrise and sunset).

L_o, N_o = denote the values of $L(x)$, $N(x)$ at the point where the waste is added to the stream ($x=0$)

The analytical solution of the above equation is given in the reference. The part of the solution corresponding to photosynthesis is expressed in Fourier series.

The model was applied to five rivers (Grand, Clinton, Flint, Truckee and Ivel River) and the computations agree reasonably well with the observations. K_2 was calculated from

$$K_2 = \frac{(D_m U)^{1/2}}{H^{3/2}} \qquad (9)$$

where D_m is the molecular diffusivity of O_2 in water.

2. Stochastic models

Stochastic models are based on the same transport equations as the deterministic models, but the various rate constants, and initial conditions if desired, are interpreted as expected values and represented by a probability distribution (usually gaussian) and the solution for the pollution (BOD) or the D.O. concentration has also the form of a probability distribution. This is much more important, because "having enough oxygen averagely is not sufficient to prevent fish kills" [Thayer and Krutchkof, 1967].

Stochastic models are more complicated and will not be presented here in detail. Only the basic concepts and results will be given.

The first stochastic model was developed by Thayer and Krutchkof [1967], who considered the following factors:

1) The pollution (BOD) and D.O. are both decreased by the action of bacteria. The rate is assumed proportional to the amount of pollution present. It is also assumed that there is always some oxygen present.

2) The D.O. is increased due to the process of reaeration.

3) The pollution only is decreased by sedimentation and adsorption on the rocks. The rate is again proportional to the amount of pollution present.

4) The pollution is increased from small sources along the water course, the rate of increase being independent of the level of pollution.

5) The D.O. is decreased at a constant rate due to benthal demand, photosynthetic respiration and photosynthesis. (All three processes are combined in one term and photosynthesis is not modeled as a function of time.)

The developed model, according to the above assumptions, was applied to the Sacramento River. Results are presented in Figure 1.

The derived model gives much more information at downstream points than is possible by other methods. Using parameter values and initial conditions that reflect expected changes in population or industry, one can obtain the probability distributions for the future. These results can aid in sensible long term planning. One can use the expected minimum flow and the parameters associated with it to calculate the probability distributions. This would give an extra degree of protection. Pollution by tributaries can also be taken into account.

Another stochastic model was developed by Esen and Rathbun [1976]. Its application for Sacramento River is shown in Figure 2.

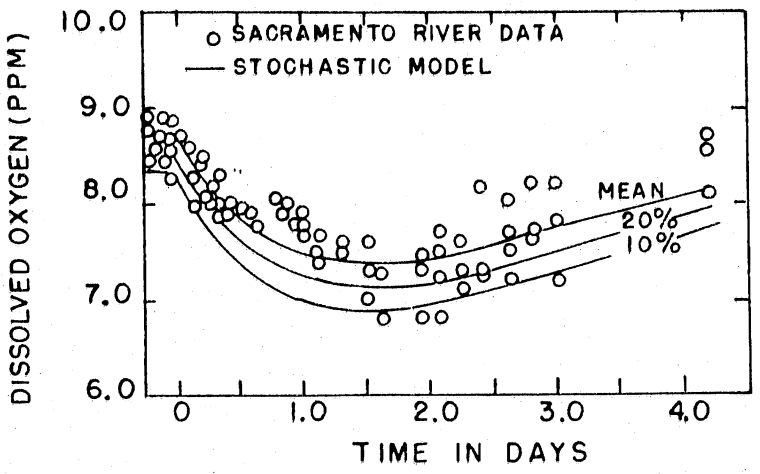

Fig. 1. Predicted D.O. concentrations (mean and lower confidence limits) by the stochastic model of Thayer and Krutchkof for Sacramento River. [From Thayer and Krutchkof, 1967].

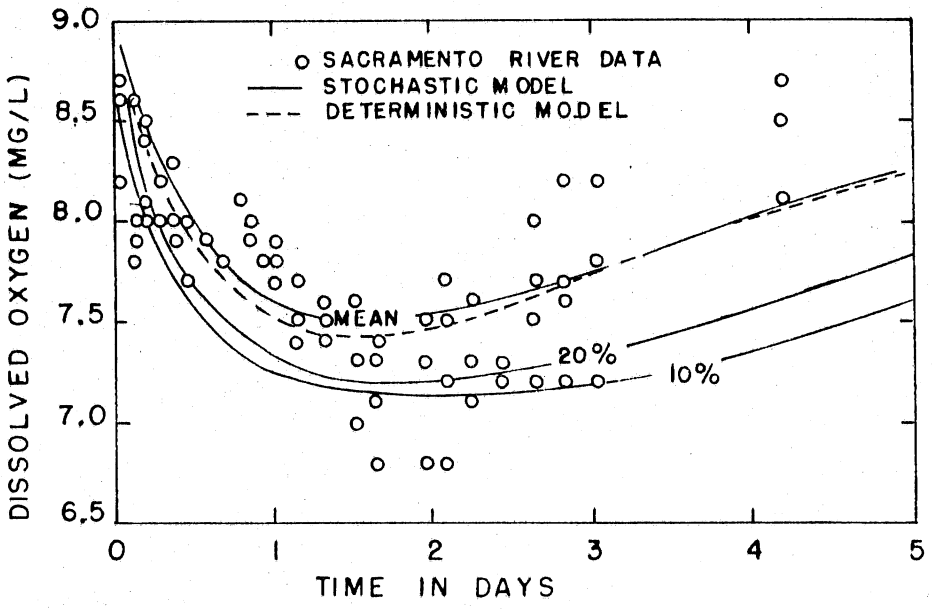

Fig. 2. Predicted D.O. concentrations (mean and lower confidence limits) by the stochastic model of Esen and Rathbun and comparison to Sacramento River data and deterministic model. [From Esen and Rathbun, 1976]

This model, using a Monte-Carlo technique for simulating a random walk process, was used to predict BOD and the distribution of D.O. deficit for points downstream from a waste source, assuming that the deoxygenation coefficient and the reaeration are normally distributed random variables. The model has the capability of considering the mean and the variance of both the reaeration and the deoxygenation coefficient as functions of the time travel through the reach. Equations for approximating the mean oxygen deficit and the variance of oxygen deficit were developed by expanding the basic equation of the stochastic model in Taylor series. The equations for the mean amounts of pollution and D.O., as derived from this model, are identical to the equations of the deterministic model presented by Dobbins [1964].

The theoretical results, especially the variance, were checked against laboratory experiments with good agreement. Application of the model to the Sacramento River yielded some interesting results:

- The variance reaches its maximum at approximately the same point at which the mean level reaches its minimum. This is an important phenomenon, because one must protect against low concentrations in order to protect the fish.

- The critical time of travel estimated from the stochastic model was always larger than the critical time of travel computed from the deterministic model. The difference decreased as the ratio of the reaeration and deoxygenation coefficient decreased.

- The critical time of travel for both the stochastic and deterministic models was extremely sensitive to the reaeration coefficient, when the deoxygenation coefficient was small, and extremely sensitive to the deoxygenation coefficient, when the reaeration coefficient was small.

- The predicted frequency distributions of the oxygen deficit became flatter and skewed to the right as travel time increased. This type of skewness is favorable in the determination of probabilistic water quality standards, because the percentile limits of the oxygen deficit will be less sensitive to errors in the values estimated for the variation of the deoxygenation and reaeration coefficient and the correlation coefficient between them.

More stochastic models, some of them including more variables, e.g. nitrogenous oxygen demand, have been developed and used in decision making in the last decade [Padgett, Schultz and Tsokos, 1977; Dewey, 1984].

Stochastic models by giving the solution in a probabilistic form provide information about the variability to be expected. The results are more realistic when the input parameters and the initial conditions are given accurate values or are modeled correctly. The reaeration coefficient is one of those parameters, and some proposed models for it are reviewed in the following section.

D. Models for Prediction of Oxygen Transfer Coefficient

Various models have been proposed for the prediction of the oxygen transfer coefficient. They can be divided into three categories: conceptual, semi-empirical and empirical models. A complete review of the models is presented by Bennett and Rathbun [1972] and Rathbun [1977]. Here only a brief review, including the most important and more commonly used models will be given. All equations presented herein were converted to the metric system (SI units: meter (m) is used for length and second (sec) for time) to facilitate comparison and be consistent. K_L is given in m/sec. A lot of existing equations in the literature involve inconsistent units and are dimensionally incorrect and one should be extremely careful when using them. The equations were also adjusted for temperature to 20°C according to the equation:

$$K_L(T) = K_L(20)\ (1.0241)^{T-20}$$

1. Conceptual models

Conceptual models are derived from equations describing an interpretation of the physical conditions governing mass transfer at a gas liquid interface. The most commonly used is the differential equation describing non-convective diffusion. The boundary conditions chosen vary from model to model. In some models the parameters arising from the solution of the differential equations with the given boundary conditions are not clearly related to the mean flow parameters such as mean velocity, depth of flow, or turbulent intensity. In such models, discovering the relation of the former parameters to the latter is a problem requiring considerable thought and experimental verification.

The models may be divided into the following general groups:

1) Film models

2) Renewal, including penetration, film penetration and surface-renewal-damped-eddy diffusivity models

3) Kinetic theory models

4) Turbulent diffusion models

The film model assumes that mass transfer takes place in a laminar layer by molecular diffusion and that the concentration gradient across the film is linear. Therefore,

$$K_L = \frac{D_m}{\delta} \tag{10}$$

where:

D_m = molecular diffusivity [L^2/T], and

δ = thickness of the film [L],

δ depends on the hydrodynamic characteristics of the flow.

The penetration model, included in the general class of renewal models, postulates that the surface of the liquid is a laminar film, the thickness of which is large with respect to the depth which can be penetrated by molecular diffusion during the life of the film. The film lifetime is the time elapsed between the formation of the film on the surface and its replacement by fresh liquid from the bulk flow. Then, the oxygen transfer coefficient is expressed as

$$K_L = \sqrt{D_m r} \tag{11}$$

where r = the average rate of surface renewal [T^{-1}] and probably is a parameter related to the average residence time of the large flow eddies at the surface. No attempt for such a correlation was made, when the model was first presented.

The film model and penetration model, as presented above, are currently the most often used and easy to deal with, due to their simple form.

The film-penetration model combines the two previous models as follows:

$$K_L = \sqrt{D_m r} \coth \left(\frac{r\delta^2}{D_m}\right)^{1/2} \tag{12}$$

but this form is more involved and not very practical because δ and r must be determined simultaneously.

A presentation of the rest of the models is given by Bennett and Rathbun [1972] and will not be given here. These models, however, for the most part cannot be used for predicting K_L of streams because of parameters such as film thickness, surface renewal rate, and eddy size, that have not been, and generally cannot be, determined for a stream.

Here only some equations, based on conceptual models and containing parameters that can be determined, will be presented. The equations are modified from their original form to give K_L in (m/sec) and all the input parameters are in SI units.

O'Connor and Dobbins [1958] presented the following equations based on the film penetration theory.

Non-isotropic turbulence

$$K_L = 1.58\left(\frac{gD_m^2 S}{H}\right)^{1/4} \tag{13}$$

Isotropic turbulence (for Chezy C > 17)

$$K_L = \left(\frac{D_m U}{H} \right)^{1/2} \qquad (14)$$

where:

S = channel slope (m/m),

D_m = molecular diffusivity of O_2 in H_2O (m^2/sec),

H = depth (m), and

U = velocity (m/sec)

The above equations do not include any adjusted constants. The validity of the assumptions for isotropic turbulence has been questioned.

Later, Dobbins [1964, 1965] presented another, more complicated equation, where some constants were obtained from experimental data. The prediction equation for K_L is

$$K_L = \frac{2.03 \times 10^{-5} B_F A E^{3/8}}{C_4^{3/2}} \coth \left(\frac{2.751 B E^{1/8}}{C_4^{1/2}} \right) \qquad (15)$$

where:

$B_F = 1 + F^2$, $F = U/\sqrt{gH}$,

$C_4 = 0.9 + F$,

$A = 9.68 + 0.054 (T-20)$,

$B = 0.976 + 0.0137 (30-T)^{3/2}$,

$E = 30.0 S U$, and

T = temperature (°C).

Another predictive equation was presented by Fortescue and Pearson [1967] based on the large-eddy model

$$K_L = 1.46 \left(\frac{D_m \overline{u'}}{\Lambda} \right)^{1/2} \qquad (16)$$

where Λ = turbulent macroscale of the flow, and

$\overline{u'}$ = longitudinal turbulence intensity.

Using the relation $\overline{u'}/\Lambda = U/H$, equation (16) yields

$$K_L = 1.46 \left(\frac{D_m U}{H}\right)^{1/2} \tag{17}$$

which is similar to Eq. (14). Thus O'Connor and Dobbin's [1958] model can be seen as a form of the large eddy model. The large-eddy model, although different in concept, is no more realistic than the other models. A more realistic relation for surface values, $\overline{u'}/\Lambda$ might improve the predictions made by the model.

2. Semiempirical models

The semiempirical models result from a consideration and combination of the factors that should affect mass transfer at a free surface. These models rely on regression correlation analysis of experimental data for establishment of a prediction equation and for verification of the assumed relations between the mass transfer coefficient and the flow parameters. In general, the steps in the derivation of these models are:

1) From intuition, a knowledge of previous conceptual models, a knowledge of the results of previous empirical studies or a combination of these, to postulate that K_L is a function of certain parameters of the flow.

2) If necessary, to manipulate the assumed relation to obtain a relation for the oxygen transfer coefficient in terms of easily measured mean flow parameters.

3) Use regression-correlation analysis to fit experimental data to the assumed relation and to check its validity.

The determination of the usefulness of these models must be based on the reliability of the data from which they were derived, or how well they predict the mass-transfer coefficient and on ease of use. Models based on the rate of energy dissipation and models in which the reaeration coefficient is correlated with the longitudinal dispersion coefficient are also included in the group of semiempirical models.

The first semiempirical models were those by Krenkel and Orlob [1963] and Thackston [1969]. Some predictive equations resulting from semiempirical models will be presented. The parameters involved are in SI units, K_L is in (m/sec) and T = 20°C.

Krenkel-Orlob

$$K_L = 2.265 \times 10^{-3} (U\ S)^{0.408}\ H^{0.34} \tag{18}$$

The model of Thackston showed some discrepancy, when applied to two different cases, indicating that some variable (may be the width of the channel) is missing, and will not be given here.

Cadwallader-McDonnel [1969]

$$K_L = 2.423 \times 10^{-3} \ (U\ S)^{0.5} \tag{19}$$

Tsivoglou-Wallace [1972]

$$K_L = 0.177 \ (U\ S\ H) \tag{20}$$

Parkhurst-Pomeroy [1972]

$$K_L = 3 \times 10^{-4} (1 + 0.17\ F^2)(U\ S)^{0.375} \tag{21}$$

(U S) is equivalent to the energy dissipated per unit mass of liquid divided by the acceleration of gravity.

Some more equations, including the shear velocity u_* or the slope of the energy gradient S_e, are also given in this group.

Thackston-Krenkel [1969]

$$K_L = 3.25 \times 10^{-4} (1 + F^{0.5}) u_* \tag{22}$$

Churchill, Elmore, Buckingham [1962]

$$K_L = 2.83 \times 10^{-7} \ U^{2.695} \ H^{-2.085} \ S_e^{-0.823} \tag{23}$$

Bennett-Rathbun [1972]

$$K_L = 4.24 \times 10^{-4} \ U^{0.413} \ S_e^{0.273} \ H^{-0.408} \tag{24}$$

Lau [1972]

$$K_L = 0.0328 \ U \left(\frac{u_*}{U} \right)^3 \tag{25}$$

3. Empirical models

The empirical prediction equations result from least squares multiple regression analysis of the variables considered pertinent by the investigator or from dimensional analysis of the mean flow and gas-liquid parameters. Empirical predictive equations usually have K_L proportional to the average flow velocity raised to some power and inversely proportional

to the average flow depth raised to some different power. All equations below are in SI units and for T = 20°C.

Churchill, Elmore and Buckingham [1962] performed many multiple regression analyses on the pertinent stream flow, gas and liquid parameters corresponding to the K_L measurements. None of the prediction equations was found to be statistically any more significant than any of the others. So, the simplest was recommended for use.

$$K_L = 5.804 \times 10^{-5} U^{0.969} H^{-0.673} \quad (26)$$

Owens, Edwards, Gibbs [1964] by analysis of their data derived

$$K_L = 8.647 \times 10^{-5} U^{0.73} H^{-0.75} \quad (27)$$

Langbein-Durum [1967]

$$K_L = 5.943 \times 10^{-5} U H^{-0.33} \quad (28)$$

Isaacs-Gaudy [1968]

$$K_L = 1.472 \times 10^{-5} C U H^{-1/2} \quad (29)$$

C = 2.44, 3.053, 3.739 for various sets of data that were analyzed. It was pointed out that C can be interpreted as $\chi[D_m^{1/2}/(\nu g)^{1/6}]_{20°C}$ where the constant χ is dimensionless and ν is the kinematic viscosity.

Negulescu-Rojanski [1969] give

$$K_L = 1.264 \times 10^{-4} U^{0.85} H^{0.15} \quad (30)$$

and

$$K_L = 35.275 D_x U^{1.63} H^{-0.63} \quad (31)$$

where D_x = longitudinal dispersion coefficient in m^2/sec.

A critical review and comparison of the above equations is given by Rathbun [1977]. Their predictive capabilities will be reviewed in Section II.F.

E. Temperature Effect

Physical properties of the liquid and gas phases are temperature dependent. However, empirical equations are usually used to account for the temperature variation. The similarity between a theoretical equation showing the dependence of K_L on the Schmidt number and the commonly used empirical formula with θ=1.0241 is presented here. The former is suggested for use, since it is applicable to all gases.

A temperature correction factor, f_c, can be defined as:

$$f_c = K_L(T)/K_L(T_r) \tag{32}$$

where $K_L(T)$ is the value of K_L at T(°C) and T_r is the reference temperature (T_r = 20°C is most commonly used and will be used herein as well). For air and water in the temperature range encountered in the field (0°C - 40°C), it is generally assumed that f_c can be expressed as a function of temperature alone, incorporating the temperature dependence of all physical properties involved.

Early approaches [Downing and Truesdale, 1955; Truesdale and Van Dyke, 1958; Elmore and West, 1961] to the problem modeled f_c as either a linear or an exponential (Arrhenius type) function of temperature:

$$f_c = 1 + \theta' (T - T_r) \tag{33}$$

$$f_c = \theta^{T - T_r} \tag{34}$$

where θ and θ' are constants.

The Arrhenius relation, derived for the temperature dependence of the equilibrium constants of ideal gas mixtures and shown to fit data for the temperature dependence of many reaction rate constants, has been used extensively. It is important to note though, that gas transfer is a diffusion process controlled largely by the hydrodynamic conditions near the interface, and K_L is not a reaction rate coefficient in contrast to the deoxygenation coefficient, K_1. Therefore, Eq. (34) for K_L is not theoretically based.

The value of θ', though, depends on the value of T_r. To convert Eq. (33) from one reference temperature, T_{r1}, to another, T_{r2}, the following relation should be used:

$$\theta_2' = \theta_1' /[1 - \theta_1' (T_{r_1} - T_{r_2})] \tag{35}$$

Thus, values of θ' reported without the corresponding T_r are of no value.

This is not true for θ. Once a θ value has been determined, Eq. (34) can be used with this θ value and any other reference temperature within the range that the equation is assumed to apply. This is a mathematical result and should not be confused with some experimental results indicating that the temperature relation changes for different temperature ranges and different θ values should be used at each range.

Equations (33) and (34) are purely empirical, and all of the data used to determine θ and θ' have been for oxygen transfer. Truesdale and Van Dyke [1958] report that values of θ'_{15} in the literature vary from 0.008 to 0.047 and suggest $\theta'_{15} = 0.015$ as the most suitable for flowing water. For θ, values ranging from 1.008 to 1.047 have been reported [Metzger, 1968]. More recently, Howe [1977] obtained values of θ less than one, but this work has been criticized by Brown and Stenstrom [1980]. Chao et al. [1987] also report K_L decreasing with temperature for very low flow velocities (0.8 cm/sec). Such velocities, however, are not representative of flows obtained in the field.

Elmore and West [1961], after reviewing prior work concluded that the effect of temperature had not been definitively established. Consequently, they performed a series of carefully controlled, high precision laboratory experiments in a stirred container and concluded that $\theta = 1.0241$ would give the most accurate results. This value has been widely used to account for the effect of temperature and is recommended in the APHA Standard Methods for the Examination of Water Wastewater [1980] and in the ASCE Standard Measurement of Oxygen Transfer in Clean Water [1984]. In some cases [Isaacs and Gaudy, 1968] $\theta = 1.0241$ has even been used to deduce functional relations between the physical properties.

Churchill, Elmore and Buckingham [1962] tried to incorporate temperature effects in the development of their empirical model. The predictive equation for K_2 with temperature correction, involving only U and R (hydraulic radius), produced as good a fit as that obtained without using the temperature correction. Some attempts to allow the effect of water temperature on reaeration rates to reveal themselves through the Schmidt number ($Sc = \nu/D_m$) were not very successful. Apparently, the distribution of observed temperatures was such that the influence of temperature in this group of field observations was not strong enough to be separated from the stronger influences of the hydraulic variables.

Although these empirical relations are convenient to use, in a complete model the temperature dependence should reveal itself through the temperature variation of the physical properties involved. Metzger and Dobbins [1967] and Metzger [1968] worked in that direction using the film penetration model (Eq. 12). For temperature dependence, they assumed that $r \propto \rho\nu^{3/4}$ and $\delta \propto \nu^{3/4}$, where ρ = density and ν = kinematic viscosity of the water. Metzger [1968] also gives $rL^3 = 1300\ \rho\nu^3$ (in SI units). The constant was determined experimentally and assumed to be applicable for all cases. With these assumptions

$$f_c = f_r \cdot \frac{\coth [a_1 f_1]}{\coth a_1} \tag{36}$$

where $a_1 = 10.91 \rho_{20}^{1/3} \nu_{20} D_{m20}^{-0.5} r_{20}^{1/6}$

$$f_1 = \frac{\rho}{\rho_{20}} \left(\frac{\nu}{\nu_{20}} \right)^{1.625} \left(\frac{T+273}{293} \right)^{0.5}$$

$$f_r = \left(\frac{T+273}{293} \right)^{0.5} \left(\frac{\nu_{20}}{\nu} \right)^{0.125}$$

and the subscript 20 denotes values of the corresponding parameters at 20°C. According to this model, f_c depends not only on temperature but also on the value of the liquid film coefficient and varies for different gases. Metzger and Dobbins [1967] presented experimental data to corroborate their theory, using helium, oxygen, argon, and nitrogen in a stirred container at a variety of mixer speeds. Metzger demonstrated that, when comparing the results of this model with Eq. (34) for a given temperature, θ varies continuously with K_L, and suggested that the value of θ to be employed should be based on K_L, as shown in Fig. 3a. This approach was used by Parkhurst and Pomeroy [1972]. However, Eq. (12) has two limits for which f_c depends only on temperature: the renewal model, $K_L = \sqrt{D_m \cdot r}$, for large values of r, and the film model, $K_L = D_m/\delta$, for small values of r. The corresponding limits of Eq. (36) are:

$$f_c \text{ (renewal)} = \left(\frac{T + 273}{293} \right)^{0.5} \left(\frac{\nu_{20}}{\nu} \right)^{0.125} = f_r \tag{37}$$

and

$$f_c \text{ (film)} = \left(\frac{T + 273}{293} \right) \frac{\rho_{20}}{\rho} \left(\frac{\nu_{20}}{\nu} \right)^{1.75} \tag{38}$$

It is interesting to note that at the limits, f_c depends only on temperature and the corresponding θ, determined from Eq. (34), is a decreasing function of temperature, whereas in the interval between the two limits θ is an increasing function of temperature and depends on K_L (20°C) and D_{m20}, as illustrated in Fig. 3b for oxygen. For all temperatures θ is a decreasing function of K_L(20°C), indicating that temperature effects are more significant when K_L is low.

Jähne et al. [1987] in their studies of the wind effects on gas transfer provide evidence that K_L is a function of the Schmidt number, $Sc = \nu/D$, via a relationship that changes from $K_L \propto Sc^{-2/3}$ to $K_L \propto Sc^{-1/2}$ with the onset of waves on the water surface. Coantic [1986] obtains the same Schmidt number dependence based on theoretical considerations. The $K_L \propto Sc^{-2/3}$ relationship results from considering the water surface as a rigid surface. This analogy holds only for very low wind and water

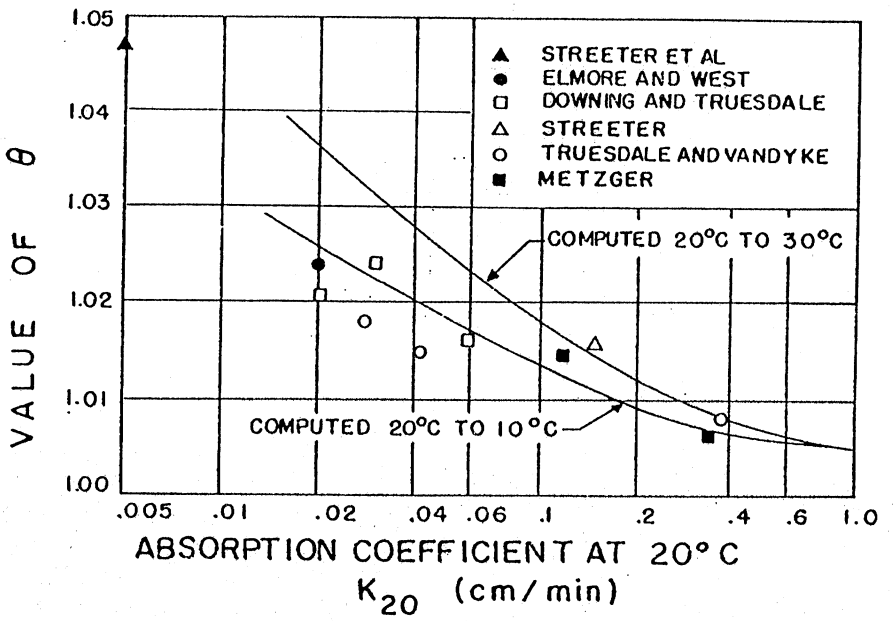

Fig. 3a. Effect of K_{20} (base e) on reported and computed values of θ [from Metzger, 1968].

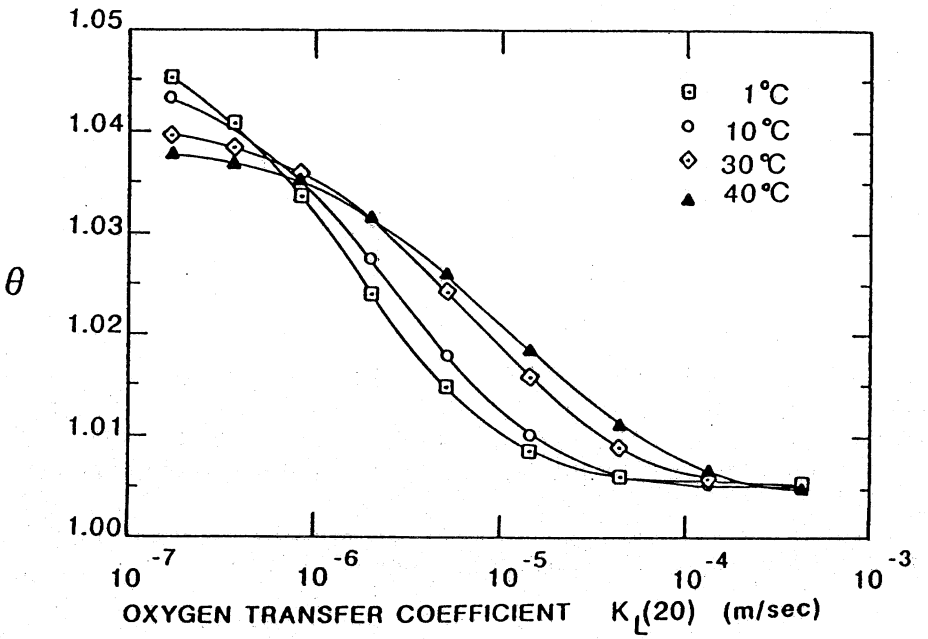

Fig. 3b. Variation of θ with K_L and temperature according to Metzger's and Dobbins' [1967] model.

velocities, which result in an undisturbed water surface and very low liquid film coefficients. When the shape of the water surface is considered deformable, the free surface regime relation, $K_L \propto Sc^{-1/2}$, is obtained. From experiments with CO_2 in the 3°C - 35°C range, Jähne et al. show that for the free surface regime the data agrees well with the $Sc^{-1/2}$ dependence. Thus, for a "rigid" surface

$$f_c = \left(\frac{Sc(20)}{Sc} \right)^{2/3} = \left(\frac{273+T}{293} \right)^{2/3} \left(\frac{\nu_{20}}{\nu} \right)^{4/3} \left(\frac{\rho_{20}}{\rho} \right)^{2/3} \qquad (39)$$

and for a "free" surface

$$f_c = \left(\frac{Sc(20)}{Sc} \right)^{1/2} = \left(\frac{273+T}{293} \right)^{1/2} \left(\frac{\nu_{20}}{\nu} \right) \left(\frac{\rho_{20}}{\rho} \right)^{1/2} \qquad (40)$$

In Fig. 4 the standard temperature correction, Eq. (34) with θ=1.0241, is compared against Eqs. (39) and (40) and the limits of Metzger and Dobbins' [1967] model, Eqs. (37) (renewal) and (38)(film). It is interesting to note that Eq. (39) is closer to Metzger and Dobbins' film model and Eq. (40) is closer to Metzger and Dobbins' renewal model, indicating that temperature effects are more pronounced for low transfer coefficients. In most cases, however, the surface of a natural water body is disturbed by wind, waves, and streamwise vortices. Moreover, cases of very low gas transfer are usually not of interest. The similarity between Eq. (34) with θ = 1.0241 and Eq. (40) with a $Sc^{-1/2}$ dependence of K_L, is striking. The maximum difference between the predicted values is 11% at T = 1°C. For the range 10°C - 40°C the values are almost identical. Thus, the correction factor which results from Elmore and West's [1961] careful laboratory experiments agrees very well with the $Sc^{-1/2}$ dependence.

Experimental data from various researchers are compared against Eq. (40) in Figure 5. Data points are scattered around Eq. (40). The scatter can be partly attributed to the difficulty in obtaining accurate gas transfer data. As an example, we refer to the preliminary experiments by Elmore and West [1961] where "the reaeration coefficient of an experiment could be more than doubled by simply removing the electrode column from the reaction flask." This was one of the main reasons that caused them to abandon the membrane electrode system. A similar sensitivity of gas transfer data has been noted by most researchers.

Although experimental data by Metzger and Dobbins [1967] follow the trend for increased temperature effect at low gas transfer rates, data reported by Downing and Truesdale [1955], as well as some data points for CO_2 by Jähne et al. [1987], experience the opposite trend. Downing and Truesdale [1955] presented data for slowly stirred and wind ruffled surfaces for distilled water, tap water and sea water. The results for the three different kinds of water were very close, but the more pronounced temperature effect was obtained for wind ruffled surfaces (with high K_L), contrary to Metzger's and Dobbins' findings. It is also unfortunate that Elmore and West [1961] report their results in terms of K_2 and do not provide necessary information for their conversion to K_L, preventing in this way any further comparison. Whether the turbulence intensity (or the

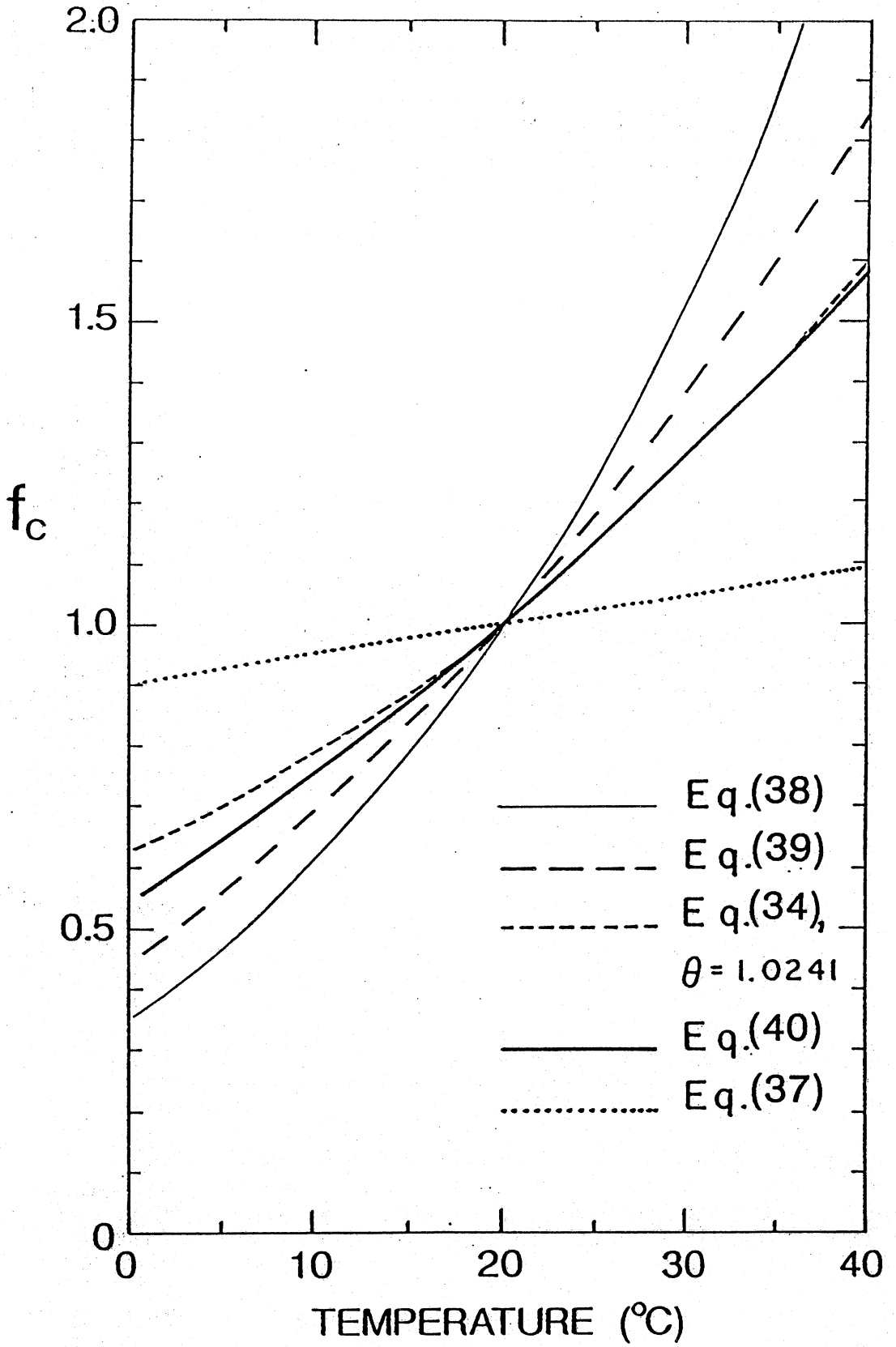

Fig. 4. Comparison of equations for the temperature correction factor, f_c, versus temperature. Eq. (34): $f_c = \theta^{T-20}$, Eqs. (37) and(38): renewal, film model by Metzger and Dobbins, Eqs. (39) and(40): Schmidt number dependence for a "rigid," "free" surface.

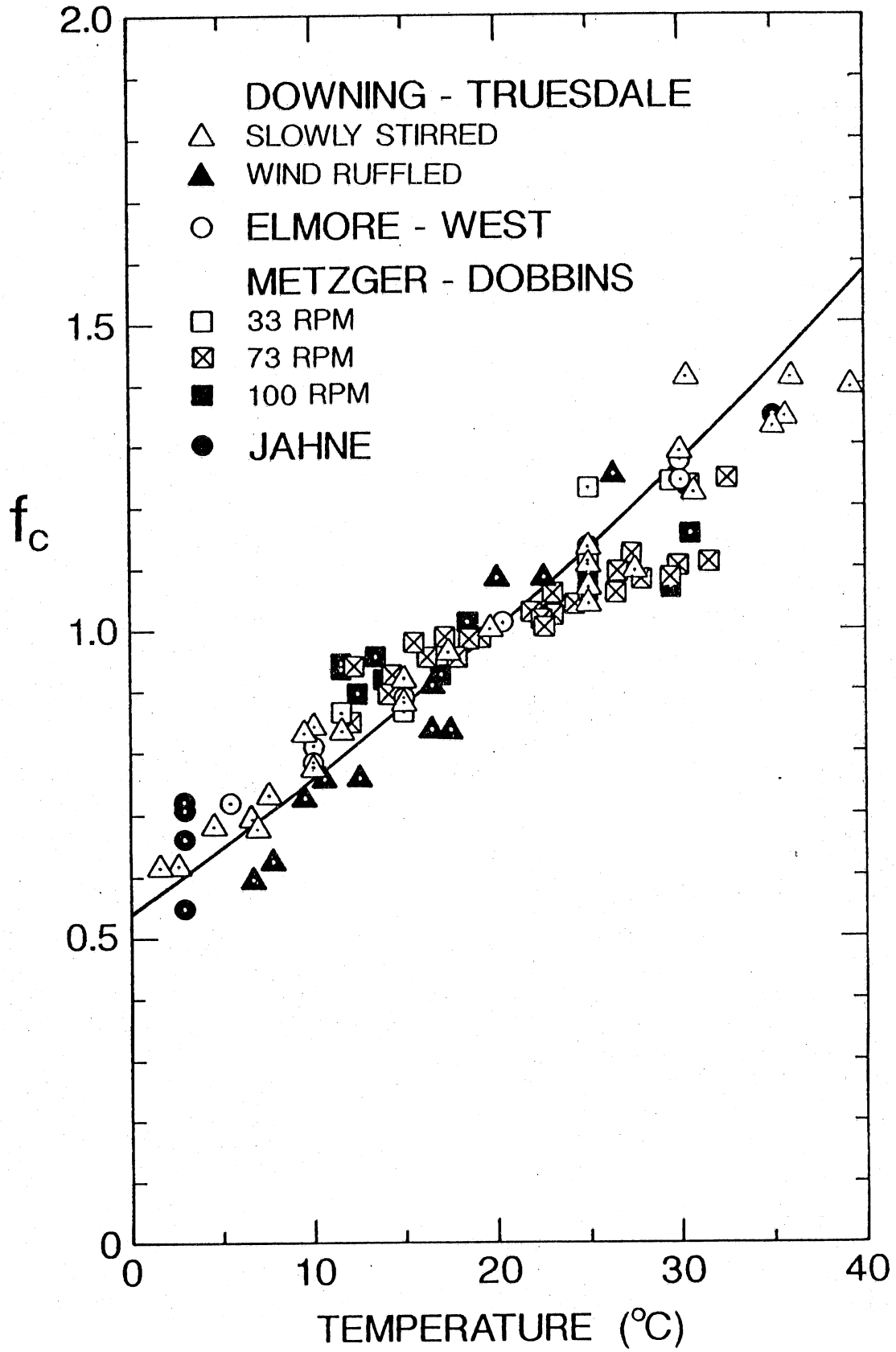

Fig. 5. Comparison of experimental data with Eq.(40): $f_c = [Sc(20)/Sc]^{1/2}$.

value of K_L) affects the value of f_c has still to be clarified, since the available data are contradictory. Until further experimental evidence, Eq. (40) seems to adequately describe the temperature effect on gas transfer for the cases of practical interest.

From the above comparison of models and equations for the prediction of a temperature correction factor, we conclude that Eq. (40), with a $Sc^{-1/2}$ dependence, derived theoretically and verified experimentally, is the appropriate one to be used for the conversion of data from one temperature to another.

Equation (34) with $\theta = 1.0241$, currently used, is a purely empirical equation for oxygen transfer which gives nearly identical results. In effect, variations in temperature have been accounted for reasonably well. The dependence on $Sc^{-1/2}$ indicates that the temperature correction factor is the same for all gases, since it depends only on water properties. In addition, it allows the translation of gas transfer coefficients between various gases.

In the preceding analysis the relationships given by Heggen [1983] were used for the evaluation of the temperature dependence of water properties. For the molecular diffusivity, a Stokes-Einstein type relation was used:

$$\frac{D_m \nu \rho}{(T+273)} = \text{const} \quad \text{or} \quad \frac{D_m}{D_{m20}} = \frac{(T+273)}{293} \frac{\nu_{20}}{\nu} \frac{\rho_{20}}{\rho} \tag{41}$$

The above equation gives very good results for the temperature range from 5°C to 40°C [Wilke and Chang, 1955]. For oxygen $D_{m(25°C)} = 2.13 \times 10^{-5}$ cm^2/s [Goldstick and Fatt, 1970].

F. Analysis of Predictive Equations

The predictive equations for the reaeration coefficient were evaluated by Bennett and Rathbun [1972], Wilson and MacLeod [1974], and Brown [1974].

Bennett and Rathbun used the following procedure: First, they compared the equations with respect to how well they predicted the reaeration coefficient (K_2) for two sets of data: the original data set, from which the equation was developed, and all applicable data. Second, a multiple linear regression analysis was completed for the data for which all four variables (depth, velocity, width and slope) were available.

It was found, that flume data equations were significantly different from field data equations, and also that the combined data equations were also significantly different from both of the others. In terms of the partial correlation coefficient, the most important variable for the field data equation was the depth of flow, followed by the average velocity and the slope of the energy gradient. The channel width had a negligible effect. For the flume data, the most important variable was the slope, followed by the width, depth, and average velocity.

Wilson and MacLeod presented a similar type analysis on a much larger body of data. They divided the predictive equations into two groups: equations involving only velocity and depth, and energy dissipation-surface renewal equations requiring the slope of the energy gradient. Flume and field data were considered as one set of data and 16 equations were evaluated. Plots of experimental coefficients vs. predicted coefficients were also presented, and it was suggested that these may be used as the primary basis for choice. Although some equations were better, considerable scatter existed. Wilson and MacLeod concluded with the suggestion that the scatter in the data is probably not entirely the result of experimental error, but of the failure to include one or more significant variables.

They also summarize the causes of predictive errors as follows:

a) experimental errors in the data as a whole,

b) errors in the data used to evaluate the model parameters, and

c) fundamental falsity of the physical model, the assumptions on which it is based, or its mathematical analysis.

A very interesting evaluation of the prediction equations is also given by Morel-Seytoux and Lau [1975]. They give a plot of k_2 vs. discharge (Q) for various equations for a particular set of data, as shown in Fig. 6. The most striking aspect of Fig. 6 is the opposite trend of the variation of k_2 with discharge displayed by the Tsivoglou-Wallace equation as compared with the others. It raises the question of whether the reaeration coefficient is a decreasing or increasing function of discharge. Perhaps, as suggested by Lau [1972] "the true values of k_2" do not "follow a smooth function of discharge." The range of discharge, where the equations converge, is also not fixed and can shift along the discharge axis, depending on the stream characteristics.

It is true that most authors of the formulas have warned the users that their formulas would be applicable only for conditions similar to those obtained during the laboratory experiments or the field measurements. This, however, leads to a serious cause of confusion.

The preceding analysis suggests that important variables, in modeling of the reaeration coefficient, have been omitted and if its prediction is to be improved, new models for the oxygen transfer coefficient in natural streams must be proposed and verified.

G. Other Parameters Affecting Gas Transfer

1. Wind

Wind can significantly increase the rate of transfer. O'Connor [1961], for example, notes that "an adjustment was made in the reaeration coefficient to allow for the increased oxygen transfer induced by the wind effect on the water surface," but no details were given in the paper apart from a reference to the unpublished manuscript, "Effects of Winds on the Oxygen Transfer Coefficient."

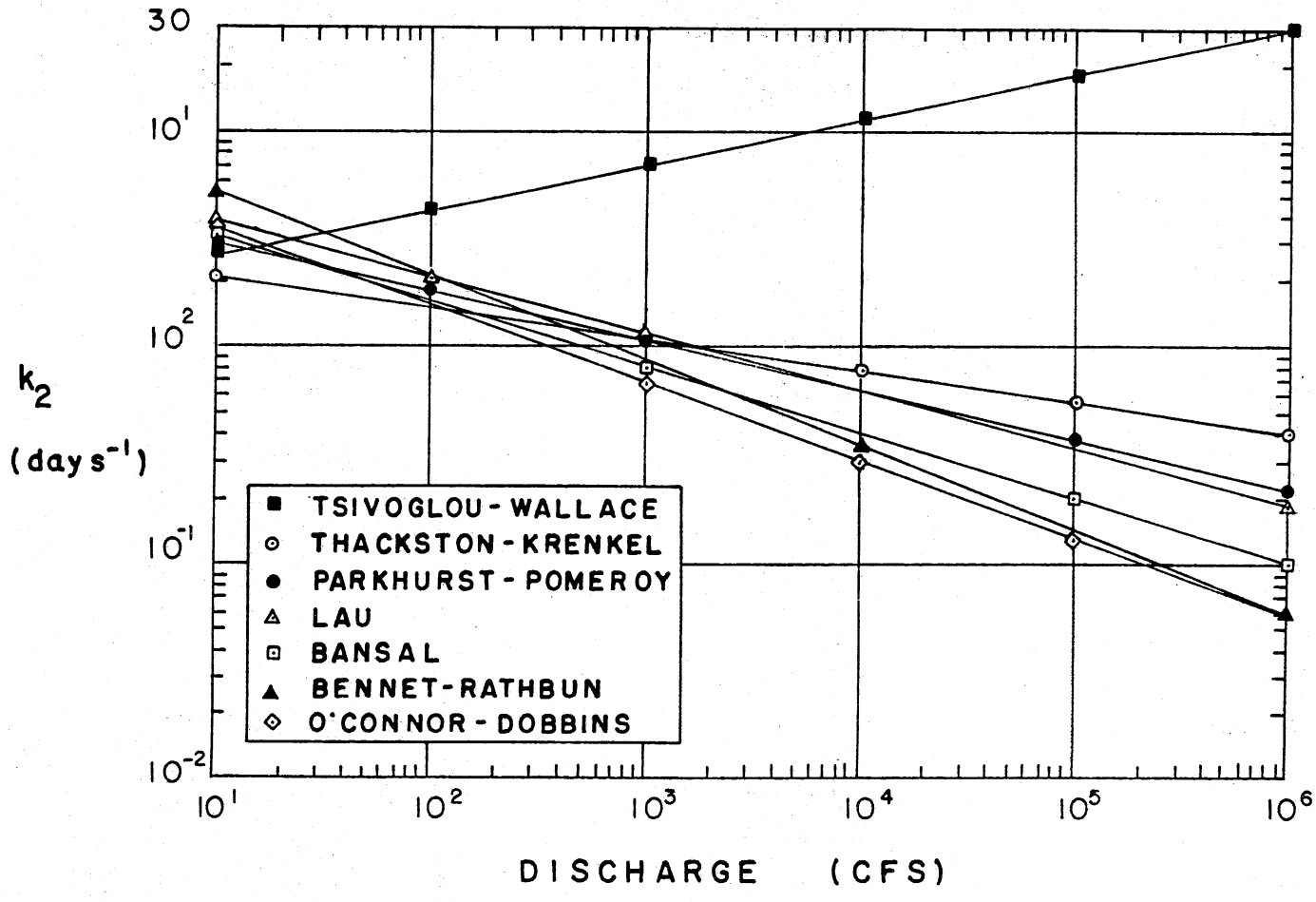

Fig. 6. Reaeration coefficient predictions as a function of discharge using Pettis' stream characteristics. [From Morel-Seytoux and Lau, 1975]

In most cases, however, the effect of wind has not been included in the prediction equations.

Wilson and MacLeod, in their analysis of predictive equations, reasoned that wind would have a slight (almost negligible) effect on the reaeration coefficient, because oxygen absorption is controlled by processes on the liquid side of the air-water interface. This is not true, because when wind blows over water, shear is exerted at the interface, establishing the structure of the boundary layers in both media. Near-surface turbulence is increased through wind shear, creating Langmuir circulations, and wind waves can develop, causing upwelling and, in the case of breaking waves, bubble entrainment. The action of wind is even more prominent in water bodies such as lakes, reservoirs, and oceans, where the effect of bottom turbulence is not so pronounced. Wind waves depend both on wind shear and wind fetch, the latter being restricted for lakes and reservoirs. The above processes determine the dynamic characteristics of the interface and, consequently, influence the rate of gas transfer between air and water.

In the last fifteen years measurements of wind influenced gas transfer coefficients have been performed and the coefficients have been related to wind velocity or wind shear velocity [Mattingly, 1977; Eloubaidy and Plate, 1972; Broecker et al., 1978; Jähne et al., 1979; Liss et al., 1981; Sivakumar and Herzog, 1978; O'Connor, 1983]. Liss [1983] presented a composite plot (Figure 7) incorporating the findings of several different wind tunnel studies. (The data were obtained using linear wind tunnels and refer to various gases with liquid-phase control.) Linear tunnels have a limited fetch. An elegant alternative is the use of circular tunnels in which the wind flows continuously over the unconstrained water surface. The results though are not in good agreement with those of the linear tunnels, the effects of wind waves being evident in the data. From Fig. 7 and other comparisons, a general trend of increased gas transfer with increasing wind velocity is evident in the data, but discrepancies exist both between different sets of laboratory data and between field and laboratory data [Jähne et al., 1985]. The relation is approximately linear for low winds, but for higher winds the dependence on wind velocity becomes stronger. Field data in general show a weaker dependence on wind speed, but the reason is not obvious, and the data are not extensive [Deacon, 1981; Liss et al., 1981; Wanninkhof et al., 1985].

Two predictive equations, for the effect of wind on oxygen transfer, based on experimental studies, are presented here.

Laboratory experiments by Mattingly [1977] indicated, that the influence of wind on the reaeration process is extremely significant. Based on the experimental results, two empirical equations were formulated:

$$\frac{K_L}{(K_L)_o} = 1 + 0.2395\ \overline{U}_A^{1.643} \qquad (r = 0.977) \qquad (41)$$

where $\overline{U}_A$, $\overline{U}_w$ = air, water velocity (m/s), and

$$(K_L)_o = 2.806 \times 10^{-5}\ \overline{U}_w^{0.607}\ H^{-0.689} \qquad \text{in (m/s)}$$

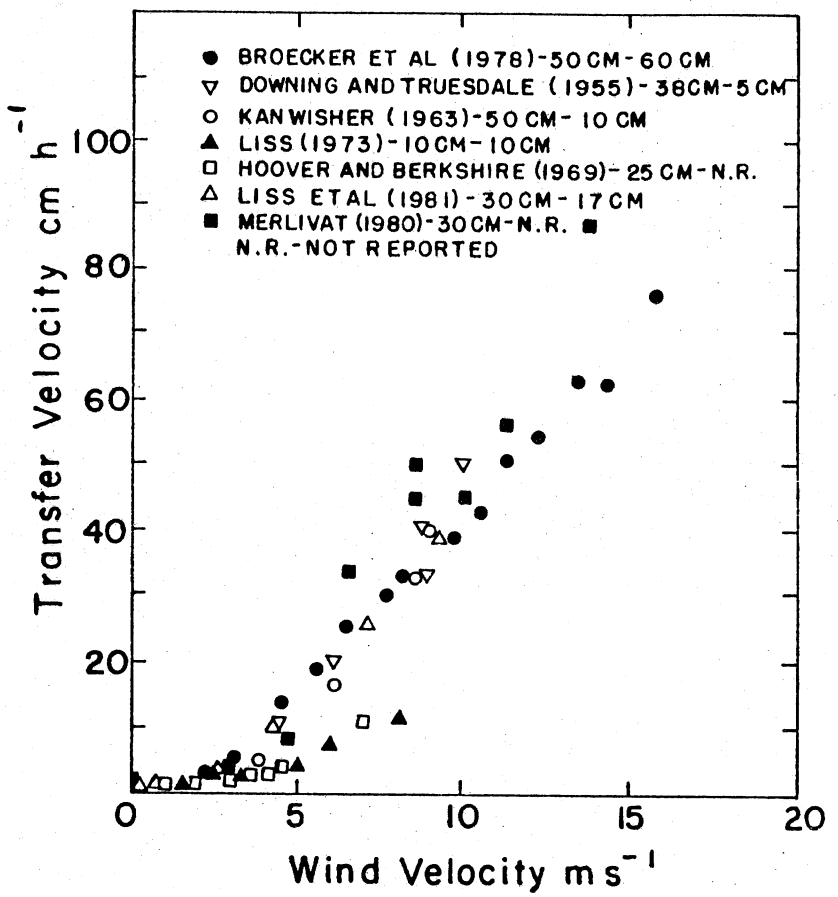

Fig. 7. Relation between air-water gas transfer velocity and wind velocity found in various wind tunnel studies. The depth of water in the tunnel and the height above the water surface at which the plotted wind velocities were measured are shown in the key. [From Liss, 1983]

as given by Bennett and Rathbun [1972] for the case when wind effects are neglected.

Another correlation was also given

$$\frac{K_L}{(K_L)_o} = 1 + 0.2588(\overline{U}_A - \overline{U}_W)^{1.618} \qquad (r = 0.978) \qquad (42)$$

Of course, it remains to be seen how these equations predict reaeration phenomena under full-scale conditions. The use of equation (42) is restricted to a certain range of values, since it cannot be used for $\overline{U}_A < \overline{U}_W$. In the conducted experiments, $\overline{U}_A$ was greater than $\overline{U}_W$.

Eloubaidy and Plate [1972] developed an equation to predict reaeration rates in natural streams and rivers with the wind blowing over the water surface, based on the concept that the reaeration rate is controlled by an effective turbulent diffusion coefficient at the surface and by the rate of surface renewal. The diffusivity of the drift current beneath the water surface was taken as a measure of the rate of surface renewal. The experimental results give support to the theoretically developed equation. The reaeration rates were found to significantly increase when waves appear on the surface. The increase is much larger than can be accounted for by the increase in surface area. The increase was attributed to the increased turbulence in the water, which finds its expression in the shear velocity of the air at the water surface. The developed equation is

$$K_L = 7.21 \times 10^{-8} R_{sh}\, u_{*c} \qquad (r = 0.989) \qquad (43)$$

where $u_{*c} = \sqrt{gHS_c}$ shear velocity of the channel bed,

H = depth,

$R_{sh} = u_{*s} h/\nu$ - shear Reynolds number - This dimensionless number has the appearance of a Reynolds number, but it arose as the ratio of eddy to kinematic viscosity, a physical concept usually not associated with a Reynolds number,

$S_c = S_e + 1/\rho g \times dp/dx$ pressure adjusted channel slope,

dp/dx = air pressure gradient in longitudinal direction,

S_e = slope of energy gradient (channel slope for uniform flow),

$u_{*s} = \sqrt{\tau_s/\rho_a}$ surface shear velocity,

ρ = water density, and

ρ_a = air density.

Because of the random nature of wind, both in direction and intensity, scatter could easily be introduced into measured reaeration coefficients as a result of wind effects. Measurements of wind speed and direction should, therefore, be a part of any experiment for gas transfer coefficient. In addition, the effects of wind sheltering, especially for small water bodies, needs to be determined.

Finally, it should be mentioned that, although in several wind-tunnel studies, the authors have noted the rapid increase in air-water gas transfer velocity, which appear to occur with the onset of waves on water [Kanwisher, 1963; Broecker et al., 1978; Jähne et al., 1979], systematic investigation of the effects of waves on gas transfer in wind tunnels has been limited and in most cases the wave characteristics have not been reported or measured.

2. Waves

As noted in the previous section, the effect of waves on gas transfer has not been investigated systematically, and almost no attempt has been made to include that effect in a predictive equation.

It is usually assumed that capillary waves are the ones affecting gas transfer. Considering the resulting increase in surface area available for gas transfer and their extent on the sea surface though, it can be argued that the enhancement of the transfer coefficient is not very important. However, capillary or gravity waves can influence gas transfer if the circulation created by the waves acts to replace the water particles on the surface. It has also been suggested that capillary waves may not be the cause of the observed enhancement in gas transfer, but may merely act as indicators of a change in the nature of the gas transfer process close to the water surface [Liss, 1983].

Only recently [Jähne et al., 1985, 1987; Merlivat and Mémery, 1983] the need for parameterization of the wave field, in order to explain the observed differences, has been realized. Coantic [1986] proposed a theoretical model incorporating the effect of capillary waves on gas transfer. Although the assumptions used need to be refined, as the author indicates, the model qualitatively explains the observed increase in gas transfer coefficients at low and moderate wind speeds. Gravity waves and wave breaking due to higher winds were not included in the model. Jähne et al. [1984, 1987] noted that the mean square slope seems to be a better parameter than the capillary wave slope, indicating an influence of gravity waves on gas transfer.

A few experiments on the effect of waves alone had been performed by Downing and Truesdale [1955] in their investigation of factors affecting oxygen transfer. They concluded that increasing the height and frequency of stable progressive waves and the height of choppy waves generated mechanically in the water caused an approximately linear increase in the rate of oxygen transfer.

Hosoi et al. [1977] presented a study on the effect of waves on reaeration; they conducted two sets of experiments. In the first set, the effect of mechanically produced waves, and in the second, the effect of

wind-waves on reaeration was investigated. Hosoi et al. concluded that a) the reaeration coefficient of wind waves is relatively high as compared to that of waves produced by a wave producing board, and it has a close relationship to the friction velocity u_* of wind above the wave surface and b) in the case of wind waves, increased input of oxygen as a result of the reentry of water particles into the water seemed to be a more influential factor than the rate of surface renewal directly below the boundary layer. However, the waves produced by the wave producing board and the wind waves in the above research were different, the former having significantly lower dominating frequency than the latter. Thus, the comparison between the two sets of experiments is not appropriate in the manner presented in (a) above. Moreover, wind waves were probably breaking ("reentry of particles") causing an increase in gas transfer.

To apply results obtained from wind tunnels to natural water bodies, proper scaling should be used. This is not simple since wave development is considerably different at the large fetches of natural water bodies and the wave effect on gas transfer has not been fully determined [Liss, 1983; Kerman, 1984; Jähne et al., 1985]. This may also explain the observed discrepancies in measured liquid film coefficient between field and laboratory data and between data from different types of wind wave flumes.

Further research is needed on the subject before the effects of waves can be incorporated in the predictive equations.

3. Bubbles

Although there is considerable theoretical and experimental information on the role of bubbles in gas transfer [Thorpe, 1982; Merlivat and Mémery, 1983], they have been largely ignored in wind tunnel experiments. Experiments by Broecker [1980] have shown an abrupt increase in the dependence of the gas transfer coefficient with wind velocity, after a critical value. The change can be attributed to the production of bubbles by breaking waves.

Breaking waves are associated with the formation of bubbles causing an additional increase in gas transfer. According to Long and Huang [1976] a wind shear velocity of approximately 30 cm/s is a critical value, independent of fetch, separating two different ranges of wave development. It can be interpreted as the transition between the moderately rough (no wave breaking) and fully rough (breaking waves) water surface regimes [Gulliver and Song, 1986]. Kerman [1984] suggested that the enhanced gas transfer at higher wind speeds results from bubble entrainment in small scale breaking waves and the enhancement is proportional to the extent of wave breaking. Monahan and Spillane [1984] using climatological and oceanographic data demonstrated a statistically significant correlation between the liquid film coefficient and whitecap coverage. The correlation was further extended to a relation between the liquid film coefficient and the third power of wind speed. Thus, the modeling of the effect of bubbles may be incorporated with that of the waves, but considerable research still needs to be done on this topic.

Although it seems clear that bubbles are important in gas transfer in the oceans for conditions under which a substantial bubble population exists, quantitative assessment of the effect is extremely difficult.

4. Pollution

As in the case of wind effects, pollution effects (detergents, etc.) are usually not included in the predictive equations.

Various pollutants alter the ability of gas molecules to enter and escape water. This alteration causes the value of the gas transfer coefficient to vary under identical hydraulic and environmental conditions, depending upon whether clean or polluted water is flowing in the stream. The pollutant effect on reaeration is not only related to the pollutant constituents and concentrations but also to the turbulent mixing regime within the fluid. In order to evaluate the effect of various pollutants on reaeration, a series of laboratory tests was conducted on both natural and artificial stream waters by Tsivoglou and Wallace [1972] and some values for the coefficient:

$$\alpha = \frac{K_2 \text{ polluted}}{K_2 \text{ unpolluted}}$$

were obtained.

The conducted experiments indicated the following:

a) LAS (linear alkylate sulfonate) and similar pollution appear to bring about the greatest reduction of reaeration capacity at water features such as rapids and shoals in streams, where reaeration would otherwise be expected to be at a most beneficial maximum.

b) Mineral oil enhances gas transfer capacity of water. Effect decreases as mixing increases (not many practical applications).

c) NTA (nitrilo triacetic acid) showed no significant effect.

The effects of pollutant films at the sea surface on gas transfer can be divided into two types: 1) Direct or static, where the film directly affects exchange by presenting a significant additional resistance to transfer as compared to the 'clean' surface and 2) Indirect or dynamic, where the film material, although possessing little or no intrinsic resistance, alters some property of the surface water, which is important in the gas transfer process.

The effect of oil films falls in the first category and was studied by Liss and Martinelli [1978]. For O_2, a thickness of 10 μm was required before a decrease in the exchange coefficient could be detected. Martinelli [1979] presented a 3 film model that provides a reasonable description of the observations. It is interesting to note that the effects of films for substances with gas-phase control is much more pronounced, since resistance of the liquid phase becomes important, where there was practically none previously.

In the second category, the major indirect effect of films reported is their ability to damp capillary waves [Garret, 1963, 1967].

There is also some evidence from laboratory tank experiments that soluble surfactants, although possessing no intrinsic transfer resistance,

can lead to significant reduction in the transfer velocity of O_2 under conditions of high stirring in aqueous phase [Mancy, 1965; Martinelli, 1979].

Due to the large number of existing pollutants and their different effect on the transfer of each gas, no further attempt will be made here either for modeling or for reporting of such effects.

H. Measurement Techniques

The developed techniques for the determination of the reaeration coefficient will be presented here briefly.

1. Dissolved oxygen balance technique

This technique was first used by Streeter and Phelps [1925] to measure K_2 in the Ohio River.

For the selected reach to be studied, all sources and sinks of dissolved oxygen except reaeration are measured or evaluated and then reaeration is determined by the difference needed to give the D.O. concentration observed at the downstream end of the reach.

Serious errors may result with this technique from the omission of one or more significant sources.

2. Disturbed equilibrium technique

The disturbed equilibrium technique was developed by the Water Pollution Research Laboratory [Gameson and Truesdale, 1959].

The technique consists of measuring the D.O. concentrations at the upstream and downstream ends of the reach at two different levels of D.O. concentration. These two levels are usually obtained by injecting sodium sulfite and a cobalt catalyst into the stream. If photosynthesis, respiration, reaeration coefficient, mean velocity, and saturation concentration remain constant during the measurements, then the reaeration coefficient can be computed. The use of this technique is generally limited to small streams because it is necessary to artificially produce a D.O. deficit. If photosynthesis is appreciable, experiments have to be done at night. We must also note that the assumption that respiration is independent of the D.O. concentration level, has been questioned. Gulliver and Stefan [1984] found respiratory inhibition at D.O. concentrations below 4 ppm.

3. Tracer technique

The tracer technique [Tsivoglou, 1965, 1967] is unique in that it does not require the measurement of any of the sources and sinks of D.O. in the stream.

The basis of the technique is the observation that the ratio of the rate coefficient for the desorption of a tracer gas from water to the rate coefficient for the absorption of oxygen by the same water is independent of temperature and flow conditions. It was found that in stirred containers, using Krypton-85 as tracer gas,

$$K_2 = \frac{K_{2G}}{0.83}$$

where K_{2G} = tracer-gas transfer coefficient. The mechanics of gas transfer in a stirred container though may not be the same as in a natural stream.

The technique uses an instantaneous injection of three tracers at a point upstream from the reach over which the reaeration coefficient is to be measured. The tracers are (1) a fluorescent dye, the purpose of which is to enable field personnel to follow the movement of the tracers; (2) tritiated water, which is used as a conservative dispersion tracer; and (3) the radioactive tracer gas Kr-85, which is used to measure the gas transfer capacity of the flow. Samples of stream water are removed from the flow as the dye peak passes the upstream end and then again as it passes the downstream end of the reach. The transfer capacity of the flow for the tracer gas is obtained from the relative concentrations of the gas and tritiated water tracers at the two ends of the reach.

The tracer technique is far superior to the other two. However, it requires the use of radioactive tracers and there are strict controls on such use in the natural environment. For this reason, the U. S. Geological Survey [Rathbun, 1979] developed a modification that does not require radioactive tracers. This modification uses low-molecular weight hydrocarbons (usually ethylene or ethylene and propane) as the tracer gas and Rhodamine-WT fluorescent dye as the dilution-dispersion tracer. Concentrations of the gas tracer are determined using a gas chromatographic technique. Results are encouraging. Recently [Wilcock, 1984] methyl chloride was also used as a tracer with good results.

4. Steady-state propane gas tracer method

Despite increasing popularity and usage of the gas tracer method, as presented in the previous section, some questions still remain concerning the accuracy and reproducibility of field data and the soundness of field procedure. A modification of the tracer method is suggested by Yotsukura et al. [1983]. In this case, the gas tracer is injected continuously at a uniform rate for a long period to produce a steady-state gas-tracer concentration in a plume that would be mixed uniformly in a cross-section. This is in contrast to the methods of Tsivoglou and Rathbun, which employ short duration injections and measure transient concentrations. Since the gas concentration with the new method is obtained under steady-state uniformly-mixed conditions, no correction is required for dispersion coefficient, and sampling errors can be easily detected.

The gas tracer measurements are restricted to small streams because a large river would not mix properly in a short distance and would require a great deal of tracer. An alternative, utilizing winter conditions, is proposed by Gulliver et al. [1980].

5. Winter measurements

Reaches of streams are chosen so that there is a long reach with ice cover upstream and a reach of open water downstream (usually due to cooling water from a thermal power plant). Saturation concentration during winter is high and D.O. concentration under ice cover is low. Consequently, a considerable D.O. deficit exists at the upstream end of the open-water reach and then D.O. measurements along the reach can yield a value of the reaeration coefficient, after taking into account the effect of respiration.

6. Analysis of errors

The following may be sources of errors in the above techniques [Bennett and Rathbun, 1972; Holley and Yotsukura, 1984]:

1) Differences between the dynamic stream condition and the quiescent conditions in the various bottle techniques developed for measuring the D.O. balance parameters.

2) The difficulty and expense of obtaining a sufficient number of representative samples to describe accurately the stream conditions and the cross-section of interest.

3) Deviations from the assumptions inherent in the derivation of the D.O. balance equation.

4) The accuracy of the D.O. measurement procedure used in the various techniques for determining the D.O. balance parameters.

5) Possible corrosion of metals in laboratory flumes is also a D.O. sink not considered [Liu et al., 1972].

6) Uncertainties of parameters used in analyzing the data. Such parameters are C_s and the ratio of transfer rate coefficients for a tracer gas and oxygen (R). C_s changes with water quality and tabulated values are usually not directly applicable for rivers.

7) Finally, random errors exist in all measurements. If these errors can be quantified, it is possible to analyze the propagation of errors through the calculations and obtain error bounds on results. In cases where many variables are involved, an alternative is sensitivity analysis or Monte Carlo simulation [Holley and Yotsukura, 1984].

III. EXPERIMENTAL PROCEDURE

A. General Description

From January 1984 through July 1984, a series of 35 experiments were carried out in order to determine the effect of waves on the process of gas transfer. The experiments were conducted in a wave tank with a mechanical wave maker. There was no net flow through the flume. The water was chemically deoxygenated and then oxygen concentration was measured over time as it increased towards a saturation value. Oxygen concentrations were determined by the Azide modification of Winkler titration method. Waves were recorded at various locations along the flume both at the beginning and the end of the experiments.

The first eight experiments (RUN1-RUN8) were preliminary. An oxygen probe was used in these experiments in addition to the Winkler samples. Use of the probe proved inconvenient because frequent calibration and temperature adjustment were needed, since the water temperature was changing in the course of the experiment. The data for RUN 1 through RUN 8 are not presented because oxygen sampling locations and frequency were insufficient for a meaningful analysis. Sampling locations were rearranged for the subsequent experiments so that information for virtually the whole length of the flume could be obtained. One capacitance and one resistance-type probe were initially used for wave recording. The resistance probe seemed to be more reliable and consequently two resistance probes were used for the rest of the experiments.

RUN 9 through RUN 35 were experiments where both waves and oxygen concentration were recorded systematically. Figure 8 shows a typical diagram of oxygen concentration versus time. The five different curves represent the five sampling locations along the flume. The difference in concentrations along the channel was initially attributed to uneven distribution of chemicals. However, this was not the case. The observed difference was mainly due to change of wave height along the channel and in some cases air entrainment near the paddle, when breaking waves were present.

In order to calculate the flux through the air-water interface for each segment of the flume, the horizontal flux in the flume needed to be determined. This was done by performing conductivity measurements. A small amount of salt was added in the area behind the paddle and conductivity measurements were taken over time along the flume. Conductivity is proportional to salt concentration (at low concentrations). A typical graph of conductivity versus time is shown in Figure 9. From these data the horizontal diffusion coefficients were determined. This was done for the last ten experiments (RUN 26 through RUN 35).

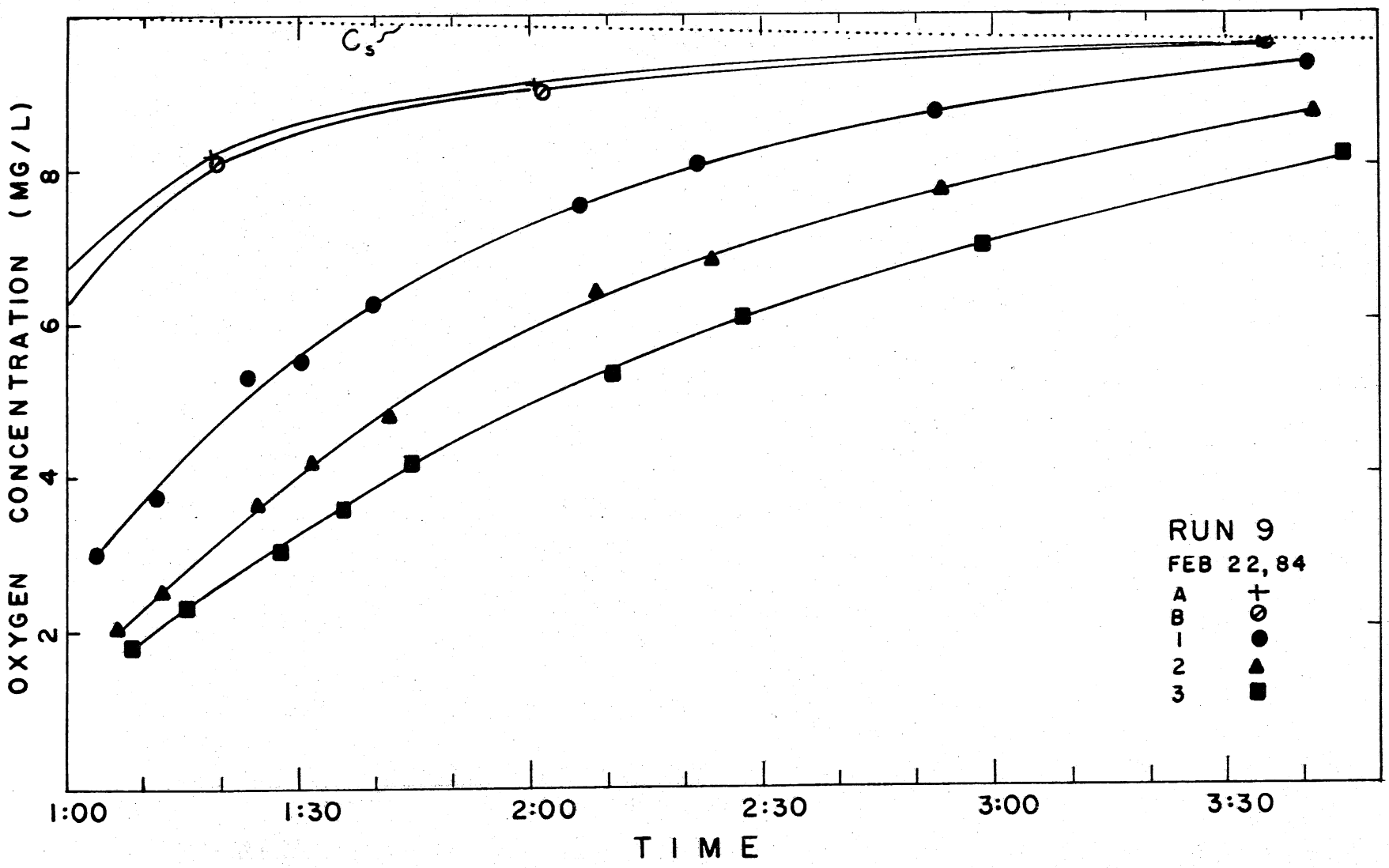

Fig. 8. Typical oxygen concentration versus time curves.

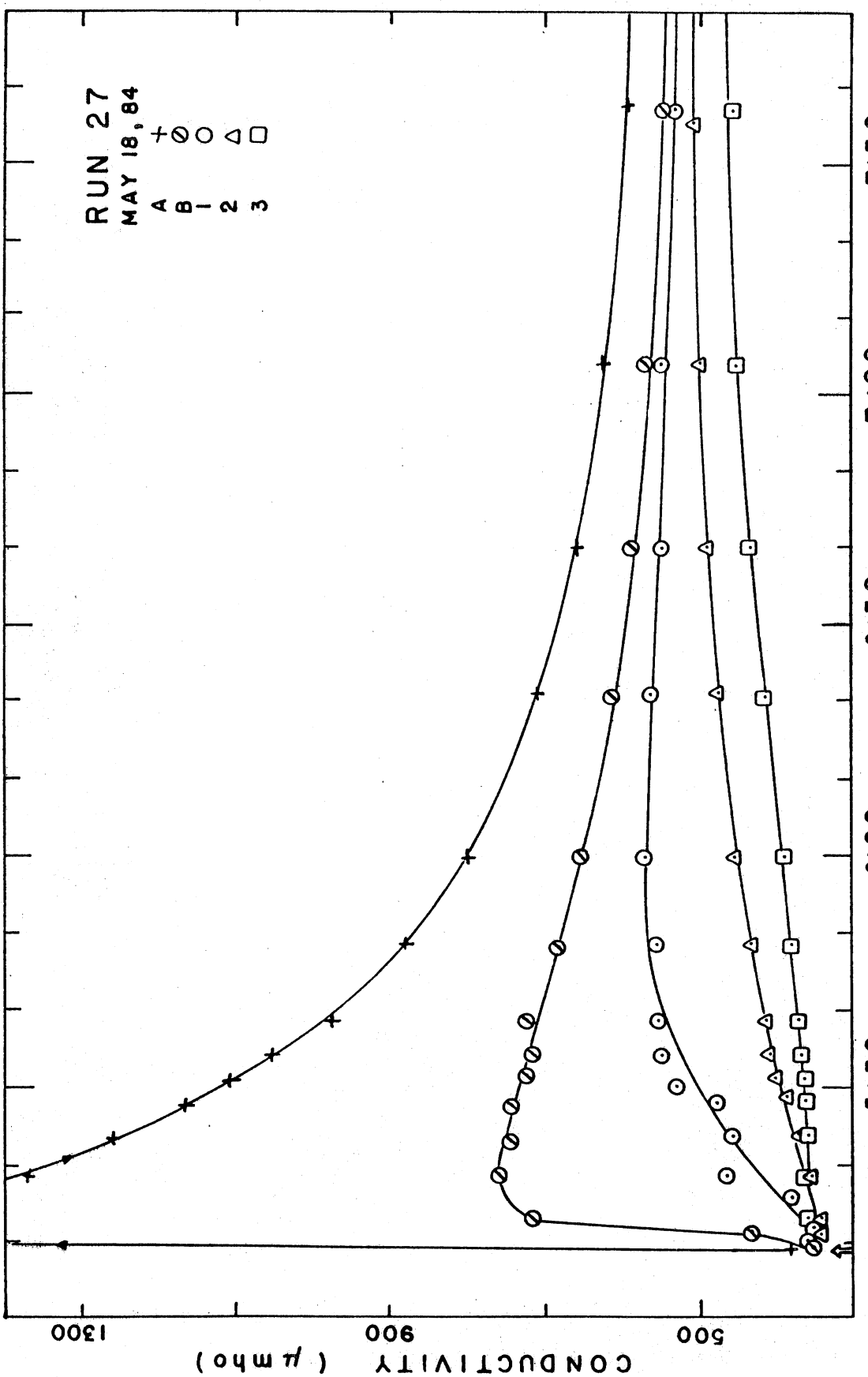

Fig. 9. Typical conductivity versus time curves.

B. Wave Flume Characteristics

Figure 10 shows a schematic diagram of the wave flume used for the experiments. The flume had metal bottom and glass sidewalls. The dimensions of the flume were 12.14x0.15x0.37 (LxWxH) in meters. The mechanical wave maker was located 1.72 m from one end of the flume, referred to as the upstream end. The frequency, amplitude and angle of rotation of the paddle movement could be controlled by the attached mechanism. Frequency and amplitude could be changed in a continuous manner. Angle of rotation could be altered by changing the location of the paddle's supporting beams. Five holes (positions) were provided for each supporting beam. In the experiments, only symmetrical positions were used. The water depth in the experiments was usually 15-25 cm. At the downstream end of the channel there was a small reservoir of approximately 0.30 m length. This was isolated from the rest of the channel and was not used in the experiments. At both ends of the flume, an inclined surface with wire mesh on top was provided to absorb waves and keep reflection to a minimum. Both beaches were pervious, and the volume under each beach was included in the water mass of the channel.

Five locations for oxygen sampling were selected along the channel. The origin of the axis (x=0) was located 2.02 m away from the upstream end of the channel. The locations selected for sampling were at x = -1.13, 0.20, 2.25, 5.35, and 8.45 m named, respectively, points A, B, 1, 2, and 3. The same locations were used for taking conductivity measurements. For the oxygen sampling, plastic tubes (3/8" outer diameter and 1/4" inner diameter) were installed at the above mentioned locations. The tubes were taped on the wall of the channel and their opening was located 7.5 cm above the bottom of the channel.

C. Wave Recording

Wave height and wave period were recorded using a two-channel Sanborn wave recorder along with two resistance probes (diameter ~ 0.5 mm). Calibration was done at the beginning and at the end of each experiment. The measurements were taken at x = 0.50, at points 1, 2, 3 and midway between points 1-2 and 2-3. Wave length was initially measured using two light probes. The light probes were moved until simultaneous flashing was achieved; then, the distance between the probes, as well as the number of wave forms between the two probes, was determined. However, this method proved difficult and required a great deal of time for adjusting. So, grids were attached to the glass wall at locations x = 0.0, 2.0, 6.0 and 8.0 m and pictures were taken with a Crown Graphic camera, from which the wave length was determined.

D. Dissolved Oxygen

1. Chemical deoxygenation

Initially, the tank was filled with water to the desired level for the experiment. Then the water was chemically deoxygenated. The reagents used for the deoxygenation were sodium sulfite (Na_2SO_3)-technical grade and

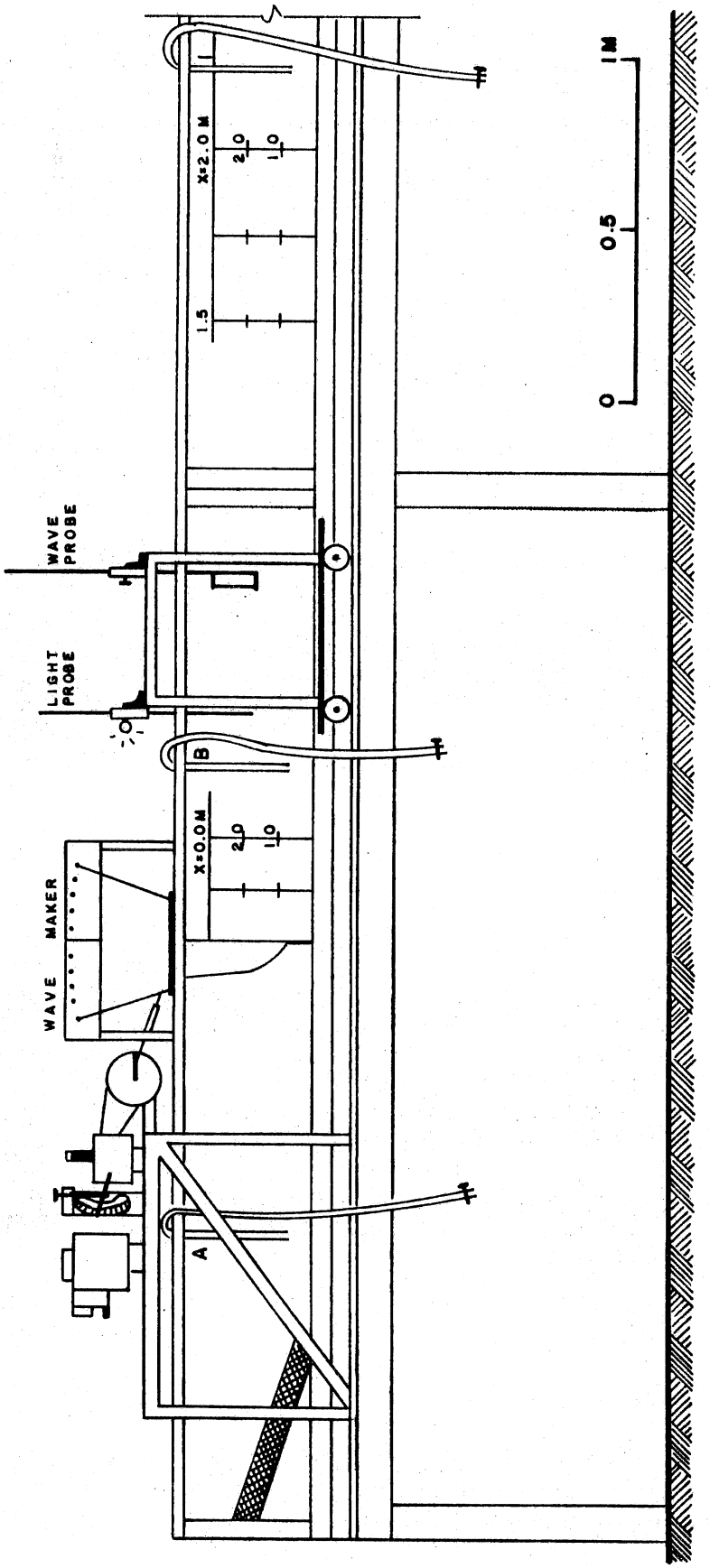

Fig. 10a. Experimental flume. "Upstream" end.

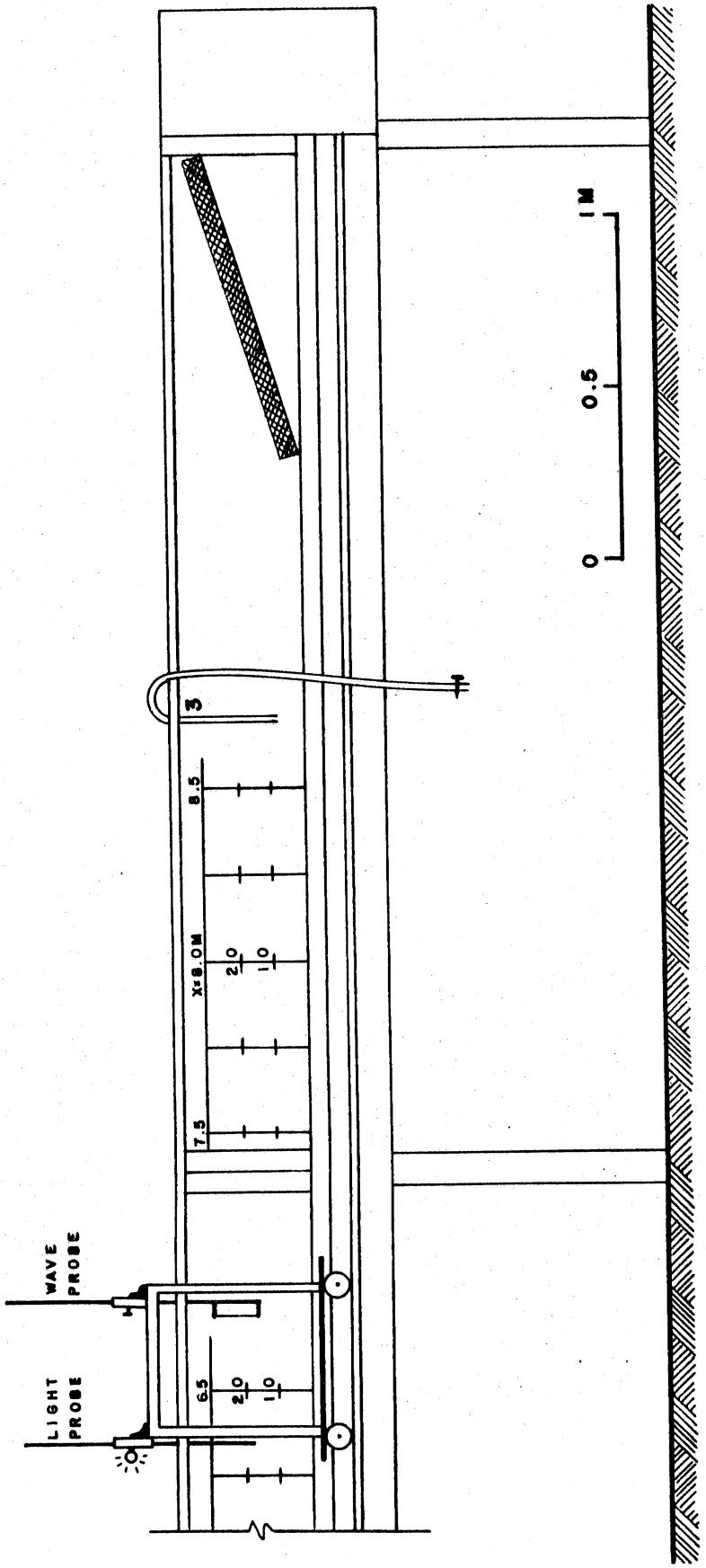

Fig. 10b. Experimental flume. "Downstream" end.

cobaltous chloride $CoCl_2 \cdot 6H_2O$ as a catalyst. The $CoCl_2$ was dissolved in warm water and added to the tank as uniformly as possible. Na_2SO_3 was also dissolved in water and added in the same manner.

Suggested quantities by Standard Methods (Sec. 208A) are 8.05 gr/m^3 $CoCl_2$ and 117 gr/m^3 Na_2SO_3 for an initial D.O. concentration of 10 mg/ℓ. The actual quantity of $CoCl_2$ to be used was calculated from the above recommendation for the desired water level of each experiment. For Na_2SO_3, the saturation concentration was first estimated using the water temperature and the existing atmospheric pressure and the above given number was adjusted accordingly. This was done in most experiments since the tap water was very close to saturation, especially during winter. However, around spring, the oxygen concentration of the water was lower. Therefore, the new practice adopted was to determine D.O. concentrations in the tank directly and thereby compute the required Na_2SO_3. In all cases, an additional 10% was added to ensure complete deoxygenation.

The saturation concentration (C_s) as a function of temperature and chloride concentration in water is given in tabular form in Standard Methods. Zero chlorinity was used and linear interpolation between the given values was employed whenever needed. C_s was then corrected for pressure.

$$C_s = C'_s \frac{p}{760}$$

where:

p = atmospheric pressure in mm Hg,

C'_s = saturation concentration obtained from table (mg/ℓ), and

C_s = actual saturation concentration.

Values of C_s from Standard Methods (for every °C) and interpolated values (for every 0.1°C) used for the experiments and data evaluation are given in Table 1.

The mean water temperature, pressure correction term, p/760, saturation concentration, C'_s, and Schmidt number for the performed experiments are given in Table 2.

2. Determination of D.O. concentration

Water samples were taken over time at the various locations along the flume to determine the D.O. concentration. The Winkler titration azide modification method was used (Standard Methods, Sec. 421.B). This method is especially effective if samples contain more than 50 µg NO_2^- N/ℓ and not more than 1 mg ferrous iron/ℓ. Other reducing or oxidizing materials should be absent. If 1 mℓ KF-solution is added before the sample is acidified and there is no delay in titration, the method is applicable in the presence of 100-200 mg ferric iron/ℓ. However, there was no need to perform this test in the experiments.

TABLE 1. VALUES OF SATURATION CONCENTRATION (C'_s)

AS A FUNCTION OF TEMPERATURE (T in °C)

T	.0	.1	.2	.3	.4	.5	.6	.7	.8	.9
6	12.43	12.40	12.37	12.34	12.31	12.28	12.24	12.21	12.18	12.15
7	12.12	12.09	12.06	12.03	12.00	11.98	11.95	11.92	11.89	11.86
8	11.83	11.80	11.77	11.75	11.72	11.69	11.66	11.63	11.61	11.58
9	11.55	11.52	11.49	11.47	11.44	11.41	11.38	11.35	11.33	11.30
10	11.27	11.24	11.22	11.19	11.17	11.14	11.11	11.09	11.06	11.04
11	11.01	10.99	10.96	10.94	10.91	10.89	10.86	10.84	10.81	10.79
12	10.76	10.74	10.71	10.69	10.66	10.64	10.62	10.59	10.57	10.54
13	10.52	10.50	10.47	10.45	10.43	10.41	10.38	10.36	10.34	10.31
14	10.29	10.27	10.25	10.22	10.20	10.18	10.16	10.14	10.11	10.09
15	10.07	10.05	10.03	10.00	9.98	9.96	9.94	9.92	9.89	9.87
16	9.85	9.83	9.81	9.79	9.77	9.75	9.73	9.71	9.69	9.67
17	9.65	9.63	9.61	9.59	9.57	9.55	9.53	9.51	9.49	9.47
18	9.45	9.43	9.41	9.39	9.37	9.36	9.34	9.32	9.30	9.28
19	9.26	9.24	9.22	9.20	9.18	9.17	9.15	9.13	9.11	9.09
20	9.07	9.05	9.04	9.02	9.00	8.99	8.97	8.95	8.93	8.92
21	8.90	8.88	8.86	8.85	8.83	8.81	8.79	8.77	8.76	8.74
22	8.72	8.70	8.69	8.67	8.66	8.64	8.62	8.61	8.59	8.58
23	8.56	8.54	8.53	8.51	8.50	8.48	8.46	8.45	8.43	8.42
24	8.40	8.38	8.37	8.35	8.34	8.32	8.30	8.29	8.27	8.26
25	8.24	8.23	8.21	8.20	8.18	8.17	8.15	8.14	8.12	8.11

TABLE 2. TEMPERATURE, SATURATION CONCENTRATION AND SCHMIDT NUMBER VALUES

Run	Mean Temp. (°C)	$\frac{P}{760}$	C_s (mg/ℓ)	Sc
9	14.3	0.961	9.82	735
10	16.4	0.970	9.48	654
11	16.1	0.977	9.60	665
12	16.8	0.981	9.51	640
13	17.1	0.974	9.38	630
14	16.7	0.979	9.51	643
15	15.9	0.963	9.50	672
16	16.4	0.968	9.46	654
17	15.5	0.970	9.66	687
18	15.3	0.981	9.81	695
19	16.9	0.979	9.47	636
20	16.1	0.973	9.56	665
21	16.8	0.973	9.43	640
22	17.8	0.977	9.27	606
23	16.5	0.959	9.35	651
24	17.5	0.974	9.30	616
25	17.6	0.973	9.27	613
26	15.0	0.984	9.91	707
27	19.9	0.970	8.82	542
28	20.6	0.977	8.76	523
29	18.0	0.980	9.26	600
30	21.9	0.977	8.54	489
31	22.0	0.974	8.49	487
32	21.9	0.977	8.54	489
33	22.9	0.974	8.36	465
34	22.6	0.968	8.34	472
35	22.8	0.971	8.34	468

The samples were collected in 300 mℓ bottles. Immediately after sampling, 1 mℓ $MnSO_4$ solution and 1 mℓ alkali-iodide-azide agent were added. The stopper was carefully replaced to exclude bubbles and then the bottle was inverted approximately five times to assure mixing. After sufficient precipitate had settled, to leave a clear supernate above the manganese hydroxide flocculant, 1.0-2.0 mℓ H_2SO_4 were added. The bottle was restoppered and mixed until dissolution was complete. Then, the sample was ready for titration.

After correction for sample loss by displacement with reagents, a volume corresponding to 200 mℓ original sample, in this case 300/(300-2) = 201 mℓ, was titrated. This assumes that only sample and no reagent is lost. Titration followed with 0.025 N $Na_2S_2O_3$ solution to a pale straw color. Near the end some starch solution was added and titration continued to first disappearance of blue color. If the point were overrun, a measured amount of sample was added and the same procedure followed. The final results were corrected for the added amount. For titration of a 200 mℓ sample

$$1 \text{ mℓ } 0.025N \ Na_2S_2O_3 = 1 \text{ mg D.O./ℓ}$$

The reactions taking place are:

$$MnSO_4 + 2NaOH \rightarrow Mn(OH)_2 + Na_2SO_4$$

$$2\ Mn(OH)_2 + O_2 \rightarrow 2\ MnO(OH)_2 \downarrow$$

$$MnO(OH)_2 + 2NaI + H_2O \xrightarrow{H^+} Mn(OH)_2 + I_2 + 2NaOH$$

$$I_2 + 2S_2O_3^{-2} \rightarrow S_4O_6^{-2} + 2I^{-1}$$

All reagents used were those recommended by APHA Standard Methods [1980] and were purchased ready-made. All reagents were purchased from Mallickrodt Inc., with the exception of the Starch Indicator, which was from Fischer Scientific Co.

E. Conductivity Measurements

Conductivity measurements were performed in the last 10 experiments in order to determine the horizontal diffusion coefficient. A small amount of salt (NaCℓ), usually around 45 gr, was added in the area behind the paddle and conductivity measurements were taken along the channel over time at the same locations where oxygen samples were taken.

A Cole-Parmer 1481-50 Digital conductivity meter used for the measurements is illustrated in Fig. 11. The sensor is contained in a remote PVC probe with two stainless steel electrodes located just below the PVC cap. A probe sleeve protects the electrodes and is perforated to direct the flow of liquid during measurements. It is not possible to take

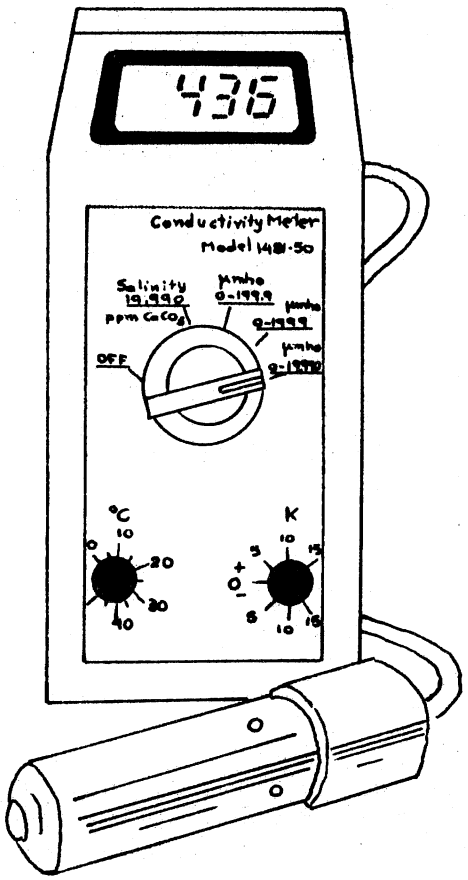

Fig. 11. Conductivity meter.

readings without the protective sleeve. The electrode is kept dry in the air and will not give a reading in a dry state. It has three ranges: 0-199.9, 0-1999.0, 0-19,990 μmho. It also has a temperature compensation and an adjustable cell constant.

The temperature compensation switch was set at 25°C because it had an insufficient resolution. Temperature correction was made using the relation

$$k_{25} = k_T/(1 + 0.0191(T-25))$$

where:

$k_{25,T}$ = conductivity at 25°C, T(°C), respectively, and

T = temperature of measurement (°C).

The above relation indicates that electrolytic conductivity increases with temperature at a rate of 1.9% per °C. This is representative of both natural waters and NaCℓ solutions. It is important to note that significant errors can result from inaccurate temperature measurements.

The meter was calibrated against the standard solution that came with it. It was also checked for linearity of conductivity versus salt concentration with KCl solutions at 25°C in the range from $1x10^{-4}$ N to $5x10^{-2}$ N. The calibration was not checked frequently because it was found to be relatively stable and the absolute value of conductivity was not of interest.

IV. DATA ANALYSIS

A. Wave Characteristics

1. Wave length (L)

Wavelength was calculated from the pictures taken during the experiment. Depending on the location, where the picture was taken, and on the wavelength of the experiment, usually 1/2 - 3½ wavelengths were included in the picture, and consequently one to four measurements of wavelength could be obtained from each picture. There were some pictures near the paddle that did not give any measurements, since the focus was on the development of the crest and air entrainment, and it was not clear what portion of a wavelength was pictured.

An average wavelength was computed for each picture and then the average of these numbers was taken to be the wavelength for the experiment. If available and reliable, the measurement of L with the light probes was also included in the averaging.

Wavelength was assumed to be constant throughout the whole flume, since no trend appeared in the measured wavelengths for the four locations along the channel.

In Table A1 (Appendix I), a summary of the wavelength computations is given. The parameters in Table A1 are:

RUN = code number of experiment,

L = wavelength of the experiment (cm),

σ_L = standard deviation when computing the final average (cm),

n = number of values used for averaging,

$$P1 = \frac{MAX1 - MIN1}{L} * 100$$

MAX1 = maximum value of averages of pictures,

MIN1 = minimum value of averages of pictures,

$$P2 = \frac{MAX2 - MIN2}{L} * 100 ,$$

MAX2 = maximum of all values computed, and

MIN2 = minimum of all values computed.

The range of wave lengths in the experiments was L = 23.7 → 62.8 cm.

2. Wave period (T)

The wave period was determined from the wave recorder charts. For a certain time period the number of waves going through were counted and T was determined. Wave period was constant for all locations and throughout the experiment, so a single value is given for each experiment in Table A1, Appendix I.

The wave period ranged from 0.380 - 0.627 sec, with a corresponding frequency (f = 1/T) in the range 1.59 - 2.63 Hz. Following a classification of ocean surface waves by frequency, as presented in Kinsman [1984], these waves fall in the ultragravity wave range.

3. Wave height (H)

Wave heights were recorded at six locations along the flume (eight for RUN 9), as described in Section III.C. At locations x = 3.80 m and x = 6.90 m, waves were recorded at various times during the experiment. At the rest of the locations waves were usually recorded at the beginning and at the end of the experiments and occasionally during the experiments. The wave height for every location was calculated separately, since it was diminishing with distance from the paddle. Calibration of the wave recorder was done both before and after each experiment. The calibration sometimes changed as much as 20 percent during the course of the experiment (3-5 h). Therefore, data sets as close to calibration time as possible were preferred in order to minimize errors. For data halfway through the experiment, linear interpolation with respect to time was employed between initial and final calibration factors.

For experiments 27 through 31 conductivity measurements were taken at the same time as oxygen measurements. Changes in conductivity affect the calibration of the wave recorder quite strongly. In this case the criterion for selection of data sets near calibration was followed even more strictly, with the additional requirement that locations recorded with the same wave probe did not have significantly different conductivity. The exact effect of conductivity changes on calibration could not be determined, since the calibration was changing even without changes in conductivity.

For every location and time, 30-60 wave heights were measured off the wave recorder chart and the arithmetic mean, the standard deviation, and the RMS (root mean square) values were computed. The wave heights were measured from trough to crest. The RMS value was taken as the representative value. These values are given in Table A2, Appendix I, for all experiments and locations. Further, these values were plotted versus distance along the channel and a wave height "profile" curve was fitted by eye, as given in Figs. A1 through A9 in Appendix I. The fitted values from these graphs were used in the computations and are given in Table A3, Appendix I. These numbers were rounded to the nearest 0.5 mm wave height, ranging from 0.70 cm to 5.35 cm.

4. Computations

Wave steepness defined as the ratio of wave height to wave length, is given in Table A4, Appendix I. The range is 0.027 - 0.1028, a small number compared to unity, allowing the waves to be classified as small amplitude waves.

Wave slope, s, is defined as the mean surface slope and is taken to be equal to $(\pi/\sqrt{2}\ H/L)$, which is exact for a sinusoidal wave.

The phase velocity or celerity, $c = L \cdot f$, was computed from the measured wave length and frequency (Table A1, Appendix I).

The group velocity, Cg, was computed from the wave recorder chart at the onset or the end of waves by measuring the distance between the two wave probes and dividing by the time required for a specific wave in the wave train to go through, as illustrated in Fig. 12.

The ratio of mean depth over wave length (h/L) was between 0.333 and 1.038 and was lower than 0.5 for only six experiments (Table A1). Therefore, in most experiments the waves could be considered deep water waves. For small amplitude waves

$$c^2 = \frac{gL}{2\pi} \tanh \frac{2\pi h}{L} \tag{44}$$

and

$$c_g = \frac{1}{2} c \left(1 + \frac{4\pi\ h/L}{\sinh \frac{4\pi h}{L}}\right) \tag{45}$$

where g is the acceleration of gravity and h is the mean water depth.

The deviation from the linear dispersion relation for deep gravity waves, $c^2 = gL/2\pi$, (expressed as $1 - \sqrt{g/(2\pi Lf^2)}$), was 2 percent on the average and was within ± 6.5 percent in all cases (Table A5, App. I). The highest errors (Run 18, Run 33) occurred along with the maximum standard deviation in the computation of the wavelength, indicating an uncertainty in estimating L, rather than a significant deviation from the deep water approximation. This also implies that the independent wave characteristics are reduced from H, L, and f to H and f (or H and L).

In the same table the values of c_g, as computed from the charts and as computed from Eq. (45), are given. The percentage error was less than 8 percent in absolute value, indicating again fairly good agreement with the sinusoidal wave formulas. The sinusoidal waves are also often referred to as first order Stokes waves.

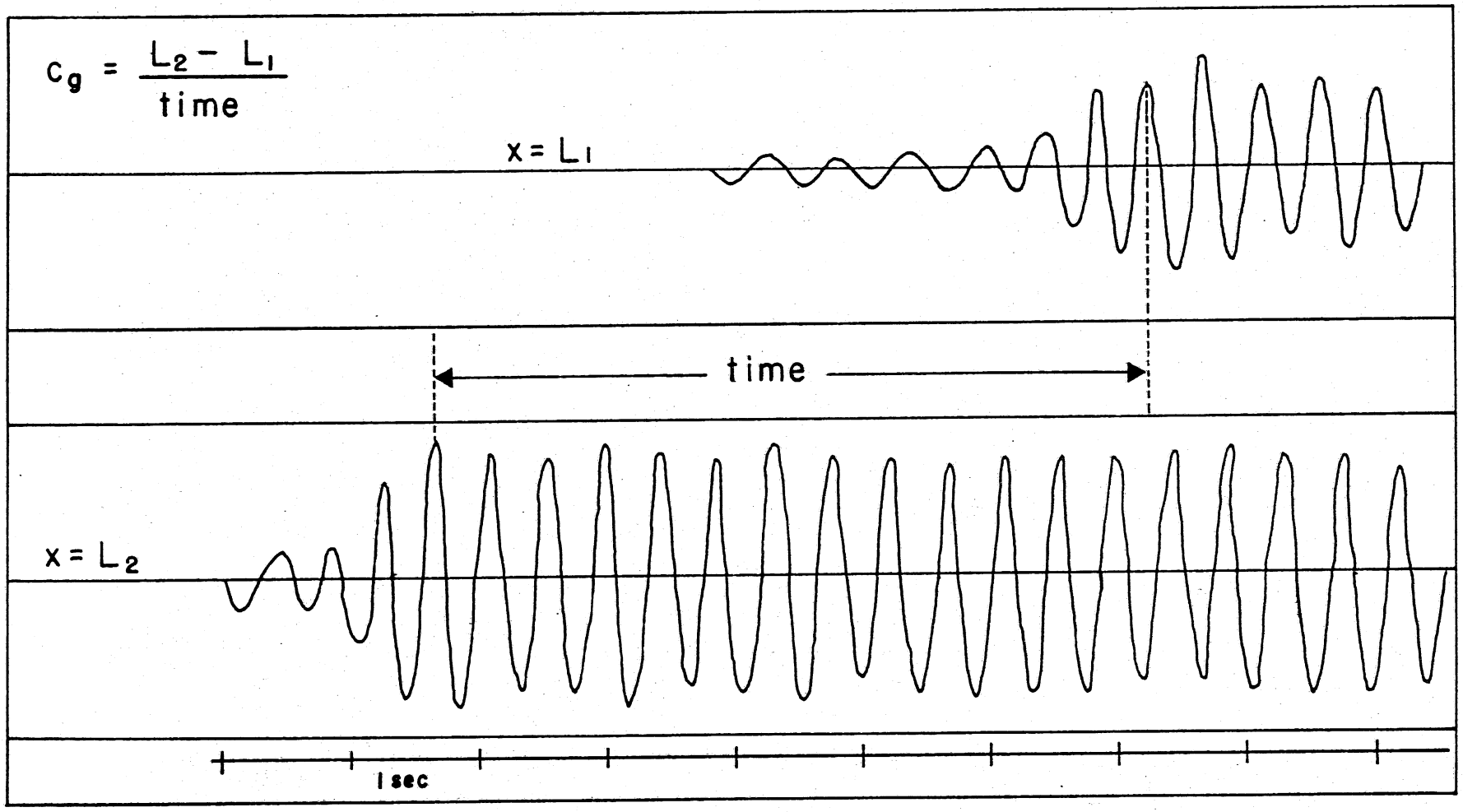

Fig. 12. Group velocity measurement.

B. Numerical Scheme for the Transport Equation

The one-dimensional transport equation can be written in the general form:

$$\frac{\partial \phi}{\partial t} + U \frac{\partial \phi}{\partial x} = \frac{\partial}{\partial x}\left(D_x \frac{\partial \phi}{\partial x}\right) + S \qquad (46)$$

where:

ϕ = concentration [M/L^3],

U = mean stream velocity [L/T],

D_x = longitudinal dispersion coefficient in the x-direction [L^2/T], and

S = source and sink terms per unit volume [$M\ L^{-3}T^{-1}$].

$S > 0$ for sources and $S < 0$ for sinks.

In the wave tank, since there is no net flow, $U = 0$ and Eq. (46) reduces to

$$\frac{\partial \phi}{\partial t} = \frac{\partial}{\partial x}\left(D_x \frac{\partial \phi}{\partial x}\right) + S$$

For oxygen gas the concentration will be denoted with C and the only source in the case of the performed experiments is oxygen transfer through the water surface.

$$S = \frac{K_L A}{V}(C_s - C) = \frac{K_L}{h}(C_s - C) \qquad (47)$$

where:

A = surface area [L^2],

V = volume [L^3],

K_L = oxygen transfer coefficient [L/T], and

h = mean water depth [L].

Samples fixed and titrated some hours after sampling showed no difference from those fixed immediately after sampling. Therefore, deoxygenation was assumed negligible and was not included in the equations. Thus, the oxygen transport equation is

$$\frac{\partial C}{\partial t} = \frac{\partial}{\partial x}\left(D_x \frac{\partial C}{\partial x}\right) + \frac{K_L}{h}(C_s - C) \qquad (48)$$

For NaCℓ the source term is zero. Since conductivity is directly proportional to NaCℓ concentration, and only differences are involved in

the equation, conductivity measurements (after temperature corrections) will be used directly to obtain the horizontal diffusivity coefficient. The transport equation becomes:

$$\frac{\partial k}{\partial t} = \frac{\partial}{\partial x}\left(D_x \frac{\partial k}{\partial x}\right) \tag{49}$$

where k = conductivity (μmhos).

Once the longitudinal dispersion coefficients have been determined, the oxygen transfer coefficients will be found using the oxygen data.

Equations (48) and (49) must be discretized for the evaluation of the coefficients from the obtained data. A control volume approach will be followed for the discretization. Equations (48) and (49) can be written as

$$\frac{\partial \phi}{\partial t} = \frac{\partial}{\partial x}\left(D_x \frac{\partial \phi}{\partial x}\right) + S \tag{50}$$

Integrating Eq. (50) over the control volume given in Fig. 13 and assuming that $\partial\phi/\partial t$ and S can be represented by their values at point i, we get:

$$\int_a^b \frac{\partial \phi}{\partial t}\, dx = \int_a^b \frac{\partial}{\partial x}\left(D_x \frac{\partial \phi}{\partial x}\right) dx + \int_a^b S\, dx \tag{51}$$

or

$$\frac{\partial \phi}{\partial t} L_i = \left[D_x \frac{\partial \phi}{\partial x}\right]_b - \left[D_x \frac{\partial \phi}{\partial x}\right]_a + S_i L_i \tag{52}$$

Using a linear profile assumption between grid points, $\partial\phi/\partial x$ can be written

$$\left.\frac{\partial \phi}{\partial x}\right|_a = \frac{\phi_i - \phi_{i-1}}{L_{i-1,i}} \qquad \left.\frac{\partial \phi}{\partial x}\right|_b = \frac{\phi_{i+1} - \phi_i}{L_{i,i+1}}$$

With these expressions, Eq. (52) becomes:

$$L_i \frac{\partial \phi}{\partial t} = \frac{D_{i,i+1}}{L_{i,i+1}}(\phi_{i+1} - \phi_i) - \frac{D_{i-1,i}}{L_{i-1,i}}(\phi_i - \phi_{i-1}) + L_i S_i \tag{53}$$

or

$$L_i \frac{\partial \phi}{\partial t} = K_{i,i+1}(\phi_{i+1} - \phi_i) - K_{i-1,i}(\phi_i - \phi_{i-1}) + L_i S_i \tag{54}$$

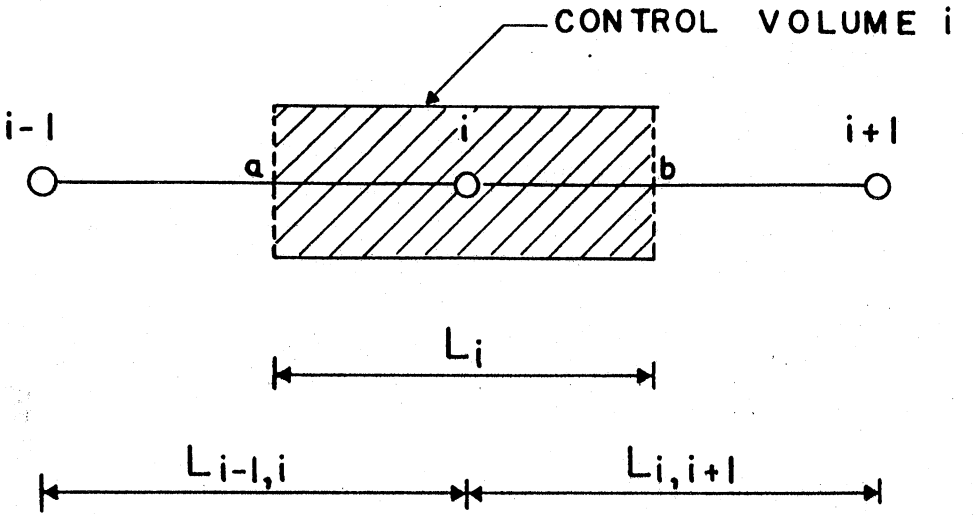

Fig. 13. Typical grid point cluster.

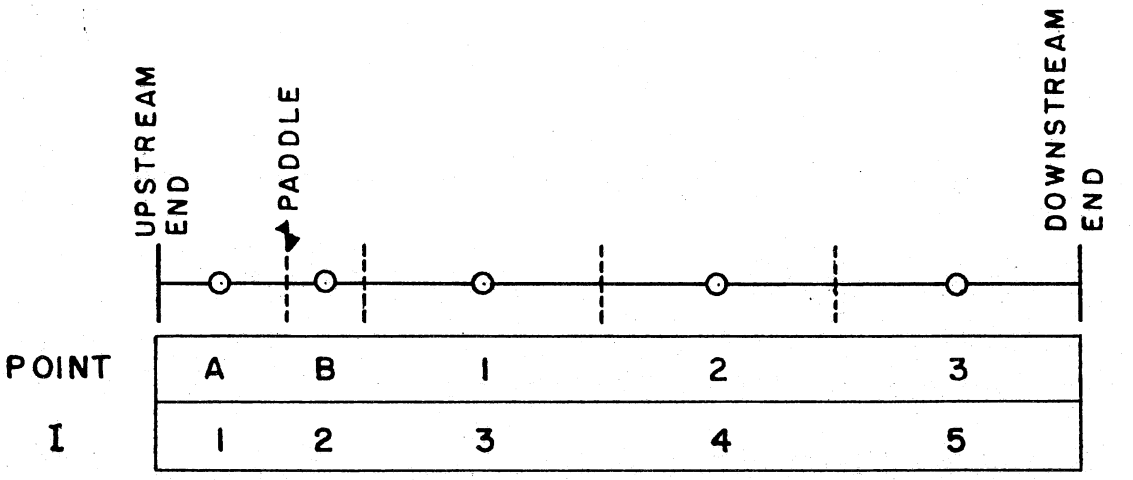

Fig. 14. Discretization grid for the wave flume.

where $K_{ij} = D_{ij}/L_{ij}$. $\partial\phi/\partial t$ can be approximated as

$$\frac{\partial \phi}{\partial t} = \frac{\phi(t+\Delta t) - \phi(t)}{\Delta t}$$

By assuming that the ϕ_i's in the right-hand side are evaluated at time $t+\Delta t$, the scheme described by Eq. (54) is fully implicit. With $S_i = (\phi_s - \phi_i)K_L/h$, Eq. (54) can be rewritten:

$$A(I)\phi_i = B(I)\phi_{i+1} + C(I)\phi_{i-1} + D(I) \qquad (55)$$

where:

$$A(I) = \frac{L_i}{\Delta t} + K_{i,i+1} + K_{i-1,i} + \frac{K_{Li}L_i}{h}$$

$$B(I) = K_{i,i+1}$$

$$C(I) = K_{i-1,i}$$

$$D(I) = \frac{L_i\,\phi_i(t)}{\Delta t} + K_{Li}\frac{L_i}{h}\,\phi_s$$

For oxygen $\phi = C$, $\phi_s = C_s$ and K_L is the oxygen transfer coefficient. For conductivity $\phi \equiv k$ and $K_L = 0$.

Equations (54) and (55) will be used to evaluate the obtained data and determine the coefficients D_x and K_L , as described in detail in the following sections. The wave flume was divided into five control volumes with no flux conditions applied at the ends. The grid used to represent the wave flume is shown in Fig. 14 and the lengths used are given in meters as:

$L_A = 1.72$ m
$L_B = 1.00$ m
$L_1 = 3.10$ m
$L_2 = 3.10$ m
$L_3 = 3.22$ m

$L_{AB} = 1.33$ m
$L_{B1} = 2.05$ m
$L_{12} = 3.10$ m
$L_{23} = 3.10$ m

Location of points A, B, 1, 2, and 3 are the same as given in Section III.B.

The set of equations presented by Eq. (55) can be easily solved using the tridiagonal matrix (TDMA) or Thomas algorithm with the no flux conditions applied as B(5) = 0 and C(1) = 0 [Patankar, 1980].

For a conservative substance (S=0) such as salt, and no flux conditions at the ends, Eq. (54) gives:

$$\sum L_i \frac{\partial k_i}{\partial t} = 0 \quad ,$$

$$\text{or} \quad \sum L_i k_i = \text{const} = \bar{k} \sum L_i$$

$$\text{where} \quad \bar{k} = \frac{\sum L_i k_i}{\sum L_i}$$

Thus, the mean value over the entire flume remains constant over time.

C. Determination of Longitudinal Dispersion Coefficient

A first attempt to determine longitudinal dispersion coefficients using Eq. (54) over every experimental time interval (Δt = time between measurements) yielded results with considerable scatter. The reason for this was probably that the computation was very sensitive to the value of the time derivative.

As a second attempt, the method of successive approximations was employed. The mean value of the first attempt was taken as the initial guess for the new method. Using Eq. (55) with $\Delta t \sim 1$ min and a measured initial conductivity distribution along the channel, conductivities were predicted for subsequent times until the end of the experiment, when computed values were compared against the experimental ones. A normalized RMS error was calculated each time as:

$$\text{RMS} = \sqrt{\frac{\frac{1}{N}\Sigma(k_{comp} - k_{expt})^2}{\frac{\Sigma k_{expt}}{N}}} \qquad (56)$$

Coefficients K_{AB}, K_{B1}, K_{12}, K_{23} were changed one at a time until a minimum RMS value was obtained.

The values of the K_{ij}'s giving the minimum RMS error were taken to be representative for the experiment in consideration. The computer program used, details of the computation, and obtained values of D_{ij} are given in Appendix II.

A correlation of the longitudinal dispersion coefficients $D_{ij} = K_{ij} L_{ij}$ was then attempted with the wave characteristics. Since D_{AB} describes the transfer across the paddle, it was expected to be different from the rest of the diffusivities, describing only the effect of waves. However, D_{AB} values follow the same trend as the rest of the diffusivities with slightly more scatter. Therefore, all D_{ij}'s were analyzed

together. Six data points were excluded from the correlation, four D_{23} values and two D_{AB} values. The D_{23} values were excluded because it was suspected that in the corresponding experiments the no flux condition at the downstream end did not hold, since the small reservoir was not completely isolated from the rest of the flume. The two D_{AB} values were excluded because they did not follow the general trend of the rest of the points.

As documented by Phillips [1977], although the Eulerian mean velocity at any point below the wave troughs is exactly zero, the Lagrangian mean velocity of all water particles is a non-zero second order quantity and is always in the wave propagation direction.

The particle displacement over one wave period due to a first order Stokes wave is given by

$$c(z) = \frac{2\pi^2 a^2}{L^2} \frac{\cosh\left(\frac{4\pi}{L}(z+h)\right)}{\sinh^2\left(\frac{2\pi h}{L}\right)} \tag{57}$$

The net area, A_1 in Fig. 15, over which the particles in a vertical line travel in one wave period, is given by the relation [Kit, 1981]:

$$A_1 = \int_{-h}^{-h_r} c(z)dz = \frac{\pi a^2}{2} \frac{\sinh\left(\frac{4\pi}{L}(h-h_r)\right)}{\sinh^2 \frac{2\pi h}{L}} \tag{58}$$

where h, h_r are water depths defined in Fig. 15. Setting $h_r = 0$ and with the deep water approximation ($h/L > 0.5$) Eq. (58) yields:

$$A_1 \simeq \frac{\pi a^2}{2} \frac{\frac{4\pi h}{L}}{\frac{2\pi h}{L}} = \pi a^2$$

If we now assume that the dispersion coefficient can be written as $D_{ij} \propto A_1/T$, we get

$$D_{ij} \propto \frac{\pi a^2}{T} = \frac{\pi}{4} \frac{H^2}{T} \approx 0.8 \frac{H^2}{T} \tag{59}$$

Consequently, an equation of the form

$$D_{ij} = \text{const.} \frac{H^2}{T} = \text{const.} \; H^2 \cdot f \tag{60}$$

was fitted to the data by least squares ($y=ax \rightarrow a = \Sigma yx/\Sigma x^2$), and the following equation was obtained:

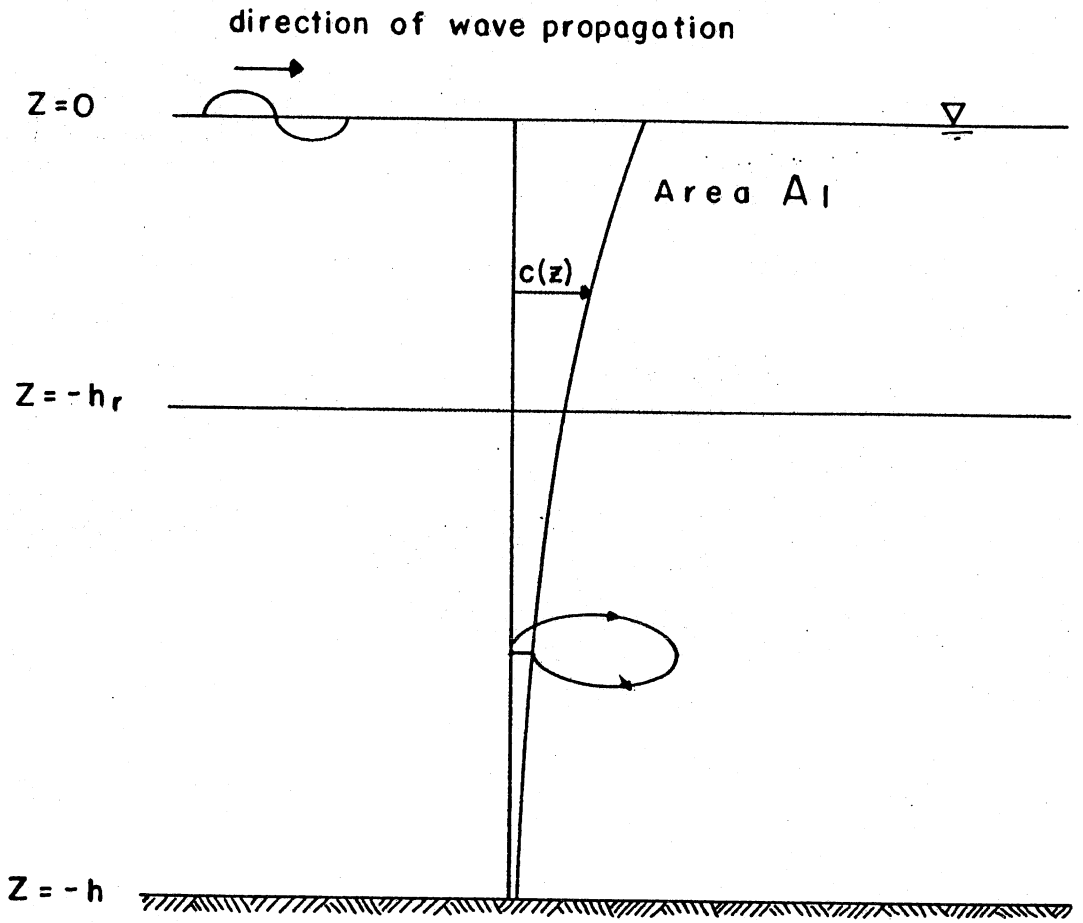

Fig. 15. Particle propagation under Stokes waves.

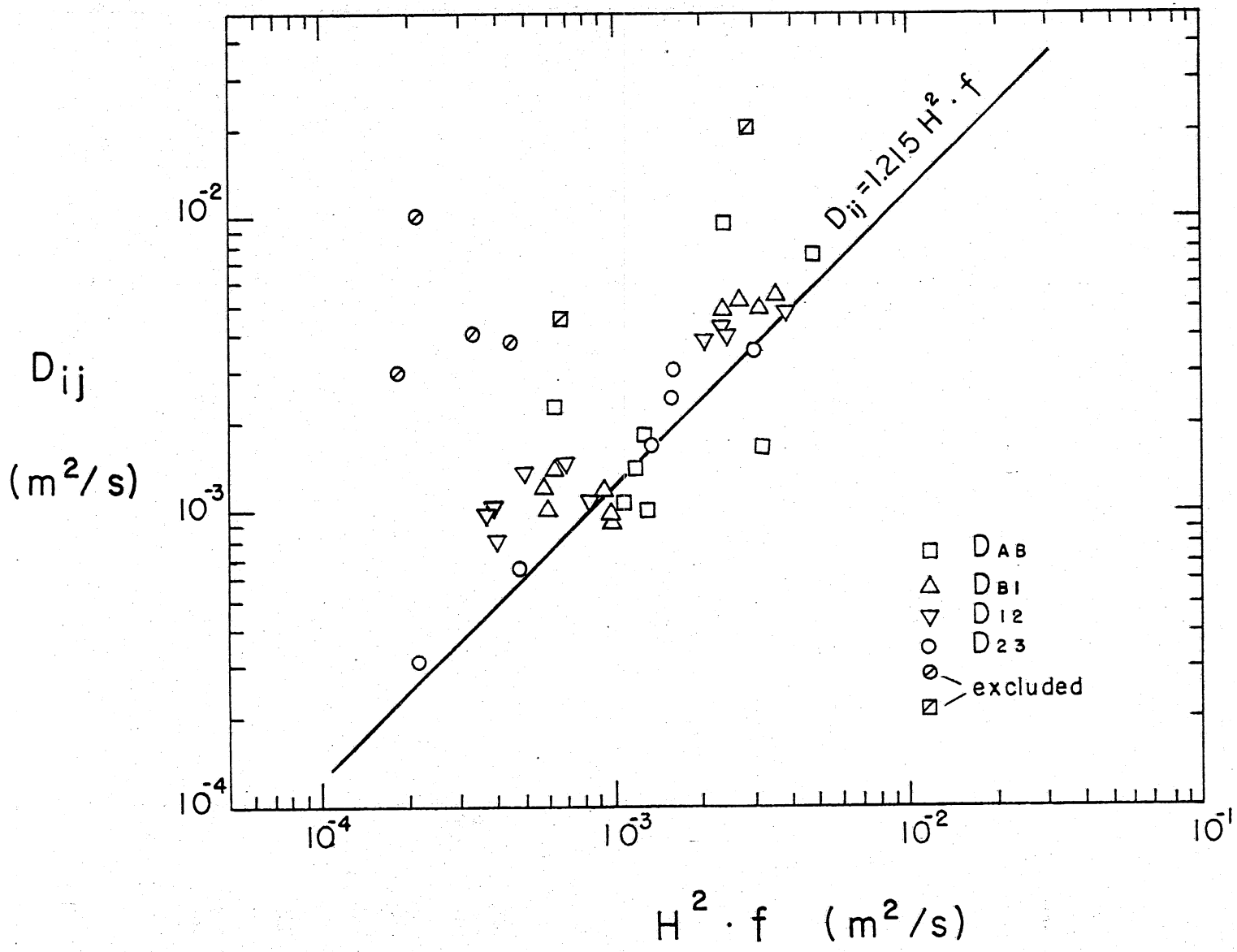

Fig. 16. Longitudinal dispersion coefficients versus $H^2 \cdot f$.

$$D_{ij} = 1.215\ H^2 \cdot f \qquad (r^2 = 0.543) \tag{61}$$

Equation (61) is shown along with the data in Fig. 16. Other attempted correlations didn't give better results. More details are presented in Appendix II.

D. Determination of Oxygen Transfer Coefficients

The oxygen transfer coefficients were initially determined for RUN 26 through RUN 35. The computations were performed using a) the dispersion coefficients obtained from the minimum RMS error procedure and b) the ones predicted from Eq. (61). Oxygen concentration profiles were determined every 10 minutes from graphs similar to the one presented in Fig. 8. The term dC/dt was also determined by measuring the slope of the curves off the graph. The oxygen transfer coefficients, proceeding from point A to point 3, were computed from Eq. (54);

$$K_{Li} = \frac{h}{C_s - C_i}\left[\frac{dC_i}{dt} - \frac{D_{i,i+1}}{L_i\, L_{i,i+1}}(C_{i+1} - C_i) + \frac{D_{i-1,i}}{L_i\, L_{i-1,i}}(C_i - C_{i-1})\right] \tag{62}$$

The temporal mean value of the obtained coefficients for every point was calculated.

Then, specifying a measured initial oxygen concentration distribution along the channel, and the oxygen transfer coefficients as determined from the above procedure, the oxygen concentration curves were predicted from Eq. (55) until the end of the experiment. The RMS error between measured and predicted D.O. concentrations was computed. For the first case the mean RMS error in D.O. concentration for the seven experiments was 0.160 mg/ℓ. For the second case, it was 0.178 mg/ℓ. The difference in RMS errors for the two cases was small. Therefore, it was judged that Eq. (61) could be safely used for the rest of the experiments where no conductivity data was available. Details of the computation are given in Appendix II.

Obtained values of the oxygen transfer coefficients as well as the corresponding RMS errors in the prediction of D.O. concentration are given in Table 3. The oxygen transfer coefficients for the area near the paddle (points A, B) are generally higher than those for the main part of the flume (points 1,2,3), but the variation along the flume is not monotonous, possibly because of uncertainties in the estimation of the longitudinal dispersion coefficients.

Because of the uncertainty inherent in any experiment to measure gas transfer, only two representative values of the oxygen transfer coefficients were used for each experiment: one for the region near the paddle, K_{LAB} , and one for the main part of the flume, K_L. K_{LAB} and K_L

TABLE 3. OXYGEN TRANSFER COEFFICIENTS, K_{L1} (m/s), AND RMS ERROR (mg/ℓ)

Run	K_{LA}	K_{LB}	K_{L1}	K_{L2}	K_{L3}	RMS Error (mg/ℓ)
9	9.25×10^{-5}	3.53×10^{-4}	3.23×10^{-5}	3.43×10^{-5}	2.66×10^{-5}	0.142
10	6.12×10^{-5}	2.61×10^{-4}	2.12×10^{-5}	3.24×10^{-5}	8.84×10^{-6}	0.128
11	1.20×10^{-4}	8.61×10^{-5}	4.21×10^{-5}	2.14×10^{-5}	6.31×10^{-5}	0.106
12	5.81×10^{-5}	5.04×10^{-5}	4.37×10^{-5}	1.60×10^{-5}	3.14×10^{-5}	0.146
13	3.95×10^{-5}	4.28×10^{-5}	2.87×10^{-5}	7.25×10^{-6}	1.65×10^{-5}	0.185
14	7.11×10^{-5}	1.29×10^{-4}	2.30×10^{-5}	3.60×10^{-5}	3.08×10^{-5}	0.185
15	7.95×10^{-5}	1.58×10^{-4}	1.13×10^{-5}	2.58×10^{-5}	2.43×10^{-5}	0.158
16	5.15×10^{-5}	4.79×10^{-5}	3.18×10^{-5}	1.75×10^{-5}	2.30×10^{-5}	0.153
17	3.37×10^{-4}	9.38×10^{-5}	2.17×10^{-5}	3.97×10^{-5}	3.96×10^{-5}	0.176
18	6.44×10^{-5}	6.77×10^{-5}	3.13×10^{-5}	3.21×10^{-5}	3.28×10^{-5}	0.159
19	4.16×10^{-5}	6.00×10^{-6}	4.06×10^{-5}	2.08×10^{-6}	1.46×10^{-5}	0.200
20	3.83×10^{-5}	2.38×10^{-5}	2.32×10^{-5}	1.52×10^{-5}	8.02×10^{-6}	0.141
21	1.06×10^{-4}	4.27×10^{-5}	2.92×10^{-5}	3.89×10^{-5}	1.88×10^{-5}	0.254
22	1.36×10^{-4}	1.47×10^{-4}	3.92×10^{-5}	4.25×10^{-5}	4.69×10^{-5}	0.094
23	9.71×10^{-5}	3.34×10^{-4}	8.06×10^{-6}	3.93×10^{-5}	3.58×10^{-5}	0.124
24	9.29×10^{-5}	2.80×10^{-4}	1.77×10^{-5}	3.30×10^{-5}	3.37×10^{-5}	0.093
25	9.37×10^{-5}	3.30×10^{-4}	1.62×10^{-5}	2.73×10^{-5}	3.51×10^{-5}	0.200
26	9.21×10^{-4}	1.01×10^{-3}	2.03×10^{-5}	3.15×10^{-5}	6.36×10^{-5}	0.131
27	2.24×10^{-4}	8.08×10^{-5}	4.50×10^{-5}	4.88×10^{-5}	5.44×10^{-5}	0.255
28	2.30×10^{-4}	6.75×10^{-4}	3.66×10^{-5}	5.15×10^{-5}	4.85×10^{-5}	0.212
29	2.08×10^{-4}	7.93×10^{-4}	1.48×10^{-5}	4.26×10^{-5}	5.18×10^{-5}	0.121
30	3.28×10^{-5}	8.49×10^{-5}	1.61×10^{-5}	*	*	*
31	3.18×10^{-5}	5.51×10^{-5}	1.35×10^{-5}	8.05×10^{-6}	7.77×10^{-6}	*
32	5.84×10^{-5}	5.56×10^{-5}	1.56×10^{-5}	2.03×10^{-5}	2.38×10^{-5}	0.200
33	3.30×10^{-5}	8.73×10^{-5}	1.75×10^{-5}	2.53×10^{-5}	6.09×10^{-6}	*
34	3.27×10^{-5}	3.52×10^{-5}	2.10×10^{-5}	1.95×10^{-5}	1.43×10^{-5}	0.193
35	2.68×10^{-5}	9.46×10^{-6}	1.70×10^{-5}	1.71×10^{-5}	1.38×10^{-5}	0.133

*Not enough data available for computation of K_L, RMS error

were obtained as weighted averages (by length) of K_{LA}, K_{LB}, and K_{L1}, K_{L2}, K_{L3}, respectively and correlated with the wave characteristics of points B and 2. It was assumed that the wave characteristics in the area behind and in front of the paddle were similar. K_{LAB} and K_L values are given in Table 4, along with the corresponding $H \cdot f$ values which were used in the finally proposed correlation.

TABLE 4. AVERAGE OXYGEN TRANSFER COEFFICIENTS AND H•f VALUES

RUN	K_{LAB} (m/sec)	H•f at point B (m/sec)	K_L (m/sec)	H•f at point 2 (m/sec)
9	1.88x10-4	0.0588	3.10x10-5	0.0407
10	1.35x10-4	0.0550	2.07x10-5	0.0288
11	1.08x10-4	0.0718	4.25x10-5	0.0654
12	5.53x10-5	0.0625	3.04x10-5	0.0490
13	4.07x10-5	0.0545	1.75x10-5	0.0380
14	9.24x10-5	0.0631	2.99x10-5	0.0401
15	1.08x10-4	0.0625	2.05x10-5	0.0409
16	5.02x10-5	0.0557	2.41x10-5	0.0452
17	2.47x10-4	0.0680	3.37x10-5	0.0420
18	6.56x10-5	0.0582	3.21x10-5	0.0403
19	2.85x10-5	0.0526	1.90x10-5	0.0383
20	3.30x10-5	0.0573	1.54x10-5	0.0372
21	8.27x10-5	0.0531	2.88x10-5	0.0305
22	1.40x10-4	0.0680	4.29x10-5	0.0530
23	1.84x10-4	0.0674	2.78x10-5	0.0411
24	1.62x10-4	0.0602	2.82x10-5	0.0359
25	1.81x10-4	0.0647	2.63x10-5	0.0439
26	9.54x10-4	0.0847	3.88x10-5	0.0755
27	1.71x10-4	0.0796	4.95x10-5	0.0605
28	3.94x10-4	0.0693	4.56x10-5	0.0574
29	4.23x10-4	0.0735	3.66x10-5	0.0619
30	4.97x10-5	0.0487	*1.61x10-5	*0.0371
31	4.04x10-5	0.0486	9.75x10-6	0.0301
32	5.74x10-5	0.0520	2.00x10-5	0.0393
33	5.30x10-5	0.0407	1.62x10-5	0.0276
34	3.36x10-5	0.0395	1.82x10-5	0.0263
35	2.04x10-5	0.0447	1.59x10-5	0.0338

*value of point 1

V. RESULTS AND DISCUSSION

A. Correlation of Experimental Data with Wave Characteristics

Dimensional analysis as well as multiple linear regression were used to correlate the measured oxygen transfer coefficients to the wave characteristics. A number of different wave parameters, e.g. $H \cdot f$, $s \cdot H \cdot f$, $g^{-1/2} H^{1.5} f^2$, $H^2 f^3/g$ etc. were developed and compared to the K_L measurements. All of these successful parameters shared a common feature: K_L could be linearly correlated with the parameter, whereas most K_{LAB} values were considerably higher without following a certain trend.

Comparing the K_{LAB} values with the pictures of the area near the paddle, a visual correlation with the intensity of wave breaking and the extent of bubbles entrained can be obtained. Experiments were classified into three categories:

(a) experiments where extensive breaking occurred,

(b) experiments with limited breaking or with a few bubbles present, and

(c) experiments where no breaking or bubbles appeared.

Breaking caused by the movement of the paddle did not extend to the rest of the flume, limiting the classification to the area near the paddle.

Figures 17a through 17h, traced from photographs, give examples for each of the above categories. Figures 17a and 17b illustrate two phases of a plunging breaker, which results in one of the highest oxygen transfer coefficients measured during the experiments. Figures 17c, 17d, and 17e show a sequence of three experiments under category (a) indicating a decreasing extent of bubbles and breaking intensity with a corresponding decrease in the oxygen transfer coefficient. In Figures 17f and 17g, a limited extent of bubbles (category b) can be observed and finally Figure 6h shows no bubble disturbance (category c). K_{LAB} values of experiments in category (c) fall in the same range as the K_L values. The higher K_{LAB} values for categories (a) and (b) indicate the importance of breaking waves in gas transfer. Though the increase in gas transfer seems to be proportional to the extent of bubbles entrained, a quantitative relation has yet to be obtained.

From the obtained equations for K_L the one including $H \cdot f$, although not having the highest coefficient of determination, provides the best comparison to data from other flumes and has a very small constant term which can be dropped without affecting the coefficient of determination (r^2).

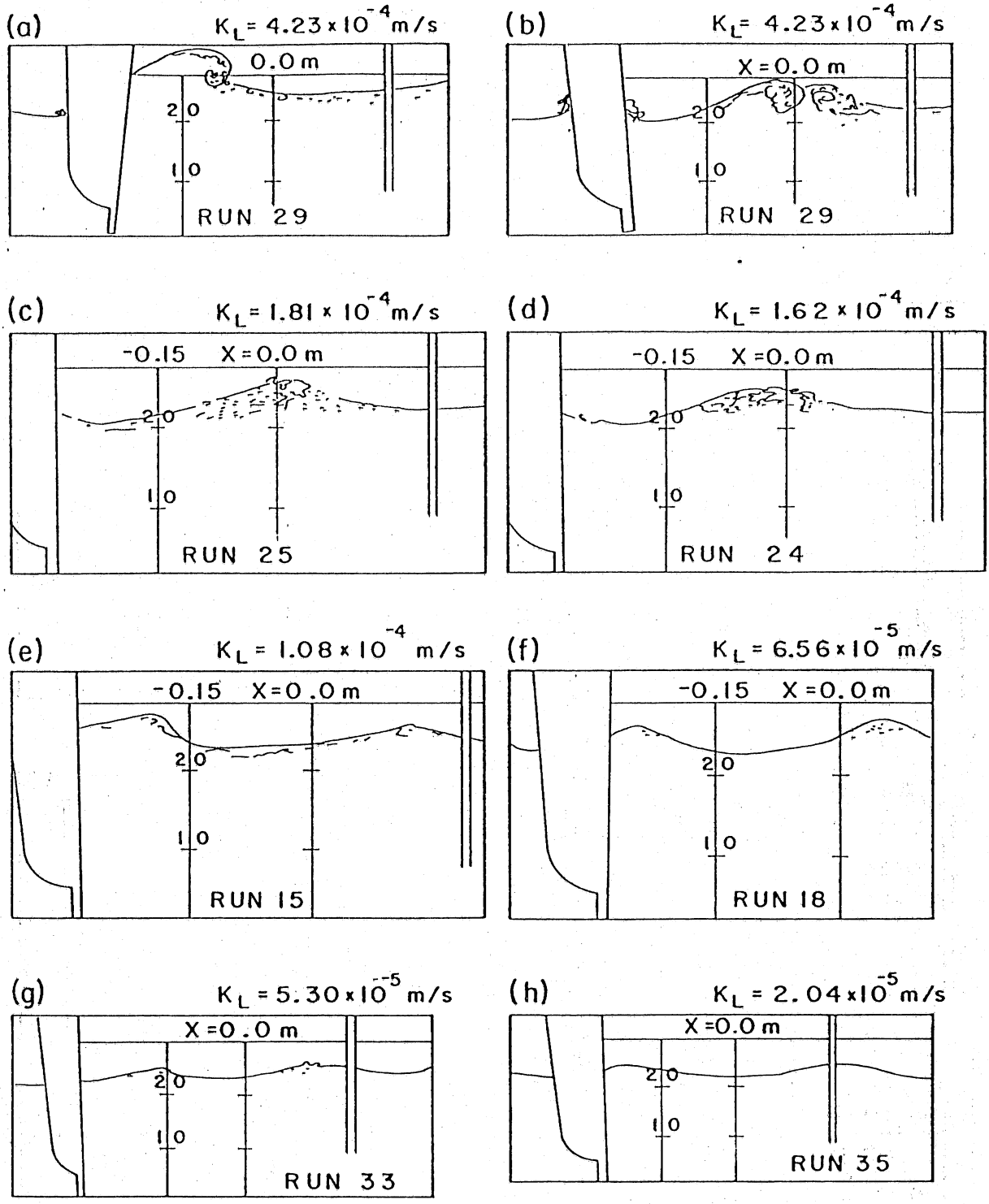

Fig. 17. Photos from the area near the paddle representative of the various categories: a,b) plunging breaker; c,d,e) limited breaking and bubbles; f,g) limited extent of bubbles; and h) undisturbed wave form.

Moreover, H·f can be related to the resultant wave velocity $\sqrt{v_x^2 + v_y^2} = \pi \cdot H \cdot f$ at the water surface for deep water waves, providing somephysical insight. The obtained equation is

$$K_L = 0.0159\ H.f\ Sc^{-1/2} \qquad (r^2 = 0.638) \qquad (63)$$

and is shown in Fig. 18 along with the K_L and K_{LAB} data. The remainder of the equations are presented in Appendix III.

Using Eq. (63) for the prediction of the liquid film coefficients K_{L1}, K_{L2} and K_{L3}, the measured K_{LAB} value for K_{LA}, K_{LB}, and the predicted longitudinal dispersion coefficients, D.O. concentrations were computed by the method described in Section IV.D. The computed and measured D.O. concentrations are compared in Fig. 19. The RMS error of the computed versus measured D.O. is given for each experiment. The comparisons are relatively good by the standard of gas transfer experiments. This is especially true when one considers that the uncertainties of both the predicted longitudinal dispersion coefficients and the liquid film coefficients are incorporated into the computations.

B. Comparison with Other Data

1. Mechanical Waves

Downing and Truesdale [1955] investigated the effect of waves on oxygen transfer in a steel tank 19 m long, 1.22 m wide and 1.22 m deep. They presented three groups of experiments:

(a) Experiments with f = 1.25 Hz (L = 99.3 cm) and varying wave height from 2.8 cm to 10.8 cm, where the oxygen transfer coefficient varied almost linearly from 2.67×10^{-5} to 1.03×10^{-4} m/sec.

(b) Experiments with H = 8 cm and varying frequency from 0.60 Hz to 1.25 Hz, corresponding to a variation of K_L between 4.06×10^{-5} and 7.56×10^{-5} m/sec.

(c) Experiments with irregular (choppy) waves at f = 1.27 Hz. In this case they reported the wave height as the mean of the wave heights of the 20% highest waves, $H_{20\%}$, varying from 6.36 cm to 13.25 cm. The liquid film coefficient varied from 3.06×10^{-5} to 6.94×10^{-5} m/sec. All waves were mechanically produced and were not breaking.

The results were plotted as three separate curves (Fig. 20). In each case K_L was plotted versus the varying wave parameter and the variation was approximately linear (their Fig. 4). Assuming that wave heights in group (c) follow the Rayleigh distribution, the reported wave height can be converted to the average height of all waves, $\bar{H} = 0.5566\ H_{20\%}$ [Longuet-Higgins, 1952]. After this conversion, curves (a) and (c) coincide. All

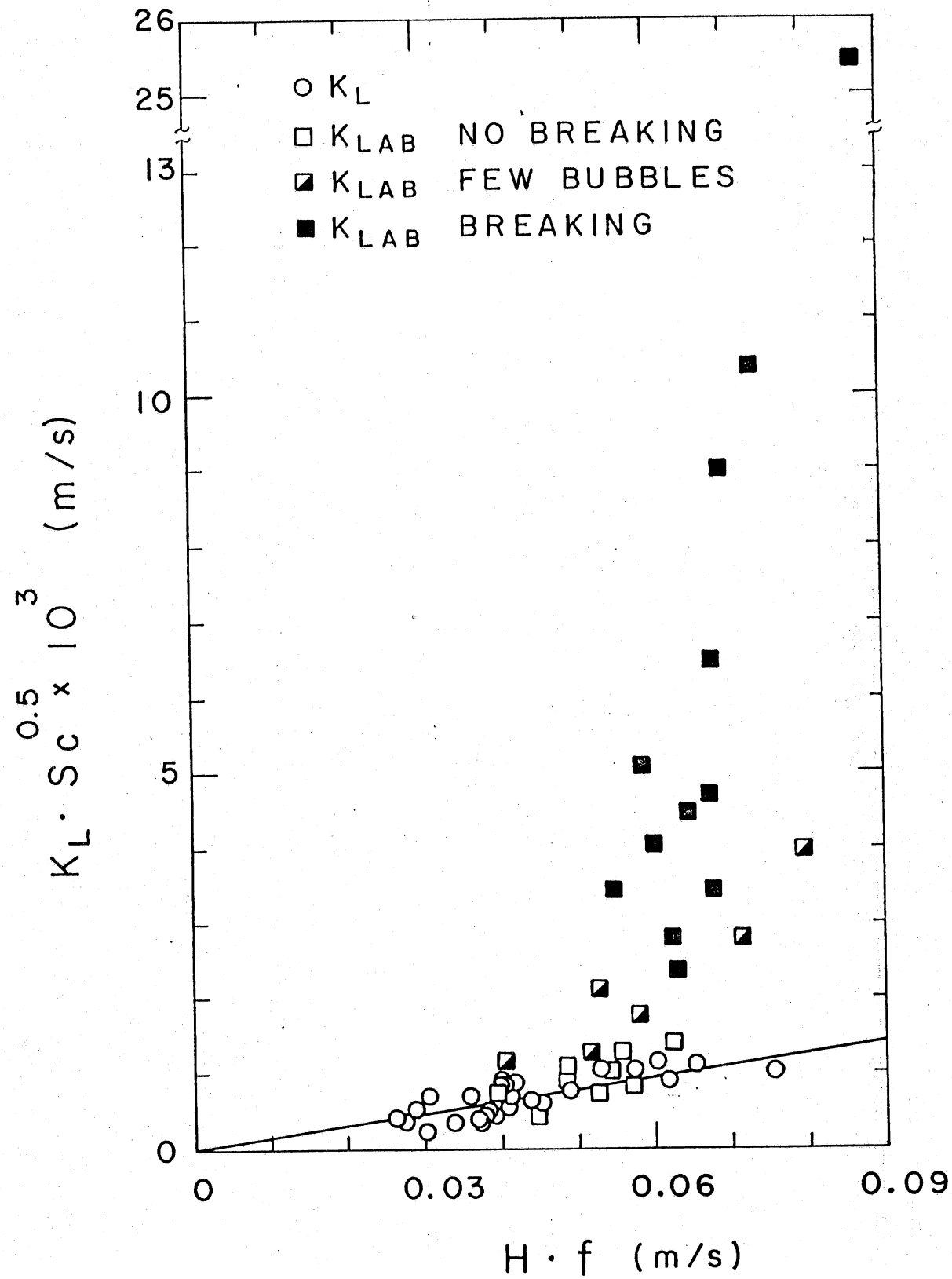

Fig. 18. Correlation of the oxygen transfer coefficients with H·f.

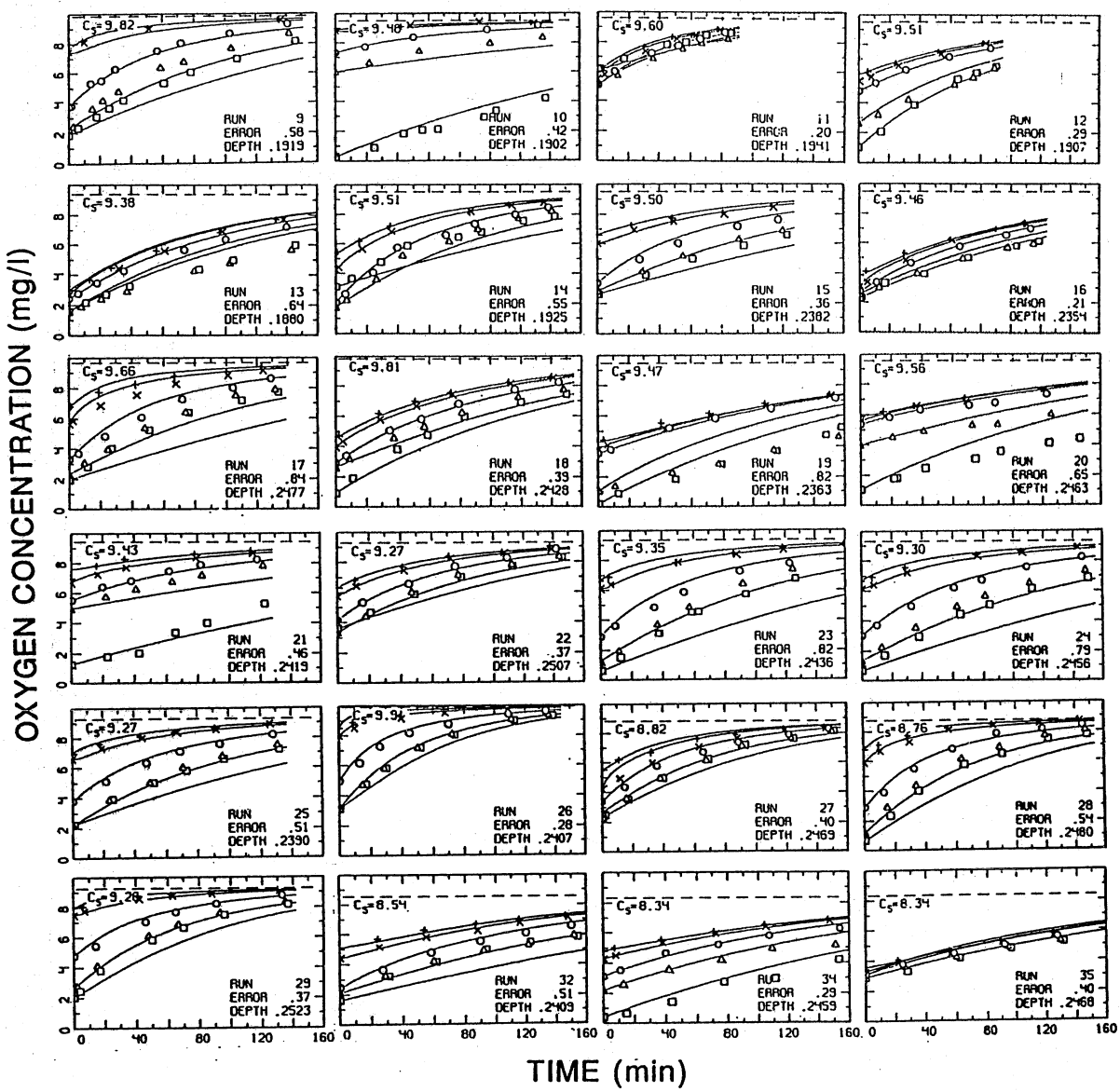

Fig. 19. D.O. data and predicted oxygen concentration curves for points A(+), B(x), 1(0), 2(Δ), and 3(□). The saturation concentration C_s and the RMS error are given in mg/ℓ. Depth is in meters.

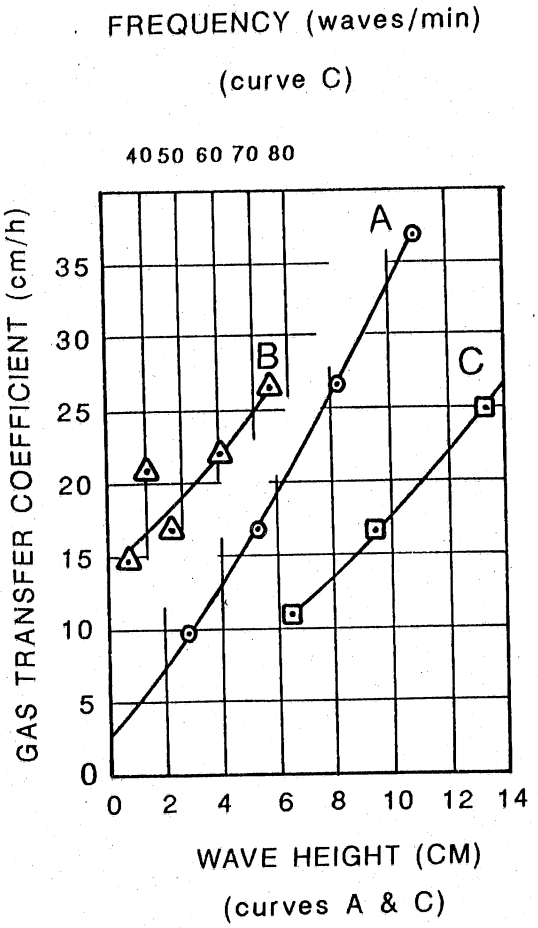

Fig. 20. Downing's and Truesdale's [1955] data for wind influenced gas transfer.

data are plotted against Eq. (63), in Fig. 21, using wave height $\overline{H}$ for curve (c) and Sc = 537 (T=20°C). The agreement is excellent. Although the range of H.f is almost twice that of our experiments, the agreement is as good in the extrapolation of Eq. (63) as in the range of our data.

Additional gas transfer data with mechanically generated waves were taken by Hosoi et al. [1977] in a 27.5 m long, 0.6 m wide and 1.2 m deep (0.35 m water depth) flume. Reported wave characteristics are the wave period and the variance, σ^2, of the water surface elevation. Wave length and height, $H=2.82\sigma$, were computed assuming a first order Stokes wave. From the wave length determination, the h/L value is shown to be between 0.11 and 0.15, indicating that the waves tend to be shallow water waves rather than deep water waves. The correlation presented in this report does not attempt to account for low h/L values and therefore the above data are not expected to agree with Eq. (63). They are plotted in Fig. 21 for comparison, and fall below the prediction line.

2. Wind waves

Equation (63) was further compared against the wind-wave data of Hosoi et al. [1977] and Jähne et al. [1984, 1985]. In Hosoi's experiments the wave height ranged from 1.08 to 4.59 cm and the frequency from 1.49 to 2.56 Hz. The transfer coefficient was between 2.58×10^{-5} and 1.15×10^{-4} m/sec. The data are compared with Eq. (63) in Fig. 22.

Jähne et al. measured the mean square slope, s^2, and frequency of the waves. For the comparison, the mean wave height was computed assuming deep water waves and $s=(\pi/\sqrt{2})H/L$. For experiments in the circular Heidelberg tunnels [Jähne et al., 1984], we estimated the dominant wave frequency and square slope from the given graphs [Jähne et al.,1984, Figs. 8 and 10]. For the large IMST facility [Jähne et al., 1985], slope and frequency measurements are reported for four different fetches. Wave data for the middle of the tunnel (fetch = 21 m) were taken as representative and used for the comparison. All data are shown in Fig. 22.

Experimental results from the Heidelberg tunnels, for CO_2 in the large facility and for O_2, He, Kr and CH_4 in the small facility, were reported normalized to $Sc^{-2}=600$ with n = 1/2. In the large IMST facility, tracer gases were He and Rn. For the He experiments both invasion and evasion experiments were performed, the invasion experiments yielding results with high scatter, as indicated by the error bars shown on Fig. 22.

Circled points indicate experiments with a wind shear velocity less than 30 cm/s which is our presumed delineation between breaking and non-breaking waves. They fall fairly close to the prediction developed herein for waves alone, with no wind shear. This is contrary to the general belief, prevalent prior to the recent work of Merlivat and Mémery [1983] and Jähne et al. [1985, 1987], that waves do not contribute significantly to air-water gas transfer. Although mechanically generated waves do not perfectly simulate wind waves, the results of the parameterization with H.f suggest that all of the gas transfer observed with non-breaking wind waves may be described by the wave parameters. This may indicate that at low wind shear waves are the primary source of gas

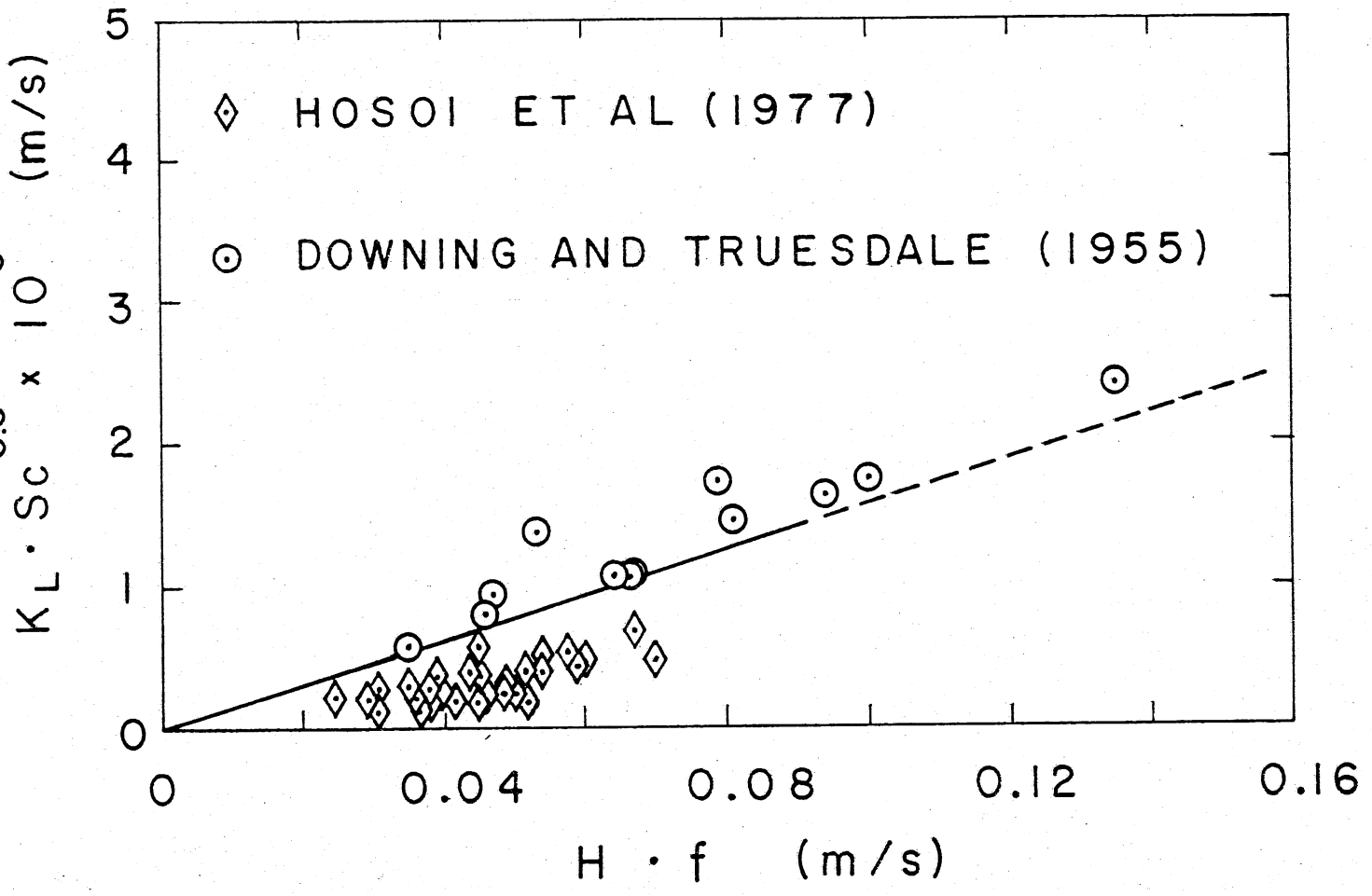

Fig. 21. Comparison of Equation 63 (solid line) with other mechanical wave data.

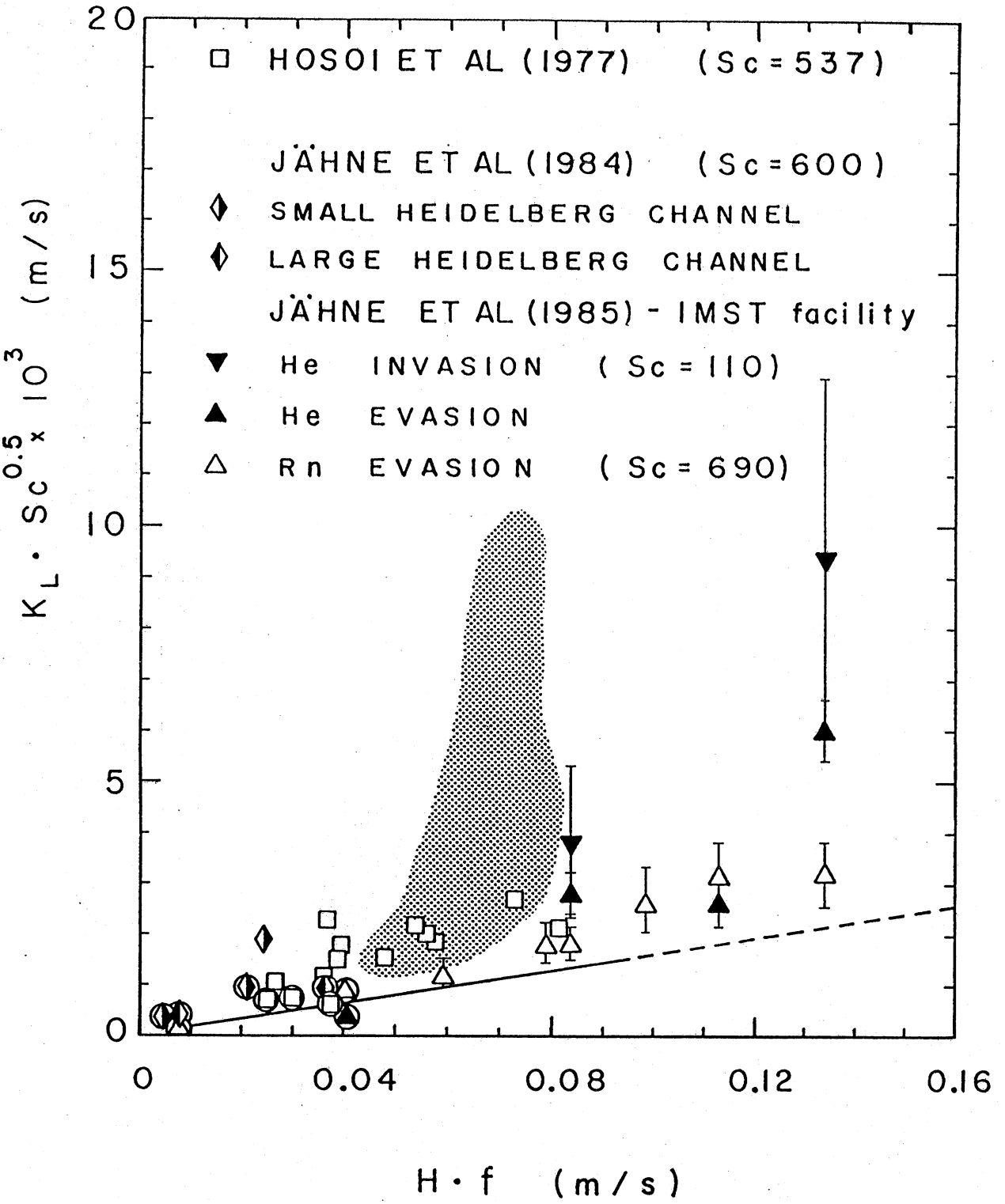

Fig. 22. Comparison of Equation 63 (solid line) for non-breaking waves, with data from wind wave flumes. Circled points indicate a wind shear velocity lower than 30 cm/sec, the presumed delineation between breaking and non-breaking wind waves. The shaded area indicates the range of our breaking waves data.

transfer, the circulation produced by the waves being more important than the water side turbulence generated by the wind. Still, the comparison of the gas transfer between mechanically generated waves and wind waves is far from ideal. The authors believe that these measurements point out the importance of waves in wind influenced gas transfer. Thus, the wave and wind shear influences should be considered simultaneously.

For experiments with wind shear velocity higher than 30 cm/s breaking waves might have been present. On the average the prediction of Eq. (63) can account for approximately 42% of the helium and oxygen transfer and 70% of the Rn transfer observed under wind waves when breaking might have been present. The shaded area in Fig. 22 indicates the range of our breaking waves data. The magnitude of the liquid film coefficients observed with mechanically generated breaking waves corresponds well to that of wind waves with a wind shear velocity greater than 30 cm/sec. The range of wave characteristics where breaking occurred, however, depends on the characteristics of the paddle. Since breaking was caused by the paddle movement and not by the steepening of the wave itself, no attempt should be made to relate them with the phenomenon of breaking in natural water bodies.

C. Fetch dependence

As proposed by Wilson [1965] and Mitsuyasu [1973], the characteristics of wind-generated wave spectra have the following dependence of fetch (F)

$$\hat{f} \sim \hat{F}^{-1/3} \tag{64}$$

$$\hat{H} \sim \hat{F}^{1/2} \tag{65}$$

where f is the dominant wave frequency, and H is a characteristic wave height. $\hat{f}$, $\hat{H}$, $\hat{F}$ are dimensionless quantities and are given by the relations: $\hat{f} = u_* f/g$, $\hat{H} = gH/u_*^2$, $\hat{F} = gF/u_*^2$. Eqs. (64) and (65) in dimensional form are:

$$f \sim g^{2/3} F^{-1/3} u_*^{-1/3} \tag{66}$$

$$H \sim g^{-1/2} F^{1/2} u_* \tag{67}$$

Using the above relations, the fetch dependence predicted by Eq. (63) can be determined as follows:

$$H \cdot f \sim (gF)^{1/6} u_*^{2/3} \tag{68}$$

Thus, the fetch dependence is shown to be small. If Eq. (68) represents the contribution of waves to gas transfer, one must consider wind fetch in the application of wind-wave flume results. For example, the wave

enhancement of gas transfer due to the waves themselves compared to a 10 m wind-wave flume, is a factor of 1.5, 2.2, 3.2, and 6.8 for a 100 m, 1 km, 10 km, and 1000 km fetch, respectively, if u_* is assumed fetch independent. At this point, however, no definite conclusion can be drawn concerning the dependence of the gas transfer coefficient on fetch, since Eq. (63) has not been derived on theoretical grounds.

VI. CONCLUSIONS

An experimental study was undertaken in order to determine the effect of deep water waves on gas transfer, using oxygen as a tracer gas. Results show that the oxygen transfer coefficient can be correlated with the wave characteristics through a power relation; a number of equations having a good fit (r^2 = 0.64 - 0.71) to the experimental data were obtained, with the wave height exponent varying from 1 to 2 and the wave frequency exponent varying from 1 to 3. Equation (63), indicating a linear dependence both on wave height and wave frequency, presented the most reasonable comparison to other data. Equation (63) predicts the gas transfer coefficient due to non-breaking waves only. Data from Downing and Truesdale [1955] for non-breaking waves agree fairly well with the proposed equation.

When breaking waves or bubbles were present, the gas transfer increased considerably. A good visual correlation of the gas transfer enhancement with breaking intensity and the extent of bubbles exists, but has not been quantified.

Comparison with data from experiments with wind waves indicate that about 50%, and possibly more, of the observed gas transfer can be accounted for by the wave forms alone.

The above comparisons imply that the wave and wind shear influences should be considered simultaneously. A wind wave flume cannot simulate the waves which occur at larger fetches. In order for experimental results to be translated for application in the field, the scaling parameters of both the wind shear and the wave influence should be identified.

If equation (63) applies to wind waves, the fetch dependence of the oxygen transfer coefficient is shown to be $F^{1/6}$, assuming u_* to be independent of fetch. This is important for application of wind-flume data, where F ~ 10 m, to field situations, where F = 100 m - 1000 km.

Additional mass transport experiments, in wind wave flumes where wave parameters and wind shear are measured, should be performed to test any theory for the delineation between wind shear and wave influences. This delineation is important because the development of waves in wind wave flumes is different from that on the open sea.

Finally, we attempted to identify the properties of the mechanically generated waves contributing to gas transfer. The following possibilities were considered:

1. The circulation and microturbulence generated by the dominant wave motion causes gas transfer by surface renewal or other

mechanism. In this case, the wave parameters developed herein, e.g. Eq. (63), would give a good indication of the gas transfer due to waves. Flow visualization experiments, though, have failed to produce visual indication of significant microturbulence near the water surface.

2. Capillary waves eminating from the side wall boundary layer of wave flumes, although relatively small, could influence a process such as gas transfer. The parameterization of the dominant waves would then be a secondary indicator of the gas transfer due to these capillary waves. Jähne et al. [1985, 1987], however, found that their wind wave flume data were better correlated with the mean wave slope than with the mean capillary wave slope. A non-intrusive technique to measure these waves is currently being investigated.

3. Secondary currents due to the no-slip condition at the boundaries and the particle velocity under the waves may also be a source of gas transfer. The secondary currents of the flume used herein were visualized and found to be insignificant.

In conclusion, it has been demonstrated that mechanically generated waves can produce a significant air-water transfer. Still, the scaling parameters should be further investigated. More experiments are currently underway in this direction focusing on the first and second mechanism.

REFERENCES

ASCE STANDARD Measurement of Oxygen Transfer in Clean Water. ASCE, July 1984.

Bennett, J. P. and R. E. Rathbun, "Reaeration in Open-Channel Flow," U. S. Geological Survey, Professional Paper 737, 1972, 75 p.

Broecker, H. Ch., J. Peterman and W. Siems, "The Influence of Wind on CO_2 Exchange in a Wind-Wave Tunnel, including the Effect of Monolayers." Jour. of Marine Research, 36, 4, 1978, 595-610.

Broecker, H. C., "Effects of Bubbles Upon the Gas Exchange Between Atmosphere and Oceans, in Berichte SFB94, Universität Hamburg, 1980, pp. 127-139.

Brown, L. C., "Statistical Evaluation of Reaeration Prediction Equations," Journal of Environ. Engineering Div., ASCE, Vol. 100, EE5, 1974, pp. 1051-1068.

Brown, L. C. and M. K. Stenstrom, "Proposed Modifications of K_2-Temperature Relation," ASCE, J. Environ. Engineering Div., Vol. 106, No. 6, 1980, pp. 1193-1202.

Brutsaert, W. and G. H. Jirka, eds. Gas Transfer at Water Surfaces, Reidel Publishing Co., 1984.

Cadwallader, T. E., "A Multivariate Analysis of Reaeration Data," Water Research, Vol. 3, 1969, pp. 731-742.

Chao, A. C., D.S. Chang, Ch. Smallwood, Jr. and W. S. Galler, "Effect of Temperature on Oxygen Transfer-Laboratory Studies," ASCE, J. Environ. Engineering, Vol. 113, No. 5, 1987, pp. 1089-1101.

Churchill, M. A., H. L. Elmore, and R. A. Buckingham, "Prediction of Stream Reaeration Rates," Journal of Sanitary Engineering Div., ASCE, Vol. 88, SA4, 1962, pp. 1-46.

Coantic, M., "A Model for Gas Transfer Across Air-Water Interfaces With Capillary Waves." J. Geophys. Res., 91, C3, 1986, pp. 3925-3943.

Deacon. E. L., "Sea-Air Gas Transfer: The Wind Speed Dependence," Boundary Layer Meteorology, 21, 1981, pp. 31-37.

Dewey, R. J., "Application of Stochastic Dissolved Oxygen Model," Jour. of Environ. Engrg., ASCE, Vol. 110, No. 2, 1984, pp. 412-429.

Dobbins, W. E., "BOD and Oxygen Relationships in Streams," Journal of Sanitary Engineering Div., ASCE, Vol. 90, SA3, 1964, pp. 53-78.

Dobbins, W. E., "Closure to BOD and Oxygen Relationships in Streams," Journal of Sanitary Engineering Div., ASCE, Vol. 91, SA5, 1965, pp. 49-55.

Downing, A. L. and G. A. Truesdale, "Some Factors Affecting the Rate of Solution of Oxygen in Water," J. Appl. Chem., 5, 1955, pp. 570-581.

Elmore, H. L. and W. F. West, "Effect of Water Temperature on Stream Reaeration," J. Sanitary Engrg. Div., ASCE, 87, SA6, 1961, pp. 59-71.

Eloubaidy, A. F. and E. J. Plate, "Wind Shear Turbulence and Reaeration Coefficient," Journal of Hydraulic Div., ASCE, Vol. 98, HY1, 1972, pp. 153-170.

Esen, I. I. and R. E. Rathbun, "A Stochastic Model for Predicting the Probability Distribution of the Dissolved Oxygen Deficit in Streams," U. S. Geological Survey, Professional Paper 913, 1976, 50 p.

Fortescue, G. E. and J.R.A. Pearson, "On Gas Absorption into a Turbulent Liquid," Chemical Engineering Sci., Vol. 22, 1967, pp. 1163-1176.

Gameson, A. L. H. and G. A. Truesdale, "Some Oxygen Studies in Streams," Inst. Water Engineers Journal, Vol. 13, No. 2, 1959, pp. 175-187.

Garret, W. D., "Damping of Capillary Waves at the Air-Sea Interface by Oceanic Surface-Active Material," Journal Marine Res., Vol. 25, 1967, pp. 279-291.

Garret, W. D. and J. D. Bultman, "Capillary Wave Damping by Insoluble Organic Monolayers," J. Colloid. Sci., Vol. 18, 1963, pp. 768-801.

Gerrard. W., Gas solubilities: Widespread Applications, Pergamon Press, 1980.

Goldstick, T. K. and I. Fatt, "Diffusion of Oxygen in Solutions of Blood Proteins, Chem. Engin. Progress, Symposium Series GG, 1970, pp. 101-113.

Gulliver, J. S., T. W. Mattke and H. G. Stefan, "Numerical and Graphical Procedures for Estimation of Community Photosynthesis and Respiration in Experimental Streams," University of Minnesota, St. Anthony Falls Hydraulic Laboratory, Project Report 198, 1980.

Gulliver, J. S. and C. S. Song, "Dynamic Roughness and the Transition Between Wind Wave Regimes," Jour. of Geophys. Res., 91, C4, April 1986, 5145-5151.

Gulliver, J. S. and H. G. Stefan, "Wind Function for a Sheltered Stream," Jour. of Environmental Engineering, ASCE, 112, 2, 1986, 387-399.

Gulliver, J. S. and H. G. Stefan, "Stream Productivity Analysis with DORM-II. Parameter Estimation and Sensitivity," Water Research, Vol. 18, No. 2, 1984, pp. 1577-1588.

Heggen, R. J., "Thermal Dependent Physical Properties of Water," Jour. of Hydraulic Engrg., ASCE, Vol. 109, No. 2, 1983, pp. 298-302.

Holley, E. R. and N. Yotsukura, "Field Techniques for Reaeration Measurements in Rivers." In Gas Transfer at Water Surfaces, W. Brutsaert and G. H. Jirka (eds.), 1984, pp. 381-401.

Hosoi, M., A. Ishida and K. Imoto, "Study on Reaeration by Waves," Coastal Engineering in Japan, Vol. 20, 1977, pp. 121-127.

Howe, R.H.L., "Proposed modification of K_2-temperature relation," ASCE, J. Environ. Engineering, Vol. 103, No. EE4, 1977, pp. 729-732.

Isaacs, W. P. and A. F. Gaudy, "Atmospheric Oxygenation in a Simulated Stream," J. Sanitary Div., ASCE, 94, SA2, 1968, pp. 319-344.

Jähne, B., K. O. Münnich and U. Siegenthaler, "Measurements of Gas Exchange and Momentum Transfer in a Circular Wind-Water Tunnel," Tellus 31, 1979, pp. 321-329.

Jähne, B., W. Huber, A. Dutzi, T. Wais and J. Imberger, "Wind/Wave-Tunnel Experiments on the Schmidt Number - and Wave Field Dependence of Air/Water Gas Exchange," In: Gas Transfer at Water Surfaces, ed. W. Brutsaert and G. H. Jirka, Reidel Publishing Co., 1984, 303-309.

Jähne, B., T. Wais, L. Mémery, G. Caulliez, L. Merlivat, K. O. Münnich and M. Coantic, "He and Rn Gas Exchange Experiments in the Large Wind-Wave Facility of IMST," Jour. of Geophys. Res., 90, C6, 1985, 11989-11997.

Jähne, B., K. O., Münnich, R. Bösinger, A. Dutzi, W. Huber, and P. Libner, "On the parameters influencing air-water gas exchange," J. Geophys. Res., 92, C2, 1987, pp. 1937-1949.

Kanwisher, J. W., "On the Exchange of Gases Between the Atmosphere and the Sea," Deep-Sea Research, Vol. 10, 1963, pp. 195-207.

Kerman, Bryan R.," A Model of Interfacial Gas Transfer for a Well-Roughened Sea," Jour. of Geophys. Res., 89, D1, 1984, 1439-1446.

Kinsman, B., Wind Waves, 1984, Dover publications.

Kit, E. and M. Stiassnie, "Particle Motion under Stokes Waves," Journal of Waterway, Coastal, and Ocean Div., ASCE, Vol. 107, No. WW3, 1981, pp. 202-204.

Krenkel, P. A. and G. T. Orlob, "Turbulent Diffusion and the Reaeration Coefficient," ASCE Transactions, Vol. 128, 1963, pp. 293-334.

Langbein, W. B. and W. H. Durum, "The Aeration Capacity of Streams," U. S. Geological Survey, Circular No. 542, 1967.

Lau, Y. L., "Prediction Equation for Reaeration in Open Channel Flow," Journal of Sanitary Engineering Div., ASCE, Vol. 98, SA6, 1972, pp. 1063-68.

Liss, P. S., P. W. Balls, F. N. Martinelli, M. Coantic, "The Effect of Evaporation and Condensation on Gas Transfer Across an Air-Water Interface," Oceanologica Acta, 4, 2, 1981, 129-138.

Liss, P.S., "Gas Transfer: Experiments and Geochemical Implication." In Air-Sea Exchange of Gases and Particles, P.S. Liss and W.G.N. Slinn (eds.), 1983, pp. 241-298.

Liss, P. S. and F. N. Martinelli, "The Effect of Oil Films on the Transfer of Oxygen and Water Vapor Across an air-water Interface," Thalassia Jugoslavica, Vol. 14, 1978, pp. 215-220.

Liu, M. S., R.M.R. Branion, and D. W. Duncan, "Oxygen Transfer to Water and to Sodium Sulfite Solutions," Journal Water Pollution Control Federation, Vol. 44, No. 1, Jan. 1972, pp. 34-40.

Long, S. R. and N. E. Huang, "On the Variation and Growth of Wave Slope Spectra in the Capillary-Gravity Range with Increasing Wind," Jour. of Fluid Mechanics, 77, 2, 1976, 209-228.

Longuet-Higgins, M.S., "On the Statistical Distribution of the Heights of Sea Waves," Jour. of Marine Research, XI, 3, 1952, 245-266.

Mancy, K. H. and D. A. Okun, "The Effects of Surface Active Agents on Aeration," Journal Water Pollution Control Federation, 37, 1965, pp. 212-227.

Martinelli, F. N., "The Effect of Surface Films on Gas Exchange Across the Air-Sea Interface," thesis, University of East Anglia, 1979, 320 p.

Mattingly, G. E., "Experimental study of Wind Effects on Reaeration," Journal of Hydraulic Div., ASCE, Vol. 103, HY3, 1977, pp. 311-323.

Merlivat, L. and L. Mémery, "Gas Exchange Across an Air-Water Interface: Experimental Results and Modeling of Bubble Contribution to Transfer," Journal Geophysical Research, Vol. 88, 1983, pp. 707-724.

Metzger, I., "Effects of Temperature on Stream Aeration," Journal of Sanitary Engineering Div., ASCE, Vol. 94, SA6, 1968, pp. 1153-1159.

Metzger, I. and W. E. Dobbins,"Role of Fluid Properties in Gas Transfer," Environmental Science and Technology, Vol. 1, No. 1, 1967, pp. 57-65.

Mitsuyasu, H., "The One-Dimensional Wave Spectra at Limited Fetch," Report of Research Institute for Applied Mechanics, Vol. XX, No. 66, 1973, pp. 37-53.

Monahan, E. C. and M. C. Spillane, "The Role of Oceanic Whitecaps in Air-Water Gas Exchange." In: Gas Transfer at Water Surfaces, ed. W. Brutsaert and G. H. Jirka, 1984, 495-503.

Morel-Seytoux, H.J. and D. H. Lau, "Statistical Evaluation of Reaeration Prediction Equations," Discussion, Journal of Environmental Engineering Div., ASCE, Vol. 101, EE5, 1975, pp. 859-861.

Negulescu, M. and V. Rojanski, "Recent Research to Determine Reaeration Coefficient," Water Research, Vol. 3, No. 3, 1969, pp. 189-202.

Nemerow, N. L., Stream, Lake, Estuary and Ocean Pollution, Von Norstand Reinhold Co., New York, 1985.

O'Connor, D. J., "Oxygen Balance of an Estuary," Transaction, ASCE, Vol. 126, Part III, 1961, pp. 556-611.

O'Connor, D. J., "Wind Effects on Gas-Liquid Transfer Coefficients," Jour. of Environmental Engineering, 109, 3, 1983, 731-752.

O'Connor, D. J. and D. M. DiToro, "Photosynthesis and Oxygen Balance in Streams," Journal of Sanitary Engineering Div., ASCE, Vol. 96, SA2, 1970, pp. 547-571.

O'Connor, D. J. and W. E. Dobbins, "Mechanism of Reaeration in Natural Streams," Transactions, ASCE, 123, 1958, pp. 641-666.

Owens, M., R. W. Edwards and J. W. Gibbs, "Some Reaeration Studies in Streams," International Journal of Air and Water Pollution, Vol. 8 No. 819, 1964, pp. 469-486.

Padgett, W. J., G. Schultz, and C. P. Tsokos, "A Random Differential Equation Approach to the Probability Distribution of BOD and DO in Streams," Soc. of Industrial and Appl. Mathematics, J. of Applied Mathematics, Vol. 32, No. 2, 1977, pp. 467-483.

Parkhurst, J. D. and R. D. Pomeroy, "Oxygen Absorption in Streams," Jour. of the Sanitary Engineering Division, ASCE, Vol. 98, No. SA1, 1972, pp. 101-124.

Patankar, S. V., Numerical Heat Transfer and Fluid Flow, McGraw Hill, 1980.

Phillips, O. M., The Dynamics of the Upper Ocean, Cambridge University Press, second edition, 1977.

Rathbun, R. E., "Reaeration Coefficients of Streams - State of the Art," Journal of Hydraulic Div., ASCE, Vol. 103, HY4, 1977, pp. 409-425.

Rathbun, R. E., "Estimating the Gas and Dye Quantities for Modified Tracer Technique. Measurements of Stream Reaeration Coefficients," U. S. Geological Survey, Water Resources Investigations 79-27, 1979, 42 p.

Sill, B. L., "Free and Forced Convection Effects on Evaporation," Jour. of Hydraulic Engineering, ASCE, Vol. 109, 9, Sept. 1983, 1216-1231.

Sivakumar, M. and A. Herzog, "A Model for the Prediction of Reaeration Coefficient in Lakes from Wind Velocity." In: Hydrodynamics of Lakes, ed. W. Graf and C. H. Mortimer, Elsevier, 1978, 331-340.

Standard Methods for Examination of Water and Wastewater, 15th ed., APHA-AWWA-WPCF, 1980.

Streeter, H. W., "The Rate of Atmospheric Reaeration of Sewage Polluted Streams," Transactions, ASCE, Vol. 89, 1926, pp. 1351-1364.

Streeter, H. W. and E. B. Phelps, "A Study of the Pollution and Natural Purification of the Ohio River," Washington, U. S. Public Health Service, Public Health Bull., 146, 1925, 75 p.

Thackston, E. L. and P. A. Krenkel, "Reaeration Prediction in Natural Streams," Journal of Sanitary Engineering Div., ASCE, Vol. 95, SA1, 1969, pp. 65-94.

Thayer, R. P. and R. G. Krutchkof, "Stochastic Model for BOD and DO in Streams," Journal of Sanitary Engineering Div., ASCE, Vol. 93, SA3, 1967, pp. 59-72.

Thorpe, S. A., "On the Clouds of Bubbles Formed by Breaking Wind-Waves in Deep Water and Their Role in Air-Sea Gas Transfer," Phil. Trans., Royal Society London, A, 304, 1982, pp. 155-210.

Truesdale, G. A. and K. G. VanDyke, "The Effect of Temperature on the Reaeration of Flowing Waters," Water and Waste Treatment Journal, Vol. 7, No. 9, 1958, pp. 9-11.

Tsivoglou, E. C., "Tracer Measurement of Stream Reaeration," Federal Water Pollution Control Adm., June 1967, 86 p.

Tsivoglou, E. C., R. L. O'Connel, C. M. Walter, P. J. Godsil, and G. S. Logsdon, "Laboratory Studies, Part I of Tracer Measurements of Atmospheric Reaeration," Journal Water Pollution Control Fed., Vol. 37, No. 10, 1965, pp. 1343-1362.

Tsivoglou, E. C. and J. R. Wallace, "Characterization of Stream Reaeration Capacity," EPA-R3-72-012, 1972.

Wannikhof, R., J. R. Ledwell and W. S. Broecker, "Gas exchange - Wind Speed Relation Measured with Sulfur Hexafluoride on a Lake," Science, 277, 1985, 1224-1226.

Wilcock, J. R., "Methylchloride as a Tracer Gas for Measuring Stream Coefficients," Water Res., 18(1), 1984, pp. 47-57.

Wilke, C. R. and P. Chang, "Correction of Diffusion Coefficients in Dilute Solutions," AIChE Journal, Vol. 1, 1955, pp. 264-270.

Wilson, B. W., "Numerical Prediction of Ocean Waves in the North Atlantic for Dec. 1959," Dtsch Hydrogr. Z, 18, 3, 1965, pp. 114-130.

Wilson, G. T. and N. Macleod, "A Critical Appraisal of Empirical Equations and Models for the Prediction of the Coefficient of Reaeration of Deoxygenated Water," Water Res., Vol., 8, No. 6, 1974, pp. 341-366.

Yotsukura, N., D. A. Stedfast, R. E. Draper and W. H. Brutsaert, "An Assessment of Steady-State Propane-Gas Tracer Method for Reaeration Coefficients - Cowaselon Creek, New York," U. S. Geological Survey, Water Res. Investigations Report 83-4183, 1983, 88 p.

APPENDIX I

TABLES A1 - A5 and FIGURES A1 - A9

TABLE A1. APPENDIX I.

WAVELENGTH, PERIOD, CELERITY AND WATER DEPTH.

SYMBOLS ARE DESCRIBED IN SECTION IV.A.1,2.

RUN	L (cm)	σ (cm)	σ/L	n	P1 (%)	P2 (%)	T (sec)	c (m/sec)	h (cm)	h/L
9	31.1	0.82	0.026	4	5	28	0.442	0.7036	19.19	0.617
10	24.5	0.61	0.025	3	5	55	0.382	0.6414	19.02	0.776
11	62.8	3.63	0.058	3	11	12	0.627	1.0016	19.41	0.309
12	43.0	1.24	0.029	6	7	12	0.520	0.8269	19.07	0.444
13	56.4	0.64	0.011	3	2	7	0.606	0.9307	18.80	0.333
14	31.6	0.94	0.030	5	8	36	0.436	0.7248	19.25	0.609
15	31.4	0.26	0.008	3	2	6	0.440	0.7136	23.82	0.759
16	60.8	2.72	0.045	6	13	13	0.619	0.9822	23.54	0.387
17	32.1	0.98	0.030	8	9	22	0.441	0.7279	24.77	0.772
18	34.1	2.10	0.062	9	19	32	0.447	0.7629	24.28	0.712
19	61.2	1.37	0.022	7	6	6	0.627	0.9761	23.63	0.386
20	42.8	0.60	0.014	9	4	5	0.524	0.8168	24.63	0.575
21	23.8	1.07	0.045	8	12	35	0.377	0.6313	24.19	1.016
22	40.2	1.09	0.027	7	8	16	0.500	0.8040	25.07	0.624
23	31.0	1.14	0.037	7	10	18	0.438	0.7078	24.36	0.786
24	30.7	0.75	0.025	7	7	31	0.432	0.7106	24.56	0.800
25	31.0	0.58	0.019	7	5	28	0.433	0.7159	23.90	0.771
26	58.4	2.03	0.035	6	11	11	0.609	0.9589	24.07	0.412
27	40.3	1.26	0.031	9	9	10	0.496	0.8125	24.69	0.613
28	41.7	1.42	0.034	7	9	14	0.505	0.8257	24.80	0.595
29	44.4	0.86	0.019	6	5	20	0.517	0.8588	25.23	0.568
30	29.2	0.41	0.014	9	4	14	0.431	0.6775	23.21	0.795
31	28.8	0.73	0.025	10	8	31	0.432	0.6667	23.62	0.820
32	30.7	0.78	0.026	9	8	40	0.433	0.7090	24.09	0.785
33	25.9	2.27	0.088	9	19	73	0.381	0.6798	25.00	0.996
34	23.7	0.48	0.020	7	5	36	0.380	0.6237	24.59	1.038
35	40.0	0.45	0.011	8	4	5	0.503	0.7952	24.68	0.617

TABLE A2. APPENDIX I: MEASURED WAVE HEIGHTS (cm).

	Start of Experiment						End of Experiment					
RUN x(m):	0.50	2.25	3.80	5.35	6.90	8.45	0.50	2.25	3.80	5.35	6.90	8.45
9	2.57	2.45[1] / 2.29[2]	2.09	1.73[3] / 1.78[4]	1.59	1.44			2.01		1.52	
10	2.34	1.53	1.40	1.21	0.86	0.80	1.78	1.58	1.25	1.13	0.95	0.72
11			4.43		4.35		4.64	4.17		3.87		3.43
12			2.82		1.99		3.24	3.19	2.68	2.50	2.56	2.45
13	3.48	3.06	2.45	2.50	2.04	2.27	2.99	3.04	2.49	2.41	1.93	2.03
14	2.99	2.89	2.07	1.85	1.45	1.34	2.42	2.24	1.94	1.69	1.43	1.23
15	2.72	2.29	1.83	1.74	1.48	1.34	2.84	2.49	2.31	1.82	1.56	1.30
16	3.69	3.53	3.10	2.90	2.79	2.42	3.23	2.96	2.59	2.71	2.23	2.09
17	3.25	2.65	2.15	1.84	1.60	1.45	2.73	2.45	2.00	2.00	1.66	1.35
18	2.66	2.42	2.15	1.74	1.41	1.25	2.54	2.50	2.26	1.85	1.58	1.33
19	3.31	3.15	2.76	2.23	1.89	2.10			2.42		2.12	
20	3.01	2.73	2.18	1.99	1.80	1.74			1.95		1.62	
21	2.09	1.87	1.41	1.05	0.83	0.67	1.72	1.65	1.39	1.09	0.87	0.68
22	3.54	3.44	2.98	2.24	2.36	1.98	3.30	3.12	3.00	2.63	2.42	2.16
23	2.91	2.57	2.14	1.82	1.40	1.32	3.01	2.66	2.14	1.83	1.40	1.26
24	2.73	2.11	1.91	1.47	1.25	1.08	2.46	2.16	1.83	1.49	1.31	1.13
25	2.90	2.51	2.03	1.90	1.59	1.41	2.70	2.34	2.17	1.98	1.62	1.33
26	5.76	5.61	4.93	4.82	4.31	4.05	4.90	4.90	4.44	4.57	4.30	4.01
27			3.37		2.85		3.90	3.89	3.19	3.04	2.86	2.39
28	3.31	3.52	3.16	2.96	2.58	2.29	3.47	3.40	3.12	2.96	2.60	2.23
29	3.83	4.22	3.63	3.12	2.72	2.76			3.40		2.90	
30	2.80	2.44	1.37	1.25	1.05	0.91	2.03	1.39	1.28	0.91	0.86	0.76
31	1.81	1.67	1.49	1.25	1.01	1.02	2.06	1.84	1.47	1.55	1.18	1.14
32	2.24	2.00	1.62	1.55	1.32	1.19	2.28	2.15	1.97	1.65	1.46	1.20
33	1.43	1.35	1.11	0.96	0.73	0.64	1.49	1.37	1.23	1.00	0.85	0.69
34	1.54	1.31	1.10	1.07	0.96	0.80	1.56	1.44	1.19	0.98	0.83	0.71
35	2.40	2.07	1.71	1.75	1.43	1.29	1.99	1.83	1.62	1.73	1.54	1.31

[1] x = 2.00m, [2] x = 2.50m, [3] x = 5.10m, [4] x = 5.60m

TABLE A3. APPENDIX I - WAVE HEIGHTS (cm) USED FOR COMPUTATIONS

RUN	X(m):	-0.30	0.20	0.70	2.25	3.80	5.35	6.90	8.45
	Point:	A-B	B	B-1	1	1-2	2	2-3	3
9		2.80	2.60	2.60	2.30	2.05	1.80	1.60	1.40
10		2.50	2.10	2.05	1.60	1.30	1.10	0.90	0.75
11		4.50	4.50	4.45	4.35	4.20	4.10	4.00	3.90
12		3.25	3.25	3.25	3.20	2.75	2.55	2.45	2.45
13		3.30	3.30	3.25	3.00	2.65	2.30	2.20	2.20
14		2.80	2.75	2.70	2.50	2.10	1.75	1.50	1.30
15		2.90	2.75	2.70	2.40	2.10	1.80	1.50	1.25
16		3.55	3.45	3.45	3.20	2.95	2.80	2.65	2.50
17		3.30	3.00	2.95	2.50	2.15	1.85	1.60	1.25
18		2.70	2.60	2.60	2.45	2.20	1.80	1.50	1.30
19		3.35	3.30	3.30	3.10	2.60	2.40	2.10	2.10
20		3.00	3.00	3.00	2.75	2.20	1.95	1.80	1.70
21		2.00	2.00	1.95	1.75	1.45	1.15	0.90	0.70
22		3.40	3.40	3.40	3.25	3.00	2.65	2.40	2.15
23		3.00	2.95	2.90	2.60	2.20	1.80	1.40	1.25
24		2.80	2.60	2.55	2.20	1.85	1.55	1.25	1.10
25		2.95	2.80	2.80	2.50	2.20	1.90	1.65	1.40
26		5.35	5.30	5.30	5.15	4.90	4.60	4.30	4.10
27		4.00	3.95	3.95	3.85	3.40	3.00	2.80	2.55
28		3.50	3.50	3.50	3.45	3.20	2.90	2.60	2.30
29		3.85	3.80	3.80	3.70	3.50	3.20	2.85	2.70
30		2.35	2.10	2.05	1.60	1.30	1.05	0.90	0.80
31		2.30	2.10	2.05	1.70	1.45	1.30	1.20	1.10
32		2.35	2.25	2.25	2.05	1.90	1.70	1.45	1.20
33		1.60	1.55	1.55	1.40	1.20	1.05	0.90	0.70
34		1.55	1.50	1.50	1.35	1.20	1.00	0.90	0.75
35		2.35	2.25	2.25	2.05	1.85	1.70	1.50	1.30

TABLE A4. APPENDIX I - WAVE STEEPNESS (H/L)

RUN	X	-0.30	0.20	0.70	2.25	3.80	5.35	6.90	8.45
	Point	A-B	B	B-1	1	1-2	2	2-3	3
9		0.0900	0.0836	0.0836	0.0740	0.0659	0.0579	0.0514	0.0450
10		0.1020	0.0857	0.0837	0.0653	0.0531	0.0449	0.0367	0.0306
11		0.0717	0.0717	0.0709	0.0693	0.0669	0.0653	0.0637	0.0621
12		0.0756	0.0756	0.0756	0.0744	0.0640	0.0593	0.0570	0.0570
13		0.0585	0.0585	0.0576	0.0532	0.0470	0.0408	0.0390	0.0390
14		0.0886	0.0870	0.0854	0.0791	0.0665	0.0554	0.0475	0.0411
15		0.0924	0.0876	0.0860	0.0764	0.0669	0.0573	0.0478	0.0398
16		0.0584	0.0567	0.0567	0.0526	0.0485	0.0461	0.0436	0.0411
17		0.1028	0.0935	0.0919	0.0779	0.0670	0.0576	0.0498	0.0389
18		0.0792	0.0762	0.0762	0.0718	0.0645	0.0528	0.0440	0.0381
19		0.0547	0.0539	0.0539	0.0507	0.0425	0.0392	0.0343	0.0343
20		0.0701	0.0701	0.0701	0.0643	0.0514	0.0456	0.0421	0.0397
21		0.0840	0.0840	0.0819	0.0735	0.0609	0.0483	0.0378	0.0294
22		0.0846	0.0846	0.0846	0.0808	0.0746	0.0659	0.0597	0.0535
23		0.0968	0.0952	0.0935	0.0839	0.0710	0.0581	0.0452	0.0403
24		0.0912	0.0847	0.0831	0.0717	0.0603	0.0505	0.0407	0.0358
25		0.0952	0.0903	0.0903	0.0806	0.0710	0.0613	0.0532	0.0452
26		0.0916	0.0908	0.0908	0.0882	0.0839	0.0788	0.0736	0.0702
27		0.0993	0.0980	0.0980	0.0955	0.0844	0.0744	0.0695	0.0633
28		0.0839	0.0839	0.0839	0.0827	0.0767	0.0695	0.0624	0.0552
29		0.0867	0.0856	0.0856	0.0833	0.0788	0.0721	0.0642	0.0608
30		0.0805	0.0719	0.0702	0.0548	0.0445	0.0360	0.0308	0.0274
31		0.0799	0.0729	0.0712	0.0590	0.0503	0.0451	0.0417	0.0382
32		0.0765	0.0733	0.0733	0.0668	0.0619	0.0554	0.0472	0.0391
33		0.0618	0.0598	0.0598	0.0541	0.0463	0.0405	0.0347	0.0270
34		0.0654	0.0633	0.0633	0.0570	0.0506	0.0422	0.0380	0.0316
35		0.0588	0.0563	0.0563	0.0513	0.0463	0.0425	0.0375	0.0325

TABLE A5. COMPARISON OF WAVE PERIOD AND GROUP VELOCITY TO THE THEORETICAL VALUES

RUN	$\sqrt{g/(2\pi Lf^2)}$	$1 - \sqrt{g/(2\pi Lf^2)}$ (%)	c_g Measured (m/sec)	C'_g from Eq. (45) (m/sec)	$\left(\frac{c'_g}{c_g} - 1\right)$ (%)
9	0.990	1.0	0.3769	0.3541	-6.
10	0.964	3.6	0.3388	0.3211	-5.
11	0.989	1.1	0.5415	0.5809	7.
12	0.991	0.9	0.4477	0.4309	-4.
13	1.008	-0.8	0.4882	0.5247	7.
14	0.969	3.1	0.3758	0.3650	-3.
15	0.981	1.9	0.3553	0.3573	1.
16	0.992	0.8	0.4921	0.5280	7.
17	0.973	2.7	0.3746	0.3644	-3.
18	0.956	4.4	0.3746	0.3823	2.
19	1.001	-0.1	0.4901	0.5251	7.
20	1.001	-0.1	0.4161	0.4127	-1.
21	0.966	3.4	0.3077	0.3157	3.
22	0.985	1.5	0.4247	0.4045	-5.
23	0.983	1.7	0.3523	0.3543	1.
24	0.974	2.6	0.3713	0.3556	-4.
25	0.972	2.8	0.3553	0.3584	1.
26	0.996	0.4	0.5487	0.5075	-8.
27	0.976	2.4	0.4276	0.4091	-4.
28	0.977	2.3	0.4261	0.4163	-2.
29	0.969	3.1	0.4276	0.4343	2.
30	0.997	0.3	0.3370	0.3391	1.
31	1.006	-0.6	0.3533	0.3336	-6.
32	0.976	2.4	0.3758	0.3549	-6.
33	0.935	6.5	0.3370	0.3399	1.
34	0.975	2.5	0.3246	0.3119	-4.
35	0.994	0.6	0.3912	0.4002	2.

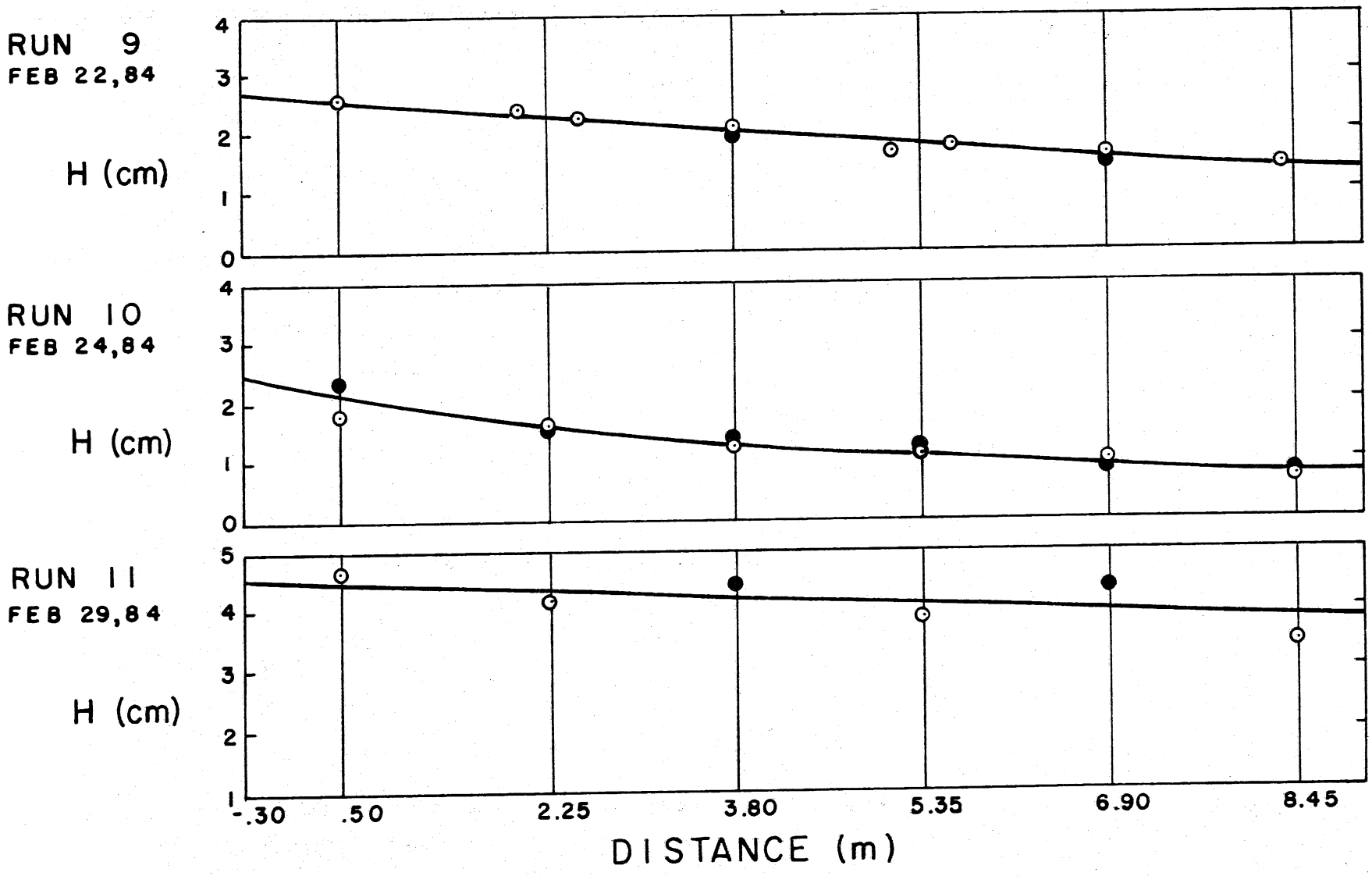

Fig. A1. Wave height versus distance along the channel for RUN 9 - RUN 11.

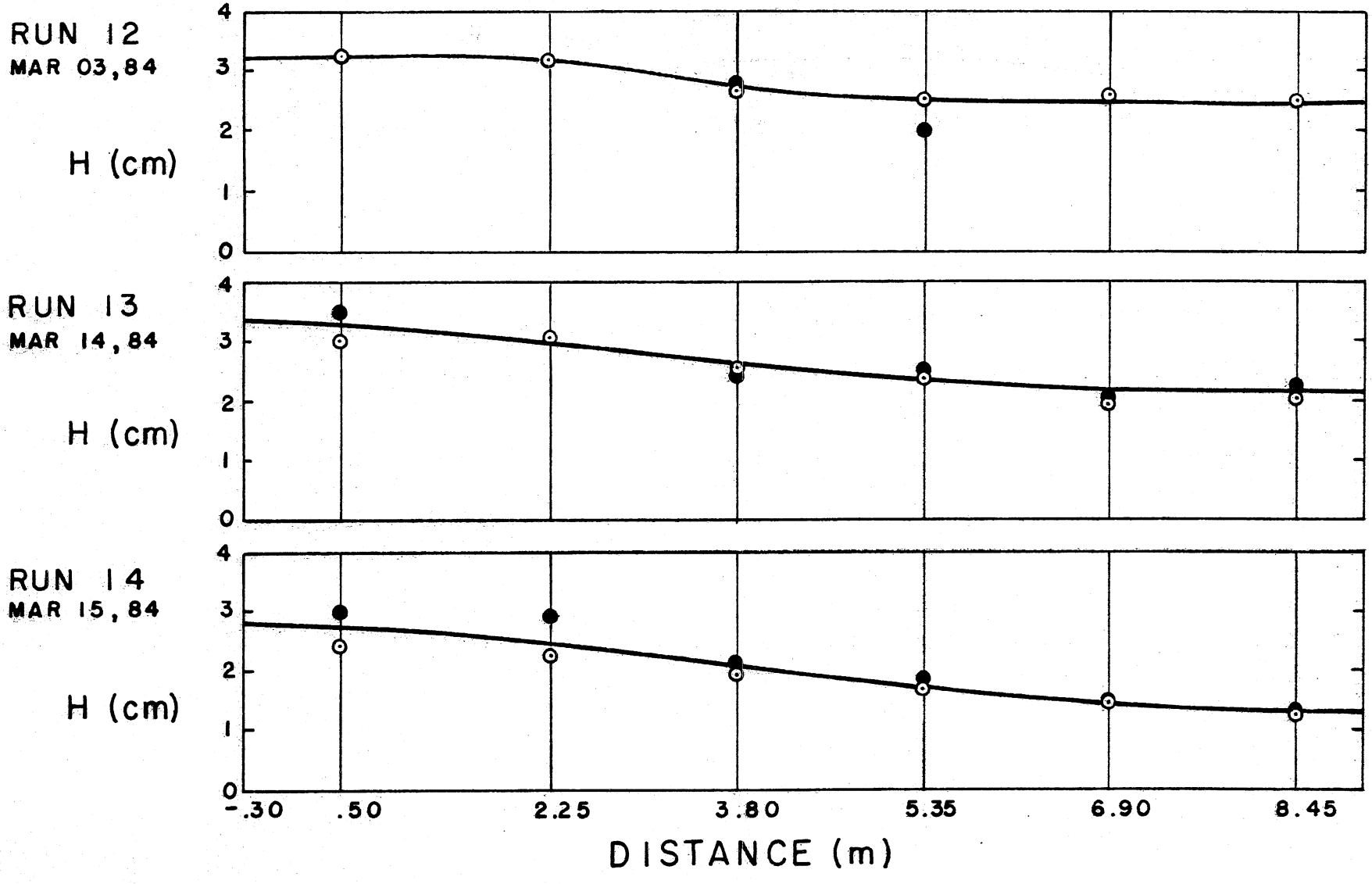

Fig. A2. Wave height versus distance along the channel for RUN 12- RUN 14.

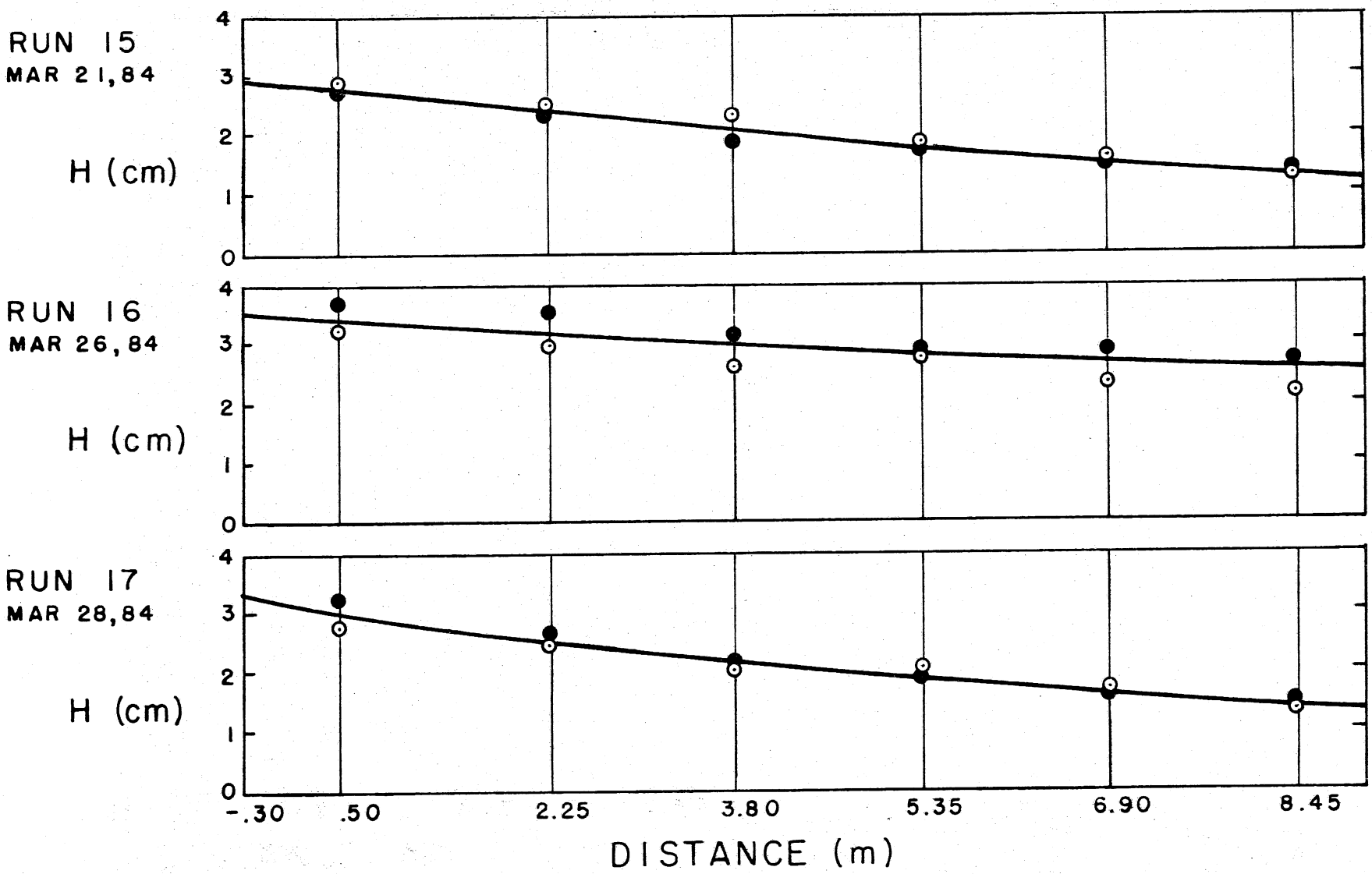

Fig. A3. Wave height versus distance along the channel for RUN 15 - RUN 17.

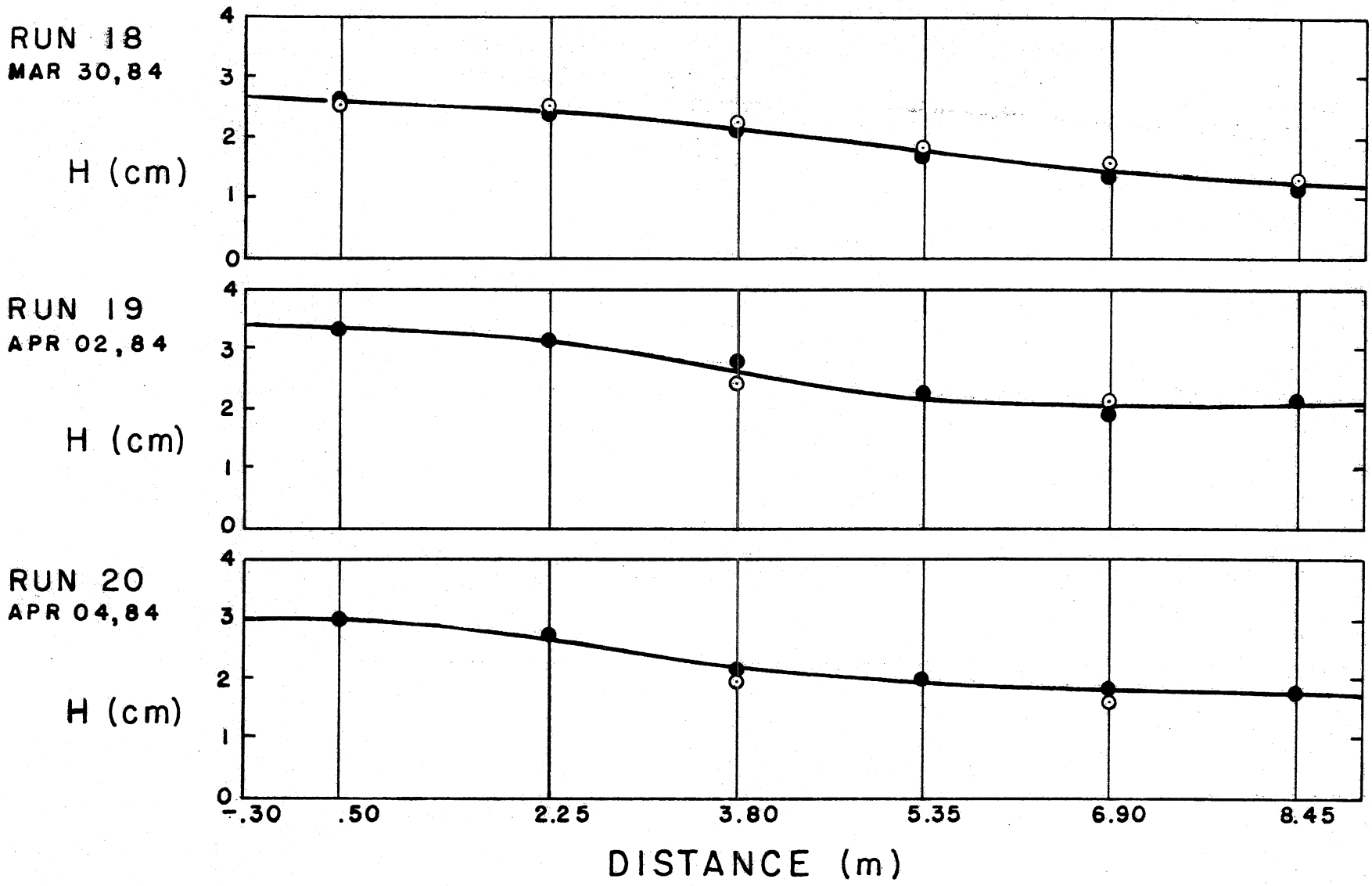

Fig. A4. Wave height versus distance along the channel for RUN 18 - RUN 20.

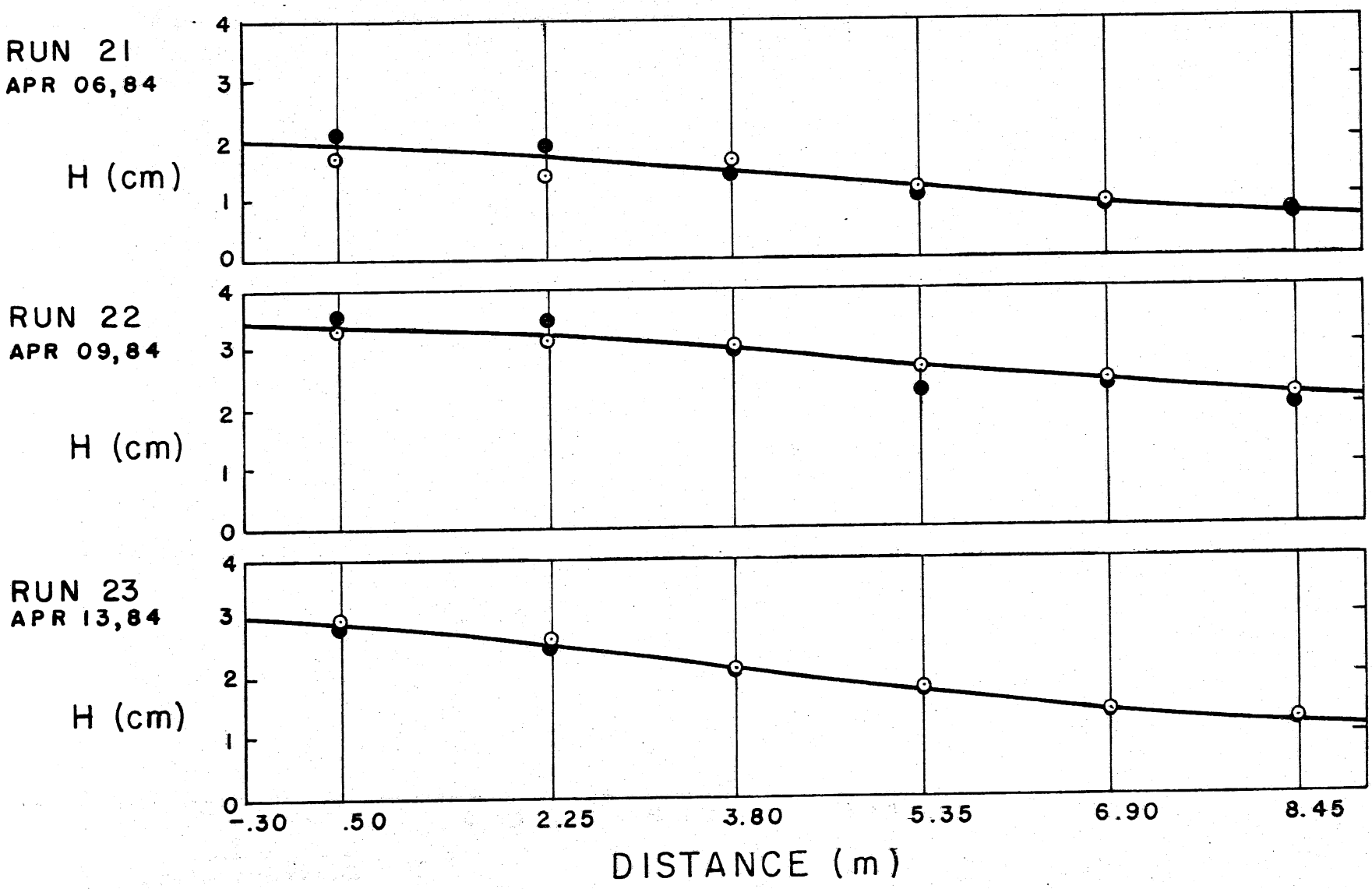

Fig. A5. Wave height versus distance along the channel for RUN 21 - RUN 23.

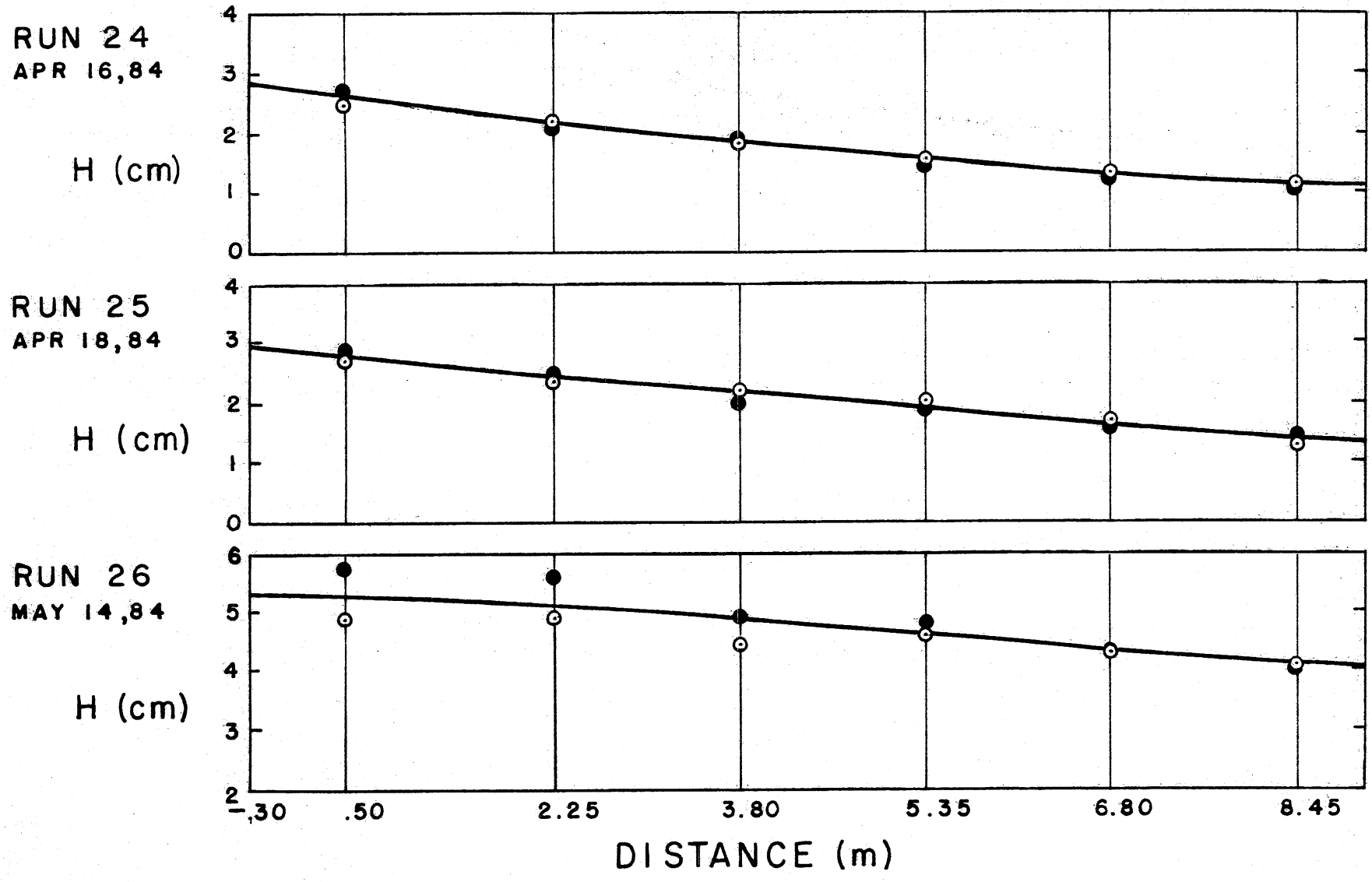

Fig. A6. Wave height versus distance along the channel for RUN 24 - RUN 26.

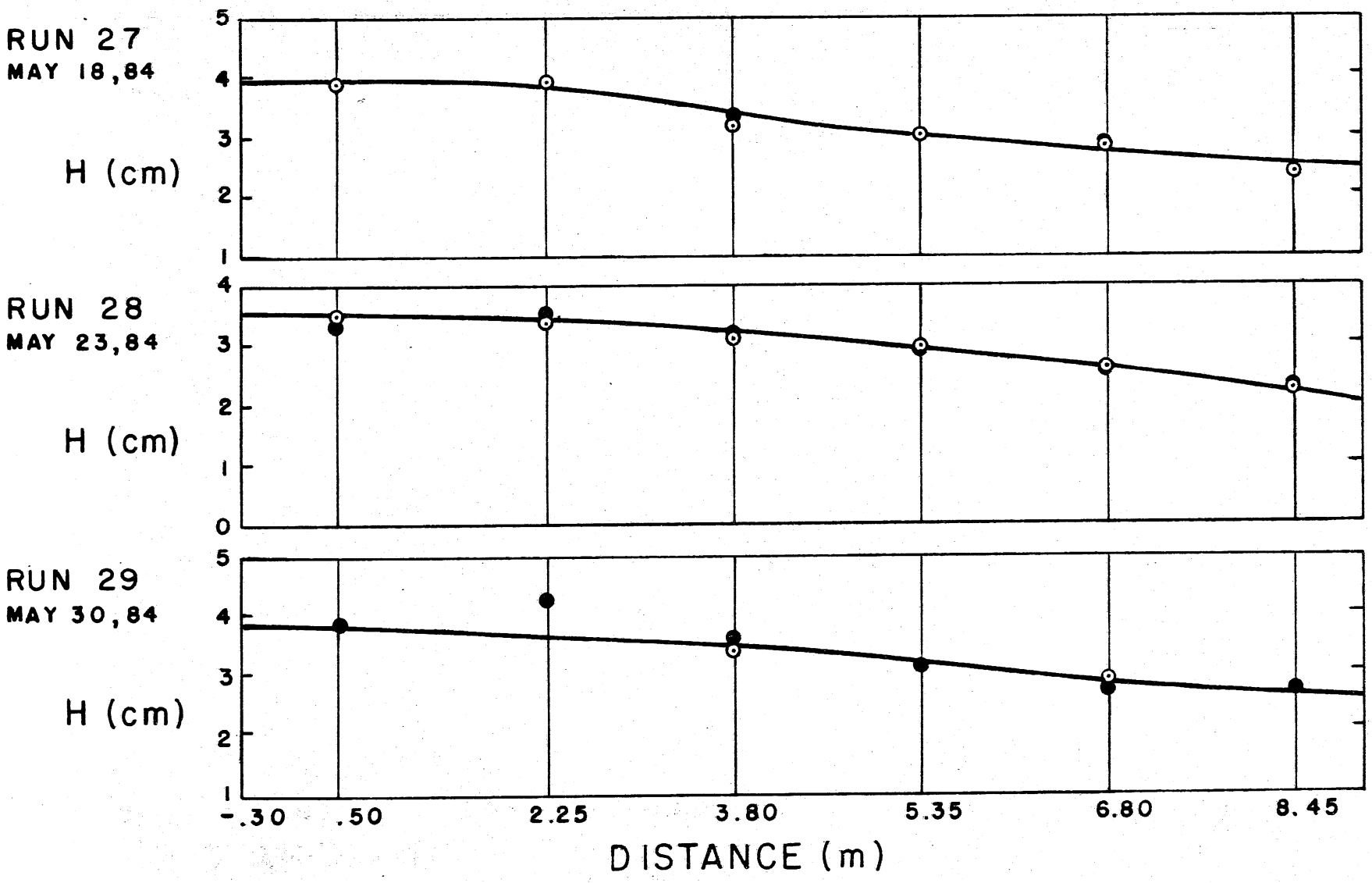

Fig. A7. Wave height versus distance along the channel for RUN 27 - RUN 29.

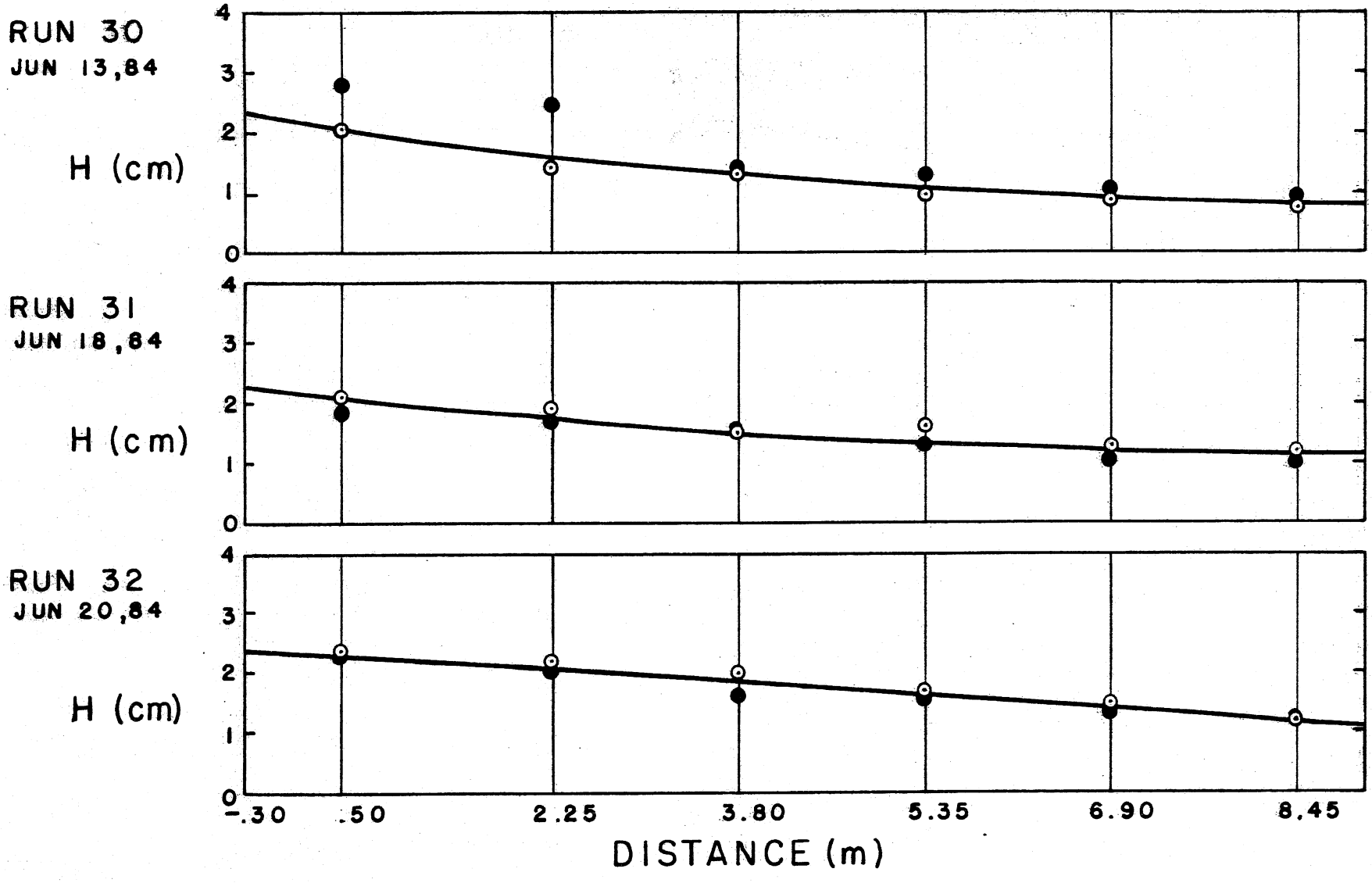

Fig. A8. Wave height versus distance along the channel for RUN 30 - RUN 32.

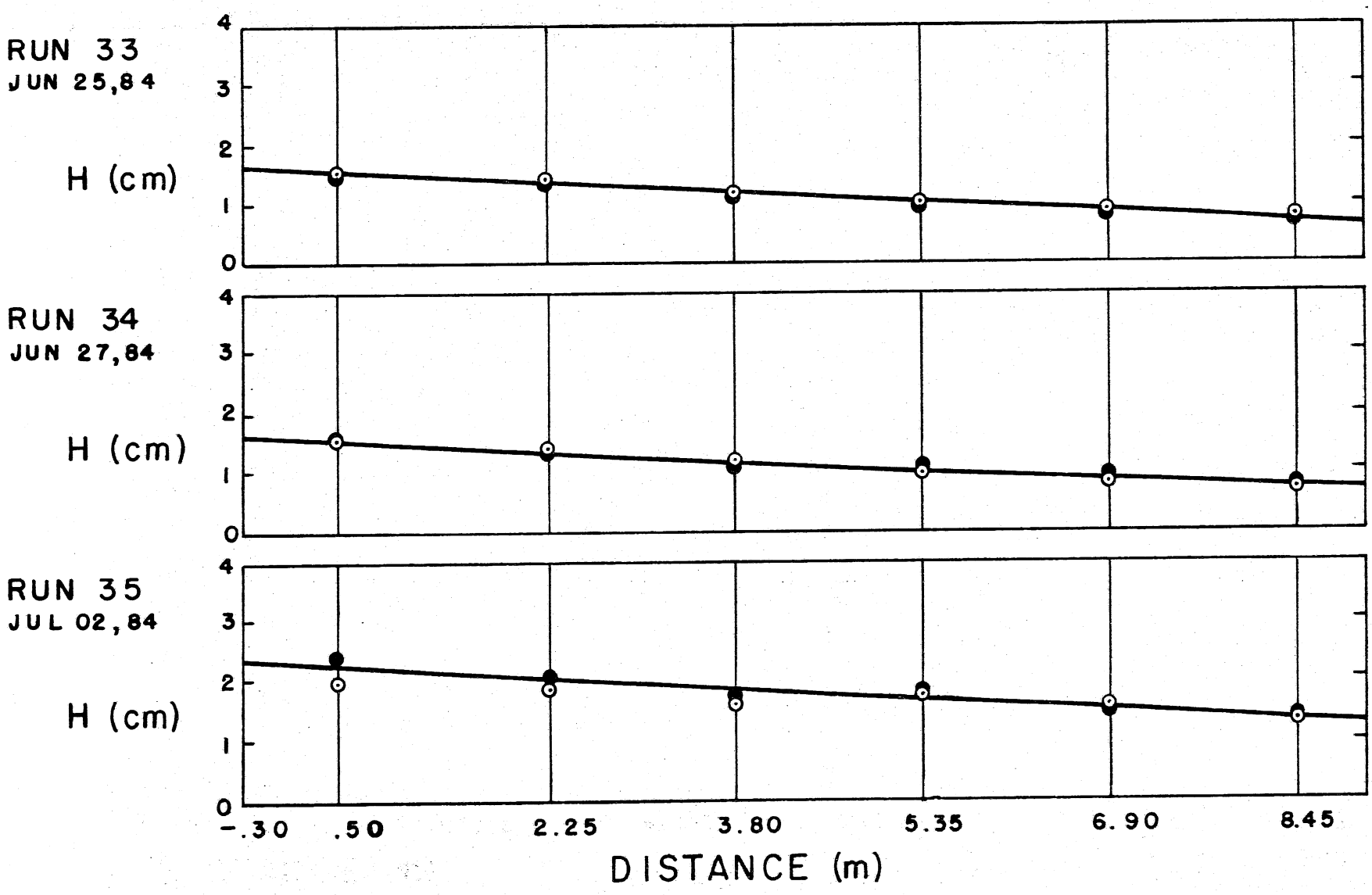

Fig. A9. Wave height versus distance along the channel for RUN 33 - RUN 35.

APPENDIX II

COMPUTER PROGRAMS

AND

COMPUTATIONAL PROCEDURE

APPENDIX II

A. Computational Procedure

1. Longitudinal Dispersion Coefficients

Conductivity values at each sampling point, measured at consecutive times during the experiment, were given in matrix form. In the computer programs, sampling locations were numbered from 1 to 5, but in the output they were printed out as A, B, 1, 2, and 3 following the experimental setup.

Program MAIK was developed to obtain a first estimation of the coefficients K_{ij} using the conductivity data. Equation (54) was used with a forward approximation for the time derivative

$$\frac{\partial k_i}{\partial t} = \frac{k_i(t+\Delta t) - k_i(t)}{\Delta t} \tag{A1}$$

and the arithmetic mean over the time interval Δt (between sampling times) for the values of k_i

$$k_i = \frac{k_i(t+\Delta t) + k_i(t)}{2} \tag{A2}$$

Solving Eq. (54) for $K_{i,i+1}$ we get:

$$K_{i,i+1} = -\frac{1}{k_i - k_{i+1}} \left[L_i \frac{\partial k_i}{\partial t} + K_{i-1,i}(k_i - k_{i-1}) \right] \tag{A3}$$

with $C(1) = K_{i-1,i} = 0$ and $B(5) = K_{i,i+1} = 0$ (no flux condition at the ends) equation (A3) can be written as

$$K_{i,i+1} = -\frac{1}{k_i - k_{i+1}} \sum_{j=1}^{i} L_i \frac{\partial k_i}{\partial t} \tag{A4}$$

Equation (A4) was used in the program for the computation of all K_{ij}'s. Dispersion coefficients were obtained as

$$D_{ij} = K_{ij} L_{ij} \tag{A5}$$

Program ALINE employs the method of successive approximations, minimizing the RMS error between experimental and predicted values of conductivities, for the determination of the horizontal diffusivities.

In Section IV.B it was proved that the conductivity values should satisfy the relation $\bar{k}$ = const. Computations showed that $\bar{k}$ was varying over time. The following could have contributed to the observed unsteadiness:

a) measured k_i values not representative mean values of the chosen control volumes.

b) errors due to temperature adjustment of data (not expected to be important).

c) Non-uniform, although not extensive, leaking along the channel.

Since there was not enough information available to include any of the above in the model, experimental data were adjusted to constant $\bar{k}$ over time. Proportional adjustment was used and $\bar{k}$ of the first sampling time was selected for each experiment. The adjusted values were obtained as:

$$k_i'(t) = k_i(t) \frac{\bar{k}(t_1)}{\bar{k}(t)} \tag{A6}$$

where $k_i'(t)$ = modified conductivity of point i at time t,

$k_i(t)$ = conductivity as obtained from the data file,

t_1 = first sampling time, and

t = any other sampling time.

An initial guess was provided for every coefficient K_{ij}. Then, using the data of the first sampling time as initial condition, conductivity values until the end of the experiment were predicted by Eq. (55). Comparison of the predicted values to the modified data yielded the corresponding RMS error (Eq. 56).

Then, for one coefficient at a time the following procedure is followed: the coefficient is changed to (1 ± AI) times the initial guess (AI = 0.3 was usually used) and the RMS errors are computed for each case to yield a set of three values of the coefficient with corresponding RMS errors. These are used for the prediction of a new value for the coefficient resulting in a smaller RMS error. Depending on the relative position of the above points, either a linear extrapolation (using the steeper slope (S) towards the minimum RMS error point and a relaxation factor) or a second order Langrangian polynomial is fitted and the value minimizing the polynomial is taken as the next guess. The various cases are illustrated in Fig. A10 (a = lowest value of K_{ij}, b = middle value of K_{ij}, c = upper value of K_{ij}). Retaining the new value and the two values used for the

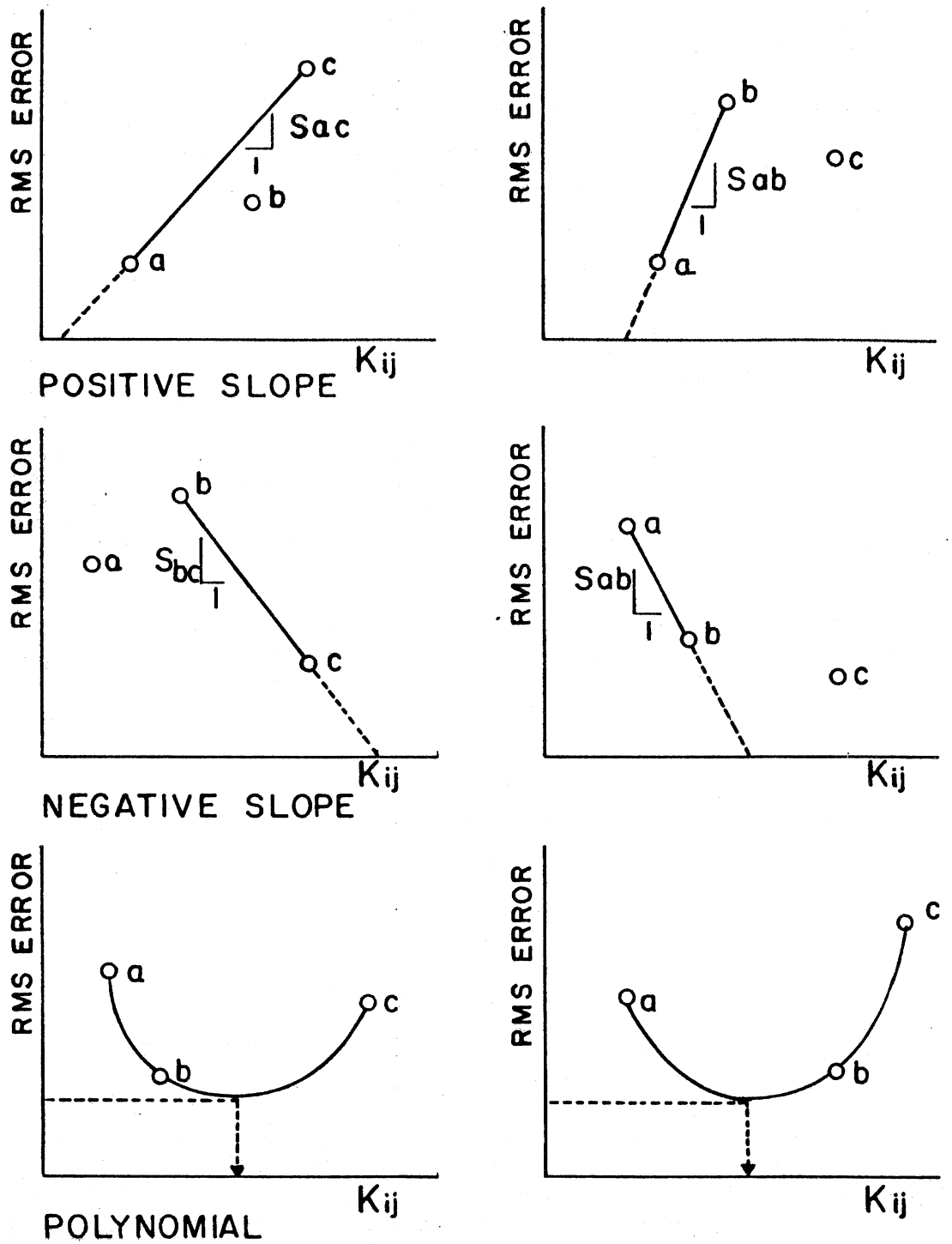

Fig. A10. Illustration of the procedure used to find the value of each dispersion coefficient resulting in min RMS error.

extrapolation or the points on each side of the new value, in the case of the polynomial, a new set is obtained and the same procedure is followed over. New values are restricted within the 1/3 to 3, times the coefficient giving the minimum RMS error, interval to avoid divergence. In the case that the new value coincides with the previous one, a new value, moved ± 10 percent away, is prescribed to allow further search for the minimum RMS error. This procedure is executed ITMAX (usually ITMAX = 5) times for every coefficient (inner iteration) and ITTM times (usually ITTM = 10) for the whole set of the four coefficients (outer iteration).

If after one outer iteration a new minimum value is not found, the computation stops. Moreover, if all coefficients changed, less than 1 percent and lead to less than 1 percent change in the minimum RMS error after one outer iteration, the computation stops. If none of the above conditions is met, the program stops after ITTM outer iterations. (This did not happen in most cases.)

When computation stops, the set of K_{ij} is printed out along with the RMS error and the predicted and modified data for this set. For the predictions a time step Δt = 1 min (or Δt = 0.5 min in some cases) is used.

Program ISSY combines the two previous programs. MAIK is included as a subroutine and is executed twice: once for the experimental data and once for the modified data and the computed K_{ij}'s are printed out. At this point the program stops and K_{ij}'s should be provided by the user. Usually K_{ij}'s as computed from the modified data, or a value between the K_{ij} from experimental and modified data was provided as initial guess. The computation continues as described for ALINE.

In Table A6 computed dispersion coefficients D_{AB}, D_{B1}, D_{12}, D_{23} and the values of H^2/T at points B, B-1, 1-2, 2-3, respectively, are given for RUN 26 through RUN 35. Predicted dispersion coefficients from equation (61) are also given in the same table.

In Table A7 values of H^2/T and predicted diffusivities (Eq. 61) are given for the rest of the experiments (RUN 9 - RUN 25).

TABLE A6. COMPUTED AND PREDICTED (USING EQUATION 61) DISPERSION COEFFICIENTS FOR RUN 26 THROUGH RUN 35

	RUN	Computed Dispersion Coefficient (m^2/s)	$H^2 \cdot f$ (m^2/s)	Dispersion Coefficient from Eq. 61	$\frac{D_{ij}comp}{D_{ij}pred}$
D_{AB}	26	7.34×10^{-3}	4.70×10^{-3}	5.71×10^{-3}	1.30
	27	1.65×10^{-3}	3.23×10^{-3}	3.92×10^{-3}	0.42
	28	9.40×10^{-3}	2.43×10^{-3}	2.95×10^{-3}	3.19
	29	2.05×10^{-2}*	2.87×10^{-3}	3.49×10^{-3}	5.87
	30	1.01×10^{-3}	1.28×10^{-3}	1.56×10^{-3}	0.65
	31	1.40×10^{-3}	1.22×10^{-3}	1.48×10^{-3}	0.95
	32	1.80×10^{-3}	1.28×10^{-3}	1.56×10^{-3}	1.15
	33	4.62×10^{-3}*	6.72×10^{-4}	8.16×10^{-4}	5.66
	34	2.23×10^{-3}	6.32×10^{-4}	7.68×10^{-4}	2.90
	35	1.06×10^{-3}	1.10×10^{-3}	1.34×10^{-3}	0.79
D_{B1}	26	5.41×10^{-3}	4.61×10^{-3}	5.60×10^{-3}	0.97
	27	4.92×10^{-3}	3.15×10^{-3}	3.83×10^{-3}	1.28
	28	4.78×10^{-3}	2.43×10^{-3}	2.95×10^{-3}	1.62
	29	5.10×10^{-3}	2.79×10^{-3}	3.39×10^{-3}	1.50
	30	9.16×10^{-4}	9.75×10^{-4}	1.18×10^{-3}	0.78
	31	1.00×10^{-3}	9.73×10^{-4}	1.18×10^{-3}	0.85
	32	9.35×10^{-4}	1.17×10^{-3}	1.42×10^{-3}	0.66
	33	1.40×10^{-3}	6.31×10^{-4}	7.67×10^{-4}	1.83
	34	1.20×10^{-3}	5.92×10^{-4}	7.19×10^{-4}	1.67
	35	6.66×10^{-4}	1.01×10^{-3}	1.23×10^{-3}	0.54
D_{12}	26	4.65×10^{-3}	3.94×10^{-3}	4.79×10^{-3}	0.97
	27	4.15×10^{-3}	2.33×10^{-3}	2.83×10^{-3}	1.47
	28	3.72×10^{-3}	2.03×10^{-3}	2.47×10^{-3}	1.51
	29	3.94×10^{-3}	2.37×10^{-3}	2.88×10^{-3}	1.37
	30	7.87×10^{-4}	3.92×10^{-4}	4.76×10^{-4}	1.65
	31	1.34×10^{-3}	4.87×10^{-4}	5.92×10^{-4}	2.26
	32	1.09×10^{-3}	8.34×10^{-4}	1.01×10^{-3}	1.08
	33	1.01×10^{-3}	3.78×10^{-4}	4.59×10^{-4}	2.20
	34	1.02×10^{-3}	3.79×10^{-4}	4.60×10^{-4}	2.22
	35	1.47×10^{-3}	6.80×10^{-4}	8.26×10^{-4}	1.78
D_{23}	26	3.50×10^{-3}	3.04×10^{-3}	3.69×10^{-3}	0.95
	27	3.05×10^{-3}	1.58×10^{-3}	1.92×10^{-3}	1.59
	28	1.97×10^{-3}	1.34×10^{-3}	1.63×10^{-3}	1.21
	29	2.37×10^{-3}	1.57×10^{-3}	1.91×10^{-3}	1.24
	30	3.00×10^{-3}*	1.88×10^{-4}	2.28×10^{-4}	13.16
	31	4.06×10^{-3}*	3.33×10^{-4}	4.05×10^{-4}	10.02
	32	6.45×10^{-4}	4.86×10^{-4}	5.90×10^{-4}	1.09
	33	3.10×10^{-4}	2.13×10^{-4}	2.59×10^{-4}	1.20
	34	1.00×10^{-2}*	2.13×10^{-4}	2.59×10^{-4}	38.61
	35	3.82×10^{-3}*	4.47×10^{-4}	5.43×10^{-4}	7.03

*Values excluded in correlations.

TABLE A7. PREDICTED DIFFUSIVITIES AND MEASURED VALUES OF H^2/T FOR RUN 9 THROUGH RUN 25.

RUN	$\frac{H^2}{T}\|_B$ (m/s)	$\frac{H^2}{T}\|_{B-1}$ (m/s)	$\frac{H^2}{T}\|_{1-2}$ (m/s)	$\frac{H^2}{T}\|_{2-3}$ (m/s)	D_{AB} (m/s)	D_{B1} (m/s)	D_{12} (m/s)	D_{23} (m/s)
9	1.77×10^{-3}	1.53×10^{-3}	9.51×10^{-4}	5.79×10^{-4}	2.15×10^{-3}	1.86×10^{-3}	1.56×10^{-3}	7.03×10^{-4}
10	1.64×10^{-3}	1.10×10^{-3}	4.42×10^{-4}	2.12×10^{-4}	1.99×10^{-3}	1.34×10^{-3}	5.37×10^{-4}	2.58×10^{-4}
11	3.23×10^{-3}	3.16×10^{-3}	2.81×10^{-3}	2.55×10^{-3}	3.92×10^{-3}	3.84×10^{-3}	3.41×10^{-3}	3.10×10^{-3}
12	2.03×10^{-3}	2.03×10^{-3}	1.45×10^{-3}	1.15×10^{-3}	2.47×10^{-3}	2.47×10^{-3}	1.76×10^{-3}	1.40×10^{-3}
13	1.80×10^{-3}	1.74×10^{-3}	1.16×10^{-3}	7.99×10^{-4}	2.19×10^{-3}	2.11×10^{-3}	1.41×10^{-3}	9.71×10^{-4}
14	1.80×10^{-3}	1.67×10^{-3}	1.01×10^{-3}	5.16×10^{-4}	2.19×10^{-3}	2.03×10^{-3}	1.23×10^{-3}	6.27×10^{-4}
15	1.91×10^{-3}	1.66×10^{-3}	1.00×10^{-3}	5.11×10^{-4}	2.32×10^{-3}	2.02×10^{-3}	1.22×10^{-3}	6.21×10^{-4}
16	2.04×10^{-3}	1.92×10^{-3}	1.41×10^{-3}	1.13×10^{-3}	2.48×10^{-3}	2.33×10^{-3}	1.71×10^{-3}	1.37×10^{-3}
17	2.47×10^{-3}	1.97×10^{-3}	1.05×10^{-3}	5.80×10^{-4}	3.00×10^{-3}	2.39×10^{-3}	1.28×10^{-3}	7.05×10^{-4}
18	1.63×10^{-3}	1.51×10^{-3}	1.08×10^{-3}	5.03×10^{-4}	1.98×10^{-3}	1.83×10^{-3}	1.31×10^{-3}	6.11×10^{-4}
19	1.79×10^{-3}	1.74×10^{-3}	1.08×10^{-3}	7.03×10^{-4}	2.17×10^{-3}	2.11×10^{-3}	1.31×10^{-3}	8.54×10^{-4}
20	1.72×10^{-3}	1.72×10^{-3}	9.24×10^{-4}	6.18×10^{-4}	2.09×10^{-3}	2.09×10^{-3}	1.12×10^{-3}	7.51×10^{-4}
21	1.06×10^{-3}	1.01×10^{-3}	5.58×10^{-4}	2.15×10^{-4}	1.29×10^{-3}	1.23×10^{-3}	6.78×10^{-4}	2.61×10^{-4}
22	2.31×10^{-3}	2.31×10^{-3}	1.80×10^{-3}	1.15×10^{-3}	2.81×10^{-3}	2.81×10^{-3}	2.19×10^{-3}	1.40×10^{-3}
23	2.05×10^{-3}	1.92×10^{-3}	1.11×10^{-3}	4.47×10^{-4}	2.49×10^{-3}	2.33×10^{-3}	1.35×10^{-3}	5.43×10^{-4}
24	1.81×10^{-3}	1.51×10^{-3}	7.92×10^{-4}	3.62×10^{-4}	2.20×10^{-3}	1.83×10^{-3}	9.62×10^{-4}	4.40×10^{-4}
25	2.01×10^{-3}	1.81×10^{-3}	1.12×10^{-3}	6.29×10^{-4}	2.44×10^{-3}	2.20×10^{-3}	1.36×10^{-3}	7.64×10^{-4}

2. Program MARKOS

Program MARKOS does not perform any iterations or computations of the coefficients. When coefficients are specified and exerpimental data provided, MARKOS predicts the values of ϕ until the end of the experiment and computes the RMS error of all data points together and of each sampling location. MARKOS can be used for conductivities as well as for oxygen concentration. Saturation concentration C'_s and water depth h should be given also in the case of conductivity, although they are not used in the computation.

In the case of conductivities RMS errors of experimental and modified data compared to predicted values are obtained. The RMS errors for conductivity measurements are given in Table A8 for the following cases:

a) D_{ij} computed from the minimum RMS error procedure.

b) D_{ij} predicted using Eq. (61).

c) D_{ij} predicted from the following equation

$$D_{ij} = 1.36\ H^2 \cdot f + 3.21 \times 10^{-4} \quad (r^2 = 0.619) \qquad \text{(A7)}$$

The difference in RMS errors for cases b and c is very small. Equation (61) was preferred for use, since it involves no constant term. Moreover, both the average and the standard deviation of the RMS errors in conductivity are smaller when Eq. (61) is used (7.04, 2.96, respectively), than the ones when Eq. (A7) is used (7.25, 3.06).

MARKOS can be used for testing various correlations either for D_{ij} or K_{Li} by comparing the resulting RMS errors of the experiments.

3. Oxygen Transfer Coefficients

The oxygen transfer coefficients were computed using Eq. (54) and a desk calculator as described in Section IV.D. Variable saturation concentration (due to varying water temperature) and decreasing water depth, as obtained from the experimental data, were used in the computations. Computations were performed using computed D_{ij}'s for RUN 26 - RUN 35 and predicted values of D_{ij}'s from Eq. (61) for all experiments.

Further, program MARKOS, assuming a mean depth and a mean saturation concentration, was used to compute RMS errors for oxygen concentrations for the following cases:

1) Dispersion coefficients as computed from the minimum RMS error procedure and oxygen transfer coefficients computed as described above (RUN 26 - RUN 35).

2) Dispersion coefficients from Eq. (61) and oxygen transfer coefficients computed with this assumption using oxygen data.

TABLE A8. RMS ERROR AS A PERCENT OF MEAN CONDUCTIVITY FOR THE EXPERIMENTAL AND MODIFIED ($\bar{k}$ = CONSTANT) DATA

	EXPERIMENTAL DATA			MODIFIED DATA ($\bar{k}$ = constant)		
	D_{ij}	D_{ij}	D_{ij}	D_{ij}	D_{ij}	D_{ij}
RUN	Computed	Eq. A7	Eq. 61	Computed	Eq. A7	Eq. 61
26	5.88	5.24	6.10	2.57	3.70	2.97
27	3.56	8.42	8.23	1.87	7.82	7.29
28	2.76	7.65	10.42	1.78	6.68	9.33
29	1.61	4.63	6.69	0.98	4.65	6.76
30	11.13	11.70	11.83	4.68	10.34	7.49
31	5.29	7.31	6.17	3.01	7.39	4.65
32	1.31	5.60	3.26	0.82	5.09	2.76
33	5.43	9.00	14.52	2.54	6.68	12.07
34	7.65	8.92	13.87	3.38	4.62	9.33
35	9.13	12.85	10.41	5.61	13.40	9.86

TABLE A9. RMS ERROR AS A PERCENT OF MEAN OXYGEN CONCENTRATION FOR EXPERIMENTAL DATA

RUN	Mean Oxygen Concentration (mg/ℓ)	Predicted D_{ij} Computed K_L (%)	Predicted D_{ij} Predicted K_L (%)	Computed D_{ij} Computed K_L (%)
9	6.41	2.21	9.05	
10	6.41	1.99	6.55	
11	7.63	1.39	2.62	
12	5.98	2.44	4.85	
13	5.10	3.62	12.55	
14	6.46	2.87	8.51	
15	6.62	2.39	5.44	
16	5.18	2.95	4.05	
17	6.75	2.60	12.44	
18	6.18	2.57	6.31	
19	4.70	4.26	17.45	
20	5.38	2.63	12.09	
21	6.65	3.82	6.92	
22	7.36	1.27	5.02	
23	6.37	1.94	12.87	
24	6.24	1.49	12.66	
25	6.81	2.93	7.49	
26	8.31	1.58	3.37	1.60
27	6.62	3.85	6.04	1.89
28	6.89	3.08	7.84	3.48
29	7.18	1.69	5.16	1.85
30	*	*	*	*
31	*	*	*	*
32	5.51	3.62	9.25	3.58
33	*	*	*	*
34	4.68	4.12	6.20	3.32
35	5.10	2.61	7.85	2.67

*Not enough oxygen data available for computation of the RMS error.

3) Dispersion coefficients from Eq. (61) and oxygen transfer coefficients from Eq. (63) for the main portion of the channel and $K_{LA} = K_{LB}$. These are the results given in Fig. 19, but here the RMS error is given a percentage of the mean oxygen concentration.

Results are given in Table A9.

LIST OF FORTRAN VARIABLES

A(5)	coefficient of ϕ_i in the TDMA algorithm
AA	relaxation factor
ADD	coefficient of the reaeration term
AI	factor used in determining the first set of values in the iteration procedure to find K_{ij}
AL(5)	length of control volume
ALS	sum of lengths of all control volumes
AMD	determines the time step in the printout
B(5)	coefficient of ϕ_{i+1} in the TDMA algorithm
C(5)	coefficient of ϕ_{i-1} in the TDMA algorithm
CEX(5,35)	experimental data, first index denotes sampling location and second sampling time
CM(35)	mean conductivity for each experimental time
CMS	the sum $\sum_{i=1}^{5} k_i L_i$
CON(5)	i in in the TDMA algorithm
CDIF	the difference $k_i - k_{i+1}$ as defined by equations A1, A2
CS	saturation concentration value
D(5)	constant term of the discretization equation in in the TDMA algorithm
DT	time step of the computation
H	water depth
HK(0:5)	coefficients K_{ij}.[HK(0)=HK(5)=0 for the no flux conditions at the ends]
HKC	K_{ij} of point b (mid value of K_{ij})
HKI(4)	K_{ij} values giving minimum RMS error during one iteration
HKM(4)	K_{ij} values giving minimum RMS error, obtained throughout the computational procedure
HKN	K_{ij} of point c (higher value of K_{ij})
HKP	K_{ij} of point a (lower value of K_{ij})
HKR(5)	reaeration coefficients K_{Li}
I	temporary index-denotes distance along the channel in subroutine SOLVE
IA(35)	counter of experimental data sets
IC,II	temporary index

IT	counter of inner iterations
ITER	iteration counter
ITMAX	maximum number of outer iterations
ITT	counter of inner iterations
ITTM	maximum number of outer iterations
J	temporary index-denotes time in SOLVE
JMAX	largest value of J for which computation is performed
K,L	temporary index
NI(5)	-used in SOLVE as a counter of values used in the computation of the RMS error for each sampling location -used in subroutine MAIK as a counter of values of K_{ij} used to compute the first estimate of K_{ij}
NM	temporary storage of N
N	number of experimental data sets
NN	counter in the computation of the RMS error
NR	code number of experimental run
OXY	when OXY=1 the reaeration term is included in the computation if OXY $\neq$ 1, $K_{Li} = 0$, i =1, 5
P(5), Q(5)	transformed coefficients in the TDMA algorithm
R	RMS error
RC	RMS error for point b
RE(5)	same as SES but for every sampling location
REF	for REF = 1 experimental data are printed out along with predicted values for the minimum RMS error case
RIM	minimum RMS error obtained during one outer iteration
RM	minimum error obtained during the whole procedure
RM(5)	same as SK but for each sampling location
RN	RMS error for point c
RP	RMS error for point a
SES	sum of squared differences between experimental and predicted values
SK	sum of experimental values
SLCN	slope Sbc
SLM	min or max slope
SLPC	slope Sab

SLPN	slope Sac
SSUM	the term $\sum_{j=1}^{i} L_i \, \partial k_i / \partial t$ in equation A4
SUM(J)	sum of all positive values of K_{ij} obtained with subroutine MAIK
TEX(35)	experimental time (sampling time)
TIME	temporary value of computational time
TIMEX	temporary value of experimental time
TMAX	maximum time for which prediction is computed

LAGPOL subroutine

AP, BP, CP	coefficients a, b, c of polynomial $ax^2 + bx + c$
HKI	value minimizing the polynomial
F(I), X(I)	values for the RMS error and K_{ij} of points a, b, c (I = 1, 3)
PP(I)	variable used in the computation of the coefficients AP, BP, CP

OUTPUT

C(A), C(B), C(1), C(2), C(3)	values of oxygen concentration at points A, B, 1, 2, 3 respectively
K(A), K(B), K(1), K(2), K(3)	values of conductivities at points A, B, 1, 2, 3 respectively
KAB, KB1, K12, K23	coefficients K_{AB}, K_{B1}, K_{12}, K_{23} (Note: $K_{ij} = D_{ij} / L_{ij}$)
KRA, KRB, KR1, KR2, KR3	oxygen transfer coefficients K_{LA}, K_{LB}, K_{L1}, K_{L2}, K_{L3}

PROGRAM MAIK

```
00100 PROGRAM MAIK(DATINA,OUTPUT,TAPE5=DATINA,TAPE6=OUTPUT)
00110 DIMENSION AL(5),HK(4),CEX(5,20),TEX(20),IA(20),SUM(4),NI(4)
00120 DATA AL /1.715,1.00,3.10,3.10,3.223/
00130C
00140 READ(5,1000)NR
00150 READ(5,1000)N
00160 READ(5,1100)((IA(I),TEX(I),(CEX(J,I),J=1,5)),I=1,N)
00170 WRITE(6,1200) NR,N
00180 WRITE(6,1500)
00190 WRITE(6,1100)((IA(I),TEX(I),(CEX(J,I),J=1,5)),I=1,N)
00200 WRITE(6,1600)
00210 1000 FORMAT(I4)
00220 1100 FORMAT(I4,F6.1,5F7.0)
00230 1200 FORMAT(/5X,'RUN',I4//5X,'N=',I2)
00240 1300 FORMAT(5X,F4.0)
00250 1400 FORMAT(9X,4E15.4)
00260 1500 FORMAT(/6X,'TIME',3X,'K(A)',3X,'K(B)',3X,'K(1)',3X,'K(2)',
00270+3X,'K(3)')
00280 1600 FORMAT(//5X,'TIME',8X,'KAB',12X,'KB1',12X,'K12',12X,'K23'/)
00290 1700 FORMAT(/5X,'MEAN VALUES'/)
00300C-----------------------------------------------------------------
00310 DO 400 J=1,4
00320 SUM(J)=0.
00330 400 NI(J)=0
00340C
00350 DO 200 I=2,N
00360 SSUM=0.
00370 WRITE(6,1300) TEX(I-1)
00380 DO 100 J=1,4
00390 SSUM=SSUM+AL(J)*(CEX(J,I)-CEX(J,I-1))/(TEX(I)-TEX(I-1))/60.
00400 CDIF=(CEX(J,I)+CEX(J,I-1)-(CEX(J+1,I)+CEX(J+1,I-1)))/2.
00410 HK(J)=-SSUM/CDIF
00420 100 CONTINUE
00430 WRITE(6,1400) (HK(L),L=1,4)
00440 DO 300 J=1,4
00450 IF(HK(J).LT.0.) GOTO 300
00460 SUM(J)=SUM(J)+HK(J)
00470 NI(J)=NI(J)+1
00480 300 CONTINUE
00490 200 CONTINUE
00500 WRITE(6,1300) TEX(N)
00510 DO 500 J=1,4
00520 500 HK(J)=SUM(J)/FLOAT(NI(J))
00530 WRITE(6,1700)
00540 WRITE(6,1400)(HK(L),L=1,4)
00550 STOP
00560 END
```

PROGRAM ALINE

```
00100 PROGRAM INA(DATINA,INPUT,OUTPUT,TAPE5=DATINA,TAPE6=OUTPUT,
00110+TAPE1=INPUT)
00120 DIMENSION HKI(4),CM(20)
00130 COMMON /D/ AL(5),HK(0:5),HKM(4)
00140 COMMON /TD/ A(5),B(5),C(5),D(5),Q(5),P(5),CON(5)
00150 COMMON /V/ CEX(5,20),TEX(20),IA(20)
00160 COMMON /V1/ JMAX,N,DT,REF,RP,RC,RN,R,RM,AA,IC,AI
00170 COMMON /LAG/ HKP,HKC,HKN
00180 DATA AL,RIM /1.715,1.00,3.10,3.10,3.223,1.E+05/
00190 DATA AA,AI,REF,HK(0),HK(5)/0.70,.3,3*0./
00200 DATA DT,ITMAX,ITTM /1.00,05,10/
00210C-----------------------------------------------------------------
00220 REWIND 5
00230 READ(5,1000) NR
00240 READ(5,1000) N
00250 READ(5,1100)((IA(I),TEX(I),(CEX(J,I),J=1,5)),I=1,N)
00260 READ(1,*) (HK(I),I=1,4)
00270 WRITE(6,1700) ITMAX,AA   ,AI   ,DT
00280 WRITE(6,1200) NR,N
00290 WRITE(6,1400)
00300 WRITE(6,1100)((IA(L),TEX(L),(CEX(J,L),J=1,5)),L=1,N)
00310C
00320 1000 FORMAT(I4)
00330 1100 FORMAT(I4,F6.1,5F7.0)
00340 1200 FORMAT(/5X,'RUN',I4//5X,'N=',I2//5X,'EXPERIMENTAL DATA'/)
00350 1400 FORMAT(/6X,'TIME',3X,'K(A)',3X,'K(B)',
00360+3X,'K(1)',3X,'K(2)',3X,'K(3)'/)
00370 1401 FORMAT(//5X,'MODIFIED DATA'/)
00380 1500 FORMAT(//5X,'ITER',8X,'KAB',7X,'KB1',7X,'K12',
00390+7X,'K23',7X,'RMS'/)
00400 1600 FORMAT(5X,2I4,4E10.4,E12.5)
00410 1700 FORMAT(//5X,'ITMAX=',I3/5X,'AA  =',F4.2/5X,'AI    =',F4.2/
00420+5X,'DT  =',F4.2//)
00430 1800 FORMAT(/5X,'RMS ERROR=',F6.4,'  PERCENT'/)
00440 1900 FORMAT(5X,'KAB=',E10.4/5X,'KB1=',E10.4/5X,'K12=',E10.4/
00450+5X,'K23=',E10.4/)
00460 2000 FORMAT (5X,60(1H-))
00470 2010 FORMAT (1X,'ITT=',I3)
00480C-----------------------------------------------------------------
00490C
00500 ALS=0.
00510 DO 101 J=1,5
00520 101 ALS=ALS+AL(J)
00530 DO 102 I=1,N
00540 CMS=0.
00550 DO 103 J=1,5
00560 103 CMS=CMS+CEX(J,I)*AL(J)
00570 102 CM(I)=CMS/ALS
00580 DO 105 I=1,N
00590 DO 105 J=1,5
00600 105 CEX(J,I)=CEX(J,I)*CM(1)/CM(I)
00610 WRITE(6,1401)
00620 WRITE(6,1400)
00630 WRITE(6,1100) (IA(L),TEX(L),(CEX(J,L),J=1,5),L=1,N)
00640 WRITE(6,1500)
00650C
00660 TMAX=TEX(N)+5
00670 JMAX=INT(TMAX/DT)
00680 ITER=0 $  IT=0
00690 CALL SOLVE
00700 WRITE(6,1600) ITER,IT,(HK(I),I=1,4),R
00710 RP=R
00720 RM=R
00730C---------------- ITERATIONS ----------------------------
00740 DO 100 ITT=1,ITTM
00750 IF(ITT.EQ.1) GOTO 190
```

```
00760 DO 120 K=1,4
00770 120 HKI(K)=HKM(K)
00780 190 RIM=RM
00790 WRITE(6,2010) ITT
00800 DO 110 IC=1,4
00810 HKC=HK(IC)
00820 HKP=(1-AI)*HK(IC)
00830 HKN=(1+AI)*HK(IC)
00840 HK(IC)=HKC
00850 CALL SOLVE
00860 RC=R  $  ITER=ITER+1
00870 WRITE(6,1600) ITER,IT,(HK(I),I=1,4),R
00880 HK(IC)=HKP
00890 CALL SOLVE
00900 RP=R  $  ITER=ITER+1
00910 WRITE(6,1600) ITER,IT,(HK(I),I=1,4),R
00920 HK(IC)=HKN
00930 CALL SOLVE
00940 RN=R  $  ITER=ITER+1
00950 DO 200 IT=1,ITMAX
00960 IF(IT.EQ.1) GO TO 3000
00970 ITER=ITER+1
00980 IF(RP.GT.RC.AND.RN.GT.RC) THEN
00990 CALL LAGPOL  $ GOTO 3000
01000 ELSE
01010 SLPC=(RC-RP)/(HKC-HKP)
01020 SLCN=(RN-RC)/(HKN-HKC)
01030 SLPN=(RN-RP)/(HKN-HKP)
01040 IF(SLPN.GT.0.) GO TO 2600
01050 IF(SLPN.LT.0.) GO TO 2700
01060 ENDIF
01070C
01080 2600 SLM=AMAX1(SLPC,SLCN,SLPN)
01090 IF(SLM.EQ.SLPC) THEN
01100 RN=RC  $  HKN=HKC
01110 RC=RP  $  HKC=HKP
01120 ELSEIF (SLM.EQ.SLPN) THEN
01130 RC=RP  $  HKC=HKP
01140 ENDIF
01150C
01160 HKP=HKC-AA*RC/SLM
01170 IF(HKP/HK(IC).GT.3.) HKP=3.*HK(IC)
01180 IF(HKP/HK(IC).LT.(1./3.)) HKP=HK(IC)/3.
01190 IF(HKP.EQ.HK(IC)) HKP=0.90*HK(IC)
01200 HK(IC)=HKP
01210 CALL SOLVE
01220 RP=R
01230 GOTO 3000
01240C
01250 2700 SLM=AMIN1(SLPC,SLCN,SLPN)
01260 IF(SLM.EQ.SLCN) THEN
01270 RP=RC  $HKP=HKC
01280 RC=RN  $  HKC=HKN
01290 ELSEIF (SLM.EQ.SLPN) THEN
01300 RC=RN  $  HKC=HKN
01310 ENDIF
01320C
01330 HKN=HKC-AA*RC/SLM
01340 IF(HKN/HK(IC).GT.3.) HKN=3.*HK(IC)
01350 IF(HKN/HK(IC).LT.1./3.) HKN=HK(IC)/3.
01360 IF(HKN.EQ.HK(IC)) HKN=1.1*HK(IC)
01370 HK(IC)=HKN
01380 CALL SOLVE
01390 RN=R
01400C
01410 3000 RM=AMIN1(RP,RC,RN,RM)
```

```
01420 IF(RM.EQ.RP) HKM(IC)=HKP
01430 IF(RM.EQ.RC) HKM(IC)=HKC
01440 IF(RM.EQ.RN) HKM(IC)=HKN
01450 WRITE(6,1600) ITER,IT,(HK(I),I=1,4),R
01460 200 CONTINUE
01470 HK(IC)=HKM(IC)
01480 WRITE(6,2000)
01490 110 CONTINUE
01500 IF(ITT.EQ.1) GOTO 100
01510 IF(RM.GE.RIM.AND.ITT.GT.1) GOTO 3010
01520 DO 130 K=1,4
01530 IF(ABS(HKI(K)-HKM(K))/HKM(K).LT.1.E-02) GOTO 130
01540 GOTO 100
01550 130 CONTINUE
01560 IF(ABS(RIM-RM)/RM.LT.1.E-02) GOTO 3010
01570 100 CONTINUE
01580C----------- PRINT OUT RESULTS FOR MIN RMS ----------------
01590 3010 R=RM
01600 REF=1.
01610 WRITE(6,1800) R*100.
01620 WRITE(6,1900) (HKM(I),I=1,4)
01630 WRITE(6,1400)
01640 CALL SOLVE
01650 WRITE(6,1800) R*100
01660 STOP
01670 END
01680C
01690C*************************************************************
01700C
01710 SUBROUTINE SOLVE
01720 COMMON/D/ AL(5),HK(0:5),HKM(4)
01730 COMMON /TD/ A(5),B(5),C(5),D(5),Q(5),P(5),CON(5)
01740 COMMON /V/ CEX(5,20),TEX(20),IA(20)
01750 COMMON /V1/ JMAX,N,DT,REF,RP,RC,RN,R,RM,AA,IC,AI
01760C-------------------------------------------------------------
01770C
01780 II=1
01790 TIME=TEX(1)
01800 DO 111 I=1,5
01810 111 CON(I)=CEX(I,1)
01820 II=II+1
01830 TIMEX=TEX(II)
01840 SES=SK=0.
01850 NN=0
01860C-------------------------------------------------------------
01870 DO 400 J=1,JMAX
01880C-------- COEFFICIENTS -----------
01890 DO 401 I=1,5
01900 B(I)=HK(I)
01910 C(I)=HK(I-1)
01920 A(I)=B(I)+C(I)+AL(I)/(DT*60.)
01930 401 D(I)=CON(I)*AL(I)/(DT*60.)
01940C------  SOLVE,PRINT  ------------
01950 TIME=TIME+DT
01960 CALL TDMA
01970 AMD=AMOD(TIME,5.)
01980 IF((AMD.NE.0).AND.(TIME.NE.TIMEX)) GOTO 400
01990 IF(REF.EQ.1.) WRITE(6,1500) TIME,(CON(K),K=1,5)
02000C---------  RMS ERROR  -----------
02010 IF(TIME.EQ.TIMEX) THEN
02020 DO 402 I=1,5
02030 SES=SES+(CON(I)-CEX(I,II))**2.
02040 SK=SK+CEX(I,II)
02050 402 NN=NN+1
02060 IF(REF.EQ.1.) THEN
02070 WRITE(6,1050) (CEX(I,II),I=1,5)
```

```
02080 WRITE(6,1051) (CON(I)-CEX(I,II),I=1,5)
02090 ENDIF
02100 II=II+1
02110 TIMEX=TEX(II)
02120 ENDIF
02130C--------------------------------
02140 400 CONTINUE
02150 R=SQRT(SES/FLOAT(NN))/(SK/FLOAT(NN))
02160C-------------------------------------------------------------
02170 1500 FORMAT(4X,F7.1,5F7.0)
02180 1050 FORMAT(11X,5F7.0)
02190 1051 FORMAT(14X,5F7.0/4X,45(1H-))
02200 RETURN
02210 END
02220C*************************************************************
02230 SUBROUTINE TDMA
02240 COMMON /TD/ A(5),B(5),C(5),D(5),Q(5),P(5),CON(5)
02250 P(1)=B(1)/A(1)
02260 Q(1)=D(1)/A(1)
02270 DO 200 I=2,5
02280       P(I)=B(I)/(A(I)-C(I)*P(I-1))
02290 200 Q(I)=(D(I)+C(I)*Q(I-1))/(A(I)-C(I)*P(I-1))
02300 CON(5)=Q(5)
02310 DO 300 I=4,1,-1
02320 300 CON(I)=P(I)*CON(I+1)+Q(I)
02330 RETURN
02340 END
02350C*************************************************************
02360 SUBROUTINE LAGPOL
02370 DIMENSION F(3),X(3),PP(3)
02380 COMMON /D/ AL(5),HK(0:5),HKM(4)
02390 COMMON /V/ CEX(5,20),TEX(20),IA(20)
02400 COMMON /V1/JMAX,N,DT,REF,RP,RC,RN,R,RM,AA,IC,AI
02410 COMMON /LAG/ HKP,HKC,HKN
02420C-------------------------------------------------------------
02430 F(1)=RP   $   X(1)=HKP
02440 F(2)=RC   $   X(2)=HKC
02450 F(3)=RN   $   X(3)=HKN
02460C
02470 DO 100 I=1,3
02480 PP(I)=1.
02490 DO 200 J=1,3
02500 IF(I.EQ.J) GOTO 200
02510 PP(I)=PP(I)*(X(I)-X(J))
02520 200 CONTINUE
02530 100 CONTINUE
02540C
02550 AP=BP=CP=0.
02560 DO 300 I=1,3
02570 AP=AP+F(I)/PP(I)
02580 BP=BP+F(I)*X(I)/PP(I)
02590 300 CP=CP+F(I)/(X(I)*PP(I))
02600 BP=BP-(X(1)+X(2)+X(3))*AP
02610 CP=CP*X(1)*X(2)*X(3)
02620 HKI=-BP/(2.*AP)
02630 HK(IC)=HKI
02640 CALL SOLVE
02650 IF(HKI.GE.HKP.AND.HKI.LE.HKC) THEN
02660 RN=RC   $   HKN=HKC
02670 RC=R    $   HKC=HKI
02680 ELSEIF (HKI.GE.HKC.AND.HKI.LE.HKN) THEN
02690 RP=RC   $   HKP=HKC
02700 RC=R    $   HKC=HKI
02710 ELSE
02720 WRITE(6,5000)
02730 5000 FORMAT (5X,'SOMETHING WRONG')

02740 ENDIF
02750 RETURN
02760C*************************************************************
02770 END
```

PROGRAM ISSY

```
00100 PROGRAM INA(DATINA,INPUT,OUTPUT,TAPE5=DATINA,TAPE6=OUTPUT,
00110+TAPE1=INPUT)
00120 DIMENSION HKI(4),CM(20)
00130 COMMON /M/ NM
00140 COMMON /D/ AL(5),HK(0:5),HKM(4)
00150 COMMON /TD/ A(5),B(5),C(5),D(5),Q(5),P(5),CON(5)
00160 COMMON /V/ CEX(5,20),TEX(20),IA(20)
00170 COMMON /V1/ JMAX,N,DT,REF,RP,RC,RN,R,RM,AA,IC,AI
00180 COMMON /LAG/ HKP,HKC,HKN
00190 DATA AL,RIM /1.715,1.00,3.10,3.10,3.223,1.E+05/
00200 DATA AA,AI,REF,HK(0),HK(5)/0.70,.3,3*0./
00210 DATA DT,ITMAX,ITTM /1.00,05,10/
00220C-------------------------------------------------------------
00230 REWIND 5
00240 READ(5,1000) NR
00250 READ(5,1000) N
00260 READ(5,1100)((IA(I),TEX(I),(CEX(J,I),J=1,5)),I=1,N)
00270 WRITE(6,1700) ITMAX,AA  ,AI  ,DT
00280 WRITE(6,1200) NR,N
00290 WRITE(6,1400)
00300 WRITE(6,1100)((IA(L),TEX(L),(CEX(J,L),J=1,5)),L=1,N)
00310C
00320 1000 FORMAT(I4)
00330 1100 FORMAT(I4,F6.1,5F7.0)
00340 1200 FORMAT(/5X,'RUN',I4//5X,'N=',I2//5X,'EXPERIMENTAL DATA'/)
00350 1400 FORMAT(/6X,'TIME',3X,'K(A)',3X,'K(B)',
00360+3X,'K(1)',3X,'K(2)',3X,'K(3)'/)
00370 1401 FORMAT(//5X,'MODIFIED DATA'/)
00380 1500 FORMAT(//5X,'ITER',8X,'KAB',7X,'KB1',7X,'K12',
00390+7X,'K23',7X,'RMS'/)
00400 1600 FORMAT(5X,2I4,4E10.4,E12.5)
00410 1700 FORMAT(//5X,'ITMAX=',I3/5X,'AA  =',F4.2/5X,'AI   =',F4.2/
00420+5X,'DT  =',F4.2//)
00430 1800 FORMAT(/5X,'RMS ERROR=',F6.4,'  PERCENT'/)
00440 1900 FORMAT(5X,'KAB=',E10.4/5X,'KB1=',E10.4/5X,'K12=',E10.4/
00450+5X,'K23=',E10.4/)
00460 2000 FORMAT (5X,60(1H-))
00470 2010 FORMAT (1X,'ITT=',I3)
00480C-------------------------------------------------------------
00490C
00500 NM=N
00510 CALL MAIK
00520 ALS=0.
00530 DO 101 J=1,5
00540 101 ALS=ALS+AL(J)
00550 DO 102 I=1,N
00560 CMS=0.
00570 DO 103 J=1,5
00580 103 CMS=CMS+CEX(J,I)*AL(J)
00590 102 CM(I)=CMS/ALS
00600 DO 105 I=1,N
00610 DO 105 J=1,5
00620 105 CEX(J,I)=CEX(J,I)*CM(1)/CM(I)
00630 WRITE(6,1401)
00640 WRITE(6,1400)
00650 WRITE(6,1100) (IA(L),TEX(L),(CEX(J,L),J=1,5),L=1,N)
00660C
00670 CALL MAIK
00680 READ(1,*) (HK(I),I=1,4)
00690 WRITE(6,1500)
00700 TMAX=TEX(N)+5
00710 JMAX=INT(TMAX/DT)
00720 ITER=0 $  IT=0
00730 CALL SOLVE
00740 WRITE(6,1600) ITER,IT,(HK(I),I=1,4),R
00750 RP=R
```

```
00760 RM=R
00770C---------- ITERATIONS ----------
00780 DO 100 ITT=1,ITTM
00790 IF(ITT.EQ.1) GOTO 190
00800 DO 120 K=1,4
00810 120 HKI(K)=HKM(K)
00820 190 RIM=RM
00830 WRITE(6,2010) ITT
00840 DO 110 IC=1,4
00850 HKC=HK(IC)
00860 HKP=(1-AI)*HK(IC)
00870 HKN=(1+AI)*HK(IC)
00880 HK(IC)=HKC
00890 CALL SOLVE
00900 RC=R  $  ITER=ITER+1
00910 WRITE(6,1600) ITER,IT,(HK(I),I=1,4),R
00920 HK(IC)=HKP
00930 CALL SOLVE
00940 RP=R  $  ITER=ITER+1
00950 WRITE(6,1600) ITER,IT,(HK(I),I=1,4),R
00960 HK(IC)=HKN
00970 CALL SOLVE
00980 RN=R  $  ITER=ITER+1
00990 DO 200 IT=1,ITMAX
01000 IF(IT.EQ.1) GO TO 3000
01010 ITER=ITER+1
01020 IF(RP.GT.RC.AND.RN.GT.RC) THEN
01030 CALL LAGPOL  $ GOTO 3000
01040 ELSE
01050 SLPC=(RC-RP)/(HKC-HKP)
01060 SLCN=(RN-RC)/(HKN-HKC)
01070 SLPN=(RN-RP)/(HKN-HKP)
01080 IF(SLPN.GT.0.) GO TO 2600
01090 IF(SLPN.LT.0.) GO TO 2700
01100 ENDIF
01110C
01120 2600 SLM=AMAX1(SLPC,SLCN,SLPN)
01130 IF(SLM.EQ.SLPC) THEN
01140 RN=RC  $  HKN=HKC
01150 RC=RP  $  HKC=HKP
01160 ELSEIF (SLM.EQ.SLPN) THEN
01170 RC=RP  $  HKC=HKP
01180 ENDIF
01190C
01200 HKP=HKC-AA*RC/SLM
01210 IF(HKP/HK(IC).GT.3.) HKP=3.*HK(IC)
01220 IF(HKP/HK(IC).LT.(1./3.)) HKP=HK(IC)/3.
01230 IF(HKP.EQ.HK(IC)) HKP=0.90*HK(IC)
01240 HK(IC)=HKP
01250 CALL SOLVE
01260 RP=R
01270 GOTO 3000
01280C
01290 2700 SLM=AMIN1(SLPC,SLCN,SLPN)
01300 IF(SLM.EQ.SLCN) THEN
01310 RP=RC  $HKP=HKC
01320 RC=RN  $  HKC=HKN
01330 ELSEIF (SLM.EQ.SLPN) THEN
01340 RC=RN  $  HKC=HKN
01350 ENDIF
01360C
01370 HKN=HKC-AA*RC/SLM
01380 IF(HKN/HK(IC).GT.3.) HKN=3.*HK(IC)
01390 IF(HKN/HK(IC).LT.1./3.) HKN=HK(IC)/3.
01400 IF(HKN.EQ.HK(IC)) HKN=1.1*HK(IC)
01410 HK(IC)=HKN
```

```
01420 CALL SOLVE
01430 RN=R
01440C
01450 3000 RM=AMIN1(RP,RC,RN,RM)
01460 IF(RM.EQ.RP) HKM(IC)=HKP
01470 IF(RM.EQ.RC) HKM(IC)=HKC
01480 IF(RM.EQ.RN) HKM(IC)=HKN
01490 WRITE(6,1600) ITER,IT,(HK(I),I=1,4),R
01500 200 CONTINUE
01510 HK(IC)=HKM(IC)
01520 WRITE(6,2000)
01530 110 CONTINUE
01540 IF(ITT.EQ.1) GOTO 100
01550 IF(RM.GE.RIM.AND.ITT.GT.1) GOTO 3010
01560 DO 130 K=1,4
01570 IF(ABS(HKI(K)-HKM(K))/HKM(K).LT.1.E-02) GOTO 130
01580 GOTO 100
01590 130 CONTINUE
01600 IF(ABS(RIM-RM)/RM.LT.1.E-02) GOTO 3010
01610 100 CONTINUE
01620C---------- PRINT OUT RESULTS FOR MIN RMS ----------------
01630 3010 R=RM
01640 REF=1.
01650 WRITE(6,1800) R*100.
01660 WRITE(6,1900) (HKM(I),I=1,4)
01670 WRITE(6,1400)
01680 CALL SOLVE
01690 WRITE(6,1800) R*100
01700 STOP
01710 END
01720C
01730C*****************************************************************
01740C
01750 SUBROUTINE SOLVE
01760 COMMON/D/ AL(5),HK(0:5),HKM(4)
01770 COMMON /TD/ A(5),B(5),C(5),D(5),Q(5),P(5),CON(5)
01780 COMMON /V/ CEX(5,20),TEX(20),IA(20)
01790 COMMON /V1/ JMAX,N,DT,REF,RP,RC,RN,R,RM,AA,IC,AI
01800C---------------------------------------------------------------
01810C
01820 II=1
01830 TIME=TEX(1)
01840 DO 111 I=1,5
01850 111 CON(I)=CEX(I,1)
01860 II=II+1
01870 TIMEX=TEX(II)
01880 SES=SK=0.
01890 NN=0
01900C---------------------------------------------------------------
01910 DO 400 J=1,JMAX
01920C-------- COEFFICIENTS -----------
01930 DO 401 I=1,5
01940 B(I)=HK(I)
01950 C(I)=HK(I-1)
01960 A(I)=B(I)+C(I)+AL(I)/(DT*60.)
01970 401 D(I)=CON(I)*AL(I)/(DT*60.)
01980C------  SOLVE,PRINT  ------------
01990 TIME=TIME+DT
02000 CALL TDMA
02010 AMD=AMOD(TIME,5.)
02020 IF((AMD.NE.0).AND.(TIME.NE.TIMEX)) GOTO 400
02030 IF(REF.EQ.1.) WRITE(6,1500) TIME,(CON(K),K=1,5)
02040C---------  RMS ERROR  -----------
02050 IF(TIME.EQ.TIMEX) THEN
02060 DO 402 I=1,5
02070 SES=SES+(CON(I)-CEX(I,II))**2.
```

```
02080 SK=SK+CEX(I,II)
02090 402 NN=NN+1
02100 IF(REF.EQ.1.) THEN
02110 WRITE(6,1050) (CEX(I,II),I=1,5)
02120 WRITE(6,1051)(CON(I)-CEX(I,II),I=1,5)
02130 ENDIF
02140 II=II+1
02150 TIMEX=TEX(II)
02160 ENDIF
02170C---------------------------------
02180 400 CONTINUE
02190 R=SQRT(SES/FLOAT(NN))/(SK/FLOAT(NN))
02200C-------------------------------------------------------------
02210 1500 FORMAT(4X,F7.1,5F7.0)
02220 1050 FORMAT(11X,5F7.0)
02230 1051 FORMAT(14X,5F7.0/4X,45(1H-))
02240 RETURN
02250 END
02260C*************************************************************
02270 SUBROUTINE TDMA
02280 COMMON /TD/ A(5),B(5),C(5),D(5),Q(5),P(5),CON(5)
02290 P(1)=B(1)/A(1)
02300 Q(1)=D(1)/A(1)
02310 DO 200 I=2,5
02320         P(I)=B(I)/(A(I)-C(I)*P(I-1))
02330 200 Q(I)=(D(I)+C(I)*Q(I-1))/(A(I)-C(I)*P(I-1))
02340 CON(5)=Q(5)
02350 DO 300 I=4,1,-1
02360 300 CON(I)=P(I)*CON(I+1)+Q(I)
02370 RETURN
02380 END
02390C*************************************************************
02400 SUBROUTINE LAGPOL
02410 DIMENSION F(3),X(3),PP(3)
02420 COMMON /D/ AL(5),HK(0:5),HKM(4)
02430 COMMON /V/ CEX(5,20),TEX(20),IA(20)
02440 COMMON /V1/JMAX,N,DT,REF,RP,RC,RN,R,RM,AA,IC,AI
02450 COMMON /LAG/ HKP,HKC,HKN
02460C-------------------------------------------------------
02470 F(1)=RP   $   X(1)=HKP
02480 F(2)=RC   $   X(2)=HKC
02490 F(3)=RN   $   X(3)=HKN
02500C
02510 DO 100 I=1,3
02520 PP(I)=1.
02530 DO 200 J=1,3
02540 IF(I.EQ.J) GOTO 200
02550 PP(I)=PP(I)*(X(I)-X(J))
02560 200 CONTINUE
02570 100 CONTINUE
02580C
02590 AP=BP=CP=0.
02600 DO 300 I=1,3
02610 AP=AP+F(I)/PP(I)
02620 BP=BP+F(I)*X(I)/PP(I)
02630 300 CP=CP+F(I)/(X(I)*PP(I))
02640 BP=BP-(X(1)+X(2)+X(3))*AP
02650 CP=CP*X(1)*X(2)*X(3)
02660 HKI=-BP/(2.*AP)
02670 HK(IC)=HKI
02680 CALL SOLVE
02690 IF(HKI.GE.HKP.AND.HKI.LE.HKC) THEN
02700 RN=RC   $   HKN=HKC
02710 RC=R    $   HKC=HKI
02720 ELSEIF (HKI.GE.HKC.AND.HKI.LE.HKN) THEN
02730 RP=RC   $   HKP=HKC
```

```
02740 RC=R    $  HKC=HKI
02750 ELSE
02760 WRITE(6,5000)
02770 5000 FORMAT (5X,'SOMETHING WRONG')
02780 ENDIF
02790 RETURN
02800C*****************************************************
02810 END
02820 SUBROUTINE MAIK
02830 COMMON /M/NM
02840 COMMON /D/ AL(5),HK(0:5),HKM(4)
02850 COMMON /V/ CEX(5,20),TEX(20),IA(20)
02860 DIMENSION SUM(4),NI(4)
02870 WRITE(6,1600)
02880 1300 FORMAT(5X,F5.1)
02890 1400 FORMAT(9X,4E15.4)
02900 1600 FORMAT(//5X,'TIME',8X,'KAB',12X,'KB1',12X,'K12',12X,'K23'/)
02910 1700 FORMAT(/5X,'MEAN VALUES'/)
02920C-------------------------------------------------------------
02930 DO 400 J=1,4
02940 SUM(J)=0.
02950 400 NI(J)=0
02960C
02970 N=NM
02980 DO 200 I=2,N
02990 SSUM=0.
03000 WRITE(6,1300) TEX(I-1)
03010 DO 100 J=1,4
03020 SSUM=SSUM+AL(J)*(CEX(J,I)-CEX(J,I-1))/(TEX(I)-TEX(I-1))/60.
03030 CDIF=(CEX(J,I)+CEX(J,I-1)-(CEX(J+1,I)+CEX(J+1,I-1)))/2.
03040 HK(J)=-SSUM/CDIF
03050 100 CONTINUE
03060 WRITE(6,1400) (HK(L),L=1,4)
03070 DO 300 J=1,4
03080 IF(HK(J).LT.0.) GOTO 300
03090 SUM(J)=SUM(J)+HK(J)
03100 NI(J)=NI(J)+1
03110 300 CONTINUE
03120 200 CONTINUE
03130 WRITE(6,1300) TEX(N)
03140 DO 500 J=1,4
03150 500 HK(J)=SUM(J)/FLOAT(NI(J))
03160 WRITE(6,1700)
03170 WRITE(6,1400)(HK(L),L=1,4)
03180 RETURN
03190 END
```

PROGRAM MARKOS

```
00100 PROGRAM INA(DATINA,INPUT,OUTPUT,TAPE5=DATINA,TAPE6=OUTPUT,
00110+TAPE1=INPUT)
00120 DIMENSION HKI(4),CM(35)
00130 COMMON /D/ AL(5),HK(0:5),HKR(5),RE(5),RM(5),NI(5)
00140 COMMON /TD/ A(5),B(5),C(5),D(5),Q(5),P(5),CON(5)
00150 COMMON /V/ CEX(5,35),TEX(35),IA(35)
00160 COMMON /V1/ JMAX,N,DT,R,CS,H,OXY
00170 DATA AL /1.715,1.00,3.10,3.10,3.223/
00180 DATA HK(0),HK(5)/2*0./
00190 DATA DT,ITTM /1.00,0/
00200C-----------------------------------------------------------------
00210 REWIND 5
00220 READ(5,1000) NR
00230 READ(5,1000) N
00240 READ(5,1100)((IA(I),TEX(I),(CEX(J,I),J=1,5)),I=1,N)
00250 READ(1,*) ((HK(I),I=1,4),(HKR(I),I=1,5))
00260 WRITE(6,1001)
00270 1001 FORMAT (/5X,'GIVE H IN METERS, CS IN MG PER LT'/
00280+5X,'OXY EQUAL 1 FOR OXYGEN'/)
00290 READ(1,*) H,CS,OXY
00300 WRITE(6,1700) DT
00310 WRITE(6,1200) NR,N
00320 IF(OXY.EQ.1) WRITE(6,1405)
00330 IF(OXY.NE.1) WRITE(6,1400)
00340 WRITE(6,1500)((IA(L),TEX(L),(CEX(J,L),J=1,5)),L=1,N)
00350C
00360 1000 FORMAT(I4)
00370 1100 FORMAT(I4,F6.1,5F7.2)
00380 1200 FORMAT(/5X,'RUN',I4//5X,'N=',I2//5X,'EXPERIMENTAL DATA'/)
00390 1400 FORMAT(/6X,'TIME',5X,'K(A)',5X,'K(B)',
00400+5X,'K(1)',5X,'K(2)',5X,'K(3)'/)
00410 1405 FORMAT(/6X,'TIME',5X,'C(A)',5X,'C(B)',
00420+5X,'C(1)',5X,'C(2)',5X,'C(3)'/)
00430 1401 FORMAT(//5X,'MODIFIED DATA'/)
00440 1500 FORMAT(I4,F6.1,5F9.2)
00450 1600 FORMAT (5X,'PERCENT RMS ERRORS'/11X,5E9.3//)
00460 1700 FORMAT(//5X,'DT  =',F4.2//)
00470 1800 FORMAT(/5X,'RMS ERROR=',E10.4,' PERCENT'/)
00480 1900 FORMAT(//5X,'KAB=',E10.4/5X,'KB1=',E10.4/5X,'K12=',E10.4/
00490+5X,'K23=',E10.4/)
00500 1905 FORMAT(5X,'KRA=',E10.4/5X,'KRB=',E10.4/5X,'KR1=',E10.4/
00510+5X,'KR2=',E10.4/5X,'KR3=',E10.4//)
00520C-----------------------------------------------------------
00530C
00540 GOTO 20
00550 30 ITTM=1
00560 ALS=0.
00570 DO 101 J=1,5
00580 101 ALS=ALS+AL(J)
00590 DO 102 I=1,N
00600 CMS=0.
00610 DO 103 J=1,5
00620 103 CMS=CMS+CEX(J,I)*AL(J)
00630 102 CM(I)=CMS/ALS
00640 DO 105 I=1,N
00650 DO 105 J=1,5
00660 105 CEX(J,I)=CEX(J,I)*CM(1)/CM(I)
00670 WRITE(6,1401)
00680 WRITE(6,1400)
00690 WRITE(6,1500) (IA(L),TEX(L),(CEX(J,L),J=1,5),L=1,N)
00700C
00710 20 TMAX=TEX(N)+5
00720 JMAX=INT(TMAX/DT)
00730C---------- PRINT OUT RESULTS  ---------------
00740 WRITE(6,1900) (HK(I),I=1,4)
00750 WRITE(6,1905) (HKR(I),I=1,5)
```

```
00760 IF(OXY.EQ.1) WRITE(6,1405)
00770 IF(OXY.NE.1) WRITE(6,1400)
00780 CALL SOLVE
00790 WRITE(6,1600) (RM(I),I=1,5)
00800 WRITE(6,1800) R*100
00810 IF(OXY.NE.1.AND.ITTM.EQ.0) GOTO 30
00820 STOP
00830 END
00840C
00850C*************************************************************
00860C
00870 SUBROUTINE SOLVE
00880 DIMENSION DIF(5)
00890 COMMON/D/ AL(5),HK(0:5),HKR(5),RE(5),RM(5),NI(5)
00900 COMMON /TD/ A(5),B(5),C(5),D(5),Q(5),P(5),CON(5)
00910 COMMON /V/ CEX(5,35),TEX(35),IA(35)
00920 COMMON /V1/ JMAX,N,DT,R,CS,H,OXY
00930C-------------------------------------------------------------
00940C
00950 II=1
00960 TIME=TEX(1)
00970 DO 111 I=1,5
00980 RE(I)=0.
00990 RM(I)=0.
01000 NI(I)=0
01010 111 CON(I)=CEX(I,1)
01020 II=II+1
01030 TIMEX=TEX(II)
01040 SES=SK=0.
01050 NN=0
01060C-------------------------------------------------------------
01070 DO 400 J=1,JMAX
01080C-------- COEFFICIENTS -----------
01090 DO 401 I=1,5
01100 ADD=HKR(I)*AL(I)/H
01110 B(I)=HK(I)
01120 C(I)=HK(I-1)
01130 A(I)=B(I)+C(I)+AL(I)/(DT*60.)+ADD
01140 401 D(I)=CON(I)*AL(I)/(DT*60.)+ADD*CS
01150C------  SOLVE,PRINT  ------------
01160 TIME=TIME+DT
01170 CALL TDMA
01180 AMD=AMOD(TIME,5.)
01190 IF((AMD.NE.0).AND.(TIME.NE.TIMEX)) GOTO 400
01200 WRITE(6,1500) TIME,(CON(K),K=1,5)
01210 IF(OXY.EQ.1.AND.AMOD(TIME,10.).EQ.0) WRITE(6,1052)
01220C---------  RMS ERROR  -----------
01230 IF(TIME.EQ.TIMEX) THEN
01240 DO 402 I=1,5
01250 IF(CEX(I,II).EQ.0) GOTO 402
01260 SES=SES+(CON(I)-CEX(I,II))**2.
01270 SK=SK+CEX(I,II)
01280 NN=NN+1
01290 RE(I)=RE(I)+(CON(I)-CEX(I,II))**2.
01300 RM(I)=RM(I)+CEX(I,II)
01310 NI(I)=NI(I)+1
01320 402 CONTINUE
01330 WRITE(6,1050) (CEX(I,II),I=1,5)
01340 DO 500 I=1,5
01350 DIF(I)=CON(I)-CEX(I,II)
01360 500 IF(CEX(I,II).EQ.0) DIF(I)=0.
01370 IF(OXY.NE.1)WRITE(6,1051) (DIF(I),I=1,5)
01380 IF(OXY.EQ.1) WRITE(6,1050)(DIF(I),I=1,5)
01390 IF(OXY.NE.1) WRITE(6,1052)
01400 II=II+1
01410 TIMEX=TEX(II)
```

```
01420 ENDIF
01430C---------------------------------
01440 400 CONTINUE
01450 R=SQRT(SES/FLOAT(NN))/(SK/FLOAT(NN))
01460 DO 510 I=1,5
01470 RM(I)=SQRT(RE(I)/FLOAT(NI(I)))/(RM(I)/FLOAT(NI(I)))
01480 510 RM(I)=RM(I)*100.
01490C-------------------------------------------------------------
01500 1500 FORMAT(4X,F7.1,5F9.2)
01510 1050 FORMAT(11X,5F9.2)
01520 1051 FORMAT(14X,5F9.2)
01530 1052 FORMAT(4X,55(1H-))
01540 RETURN
01550 END
01560C*************************************************************
01570 SUBROUTINE TDMA
01580 COMMON /TD/ A(5),B(5),C(5),D(5),Q(5),P(5),CON(5)
01590 P(1)=B(1)/A(1)
01600 Q(1)=D(1)/A(1)
01610 DO 200 I=2,5
01620         P(I)=B(I)/(A(I)-C(I)*P(I-1))
01630 200 Q(I)=(D(I)+C(I)*Q(I-1))/(A(I)-C(I)*P(I-1))
01640 CON(5)=Q(5)
01650 DO 300 I=4,1,-1
01660 300 CON(I)=P(I)*CON(I+1)+Q(I)
01670 RETURN
01680C*************************************************************
01690 END
```

APPENDIX III

ATTEMPTED CORRELATIONS FOR K_L

APPENDIX III

ATTEMPTED CORRELATIONS FOR K_L

Multiple regression between K_L , $K_L\ Sc^{1/2}$ and the wave characteristics (H, f) yielded the following empirical equations

$$K_L = 1.71 \times 10^{-3}\ H^{1.59}\ f^{2.76} \qquad (r^2=0.708) \qquad \text{(A8)}$$

$$K_L\ Sc^{1/2} = 0.0551\ H^{1.67}\ f^{2.77} \qquad (r^2=0.673) \qquad \text{(A9)}$$

Consequently, the parameters H.f, $s.H.f = \sqrt{2}\ \pi^2 H^2 f^3/g$, $H^{1.5}f^2/\sqrt{g}$, $(\nu/g^5)^{1/6}\ H^{1.5}f^{2.5}$, all having units of velocity, were developed through dimensional analysis and linearly correlated with $K_L Sc^{1/2}$. For each parameter one correlation with and one without a constant term was obtained using the method of least squares. The coefficient of determination r^2 was determined in every case. A small difference in r^2 in the two correlations of a parameter indicates that the constant term is not important and can be dropped, as in the case of Eq. (63).

The correlations have the form

$$K_L\ Sc^{1/2} = a_1\ X + b_1 \qquad (r_1^2) \qquad \text{(A10)}$$

$$K_L\ Sc^{1/2} = a_2\ X \qquad (r_2^2) \qquad \text{(A11)}$$

X, a_1, b_1, a_2, r_1^2, and r_2^2 are all given in Table A10.

One more equation was developed for K_L with the form

$$K_L = a_1 \left(\frac{H^3 f^3}{g\nu} \right)^{a_2} \sqrt{D_m.s.f} \qquad \text{(A12)}$$

Multiple regression yielded $a_1 = 0.611$, $a_2 = 0.35$ and $r^2 = 0.707$. For deep water waves Eq. (A12) gives $K_L \sim H^{1.55}\ f^{2.55}$. All the above equations were developed using K_L data only. K_{LAB} values in most cases were much higher.

The dependence of $K_L Sc^{1/2}$ on fetch and wind shear velocity, as predicted by Eqs. (66) and (67) for the equations of Table A10 is given in Table A11. The exponents of F range from -1/12 to 1/6 and the exponents of u_* range from 2/3 to 1. The fact that the exponent of F ranges from negative to postive values does not allow us to draw any definite

conclusions on the influence of fetch on gas transfer. More experimental results are needed to determine the influence of fetch on wave induced gas transfer.

Finally, an equation fitting all the data (both K_{LAB} and K_L values) reasonably well was derived:

$$K_L \, Sc^{1/2} = 2.1 \times 10^{-3} \, H.f \, e^{37H/L} \qquad (r^2=0.653) \tag{A13}$$

This equation though, cannot be used for comparison with other data, since the wave breaking was forced by the paddle and not by the steepening of the wave itself, in which case a critical value of H/L could be used as a criterion for the breaking.

In all cases the coefficient of determination was determined as

$$r^2 = 1 - \frac{\sum_{i=1}^{N} (y_i - \hat{y}_i)^2}{\sum_{i=1}^{N} (y_i - \bar{y})^2} \tag{A14}$$

where y_i = measured value; $\hat{y}_i$ = predicted value, and $\bar{y} = \Sigma \, y_i/N$.

TABLE A10. COMPARISON OF VARIOUS PREDICTIVE EQUATIONS FOR $K_L\ Sc^{1/2}$

X	a_1	b_1	r_1^2	a_2	r_2^2
H.f	1.75×10^{-2}	-7.39×10^{-5}	0.643	1.59×10^{-2}	0.638
s.H.f	8.01×10^{-2}	2.36×10^{-4}	0.640	11.48×10^{-2}	0.477
$H^{1.5}f^{2}$	4.39×10^{-2}	1.04×10^{-4}	0.670	5.08×10^{-2}	0.646
$H^{1.5}f^{2.5}$	3.57×10^{-2}	8.45×10^{-6}	0.712	3.61×10^{-2}	0.712

*Values of H in meters and f in Hz were used for the computation of all parameters.

TABLE A11. FETCH DEPENDENCE OF $K_L\ Sc^{1/2} \propto F^{c1}\ U_*^{c2}$

X	C_1	C_2
H• f	1/6	2/3
s• H• f	0	1
$H^{1.5}f^{2}$	1/12	5/6
$H^{1.5}f^{2.5}$	-1/12	2/3